U.PORTO
FEUP FACULDADE DE ENGENHARIA
UNIVERSIDADE DO PORTO

DEVELOPMENT OF FLEXIBLE AND ELECTRICALLY CONDUCTIVE SENSORS USING POLYMER COMPOSITES WITH CARBON NANOTUBES

A dissertation to the fulfilment of doctorate degree in Advanced Materials and Processing

Candidate
David Seixas Esteves

Supervisor
Professora Elsa W. Sequeiros

Co-Supervisor
Professora Maria C. Paiva

Porto, May 2025

A collaborative work between three institutions:

Acknowledgements

This thesis would not have been possible without the guidance, support, and encouragement of many people and institutions.

First and foremost, I express my deepest gratitude to my supervisor, Prof. Elsa Sequeiros, for her invaluable guidance, continuous support, and unwavering availability to discuss my work. Her encouragement and insights have been instrumental in the successful completion of this research.

I am equally thankful to my co-supervisors, Prof. Conceição Paiva and Nelson Durães. Prof. Conceição Paiva's expertise, support, and shared knowledge provided essential direction to my research, while Nelson Durães offered thoughtful guidance and practical insights, helping me approach problems and interpret results with clarity throughout these years, both in my PhD and at work.

A special acknowledgement goes to Prof. Manuel Vieira from FEUP for accepting my PhD application and for all his assistance throughout this journey.

I am grateful to CeNTI for providing the infrastructure, materials, and equipment that enabled me to conduct my research effectively.

I also extend my heartfelt thanks to all my colleagues who contributed to my experimental work, making it not only more engaging but also significantly more valuable. Their assistance and collaboration were vital in achieving the outcomes of this research.

I am deeply indebted to my family and friends for their unwavering support and encouragement throughout this journey. Without their understanding and support, this work would not have been possible.

Abstract

The increasing demand for sensors in emerging technologies, including wearable devices, smart textiles, and flexible electronics, has driven significant research into developing innovative composites with high conductivity, mechanical flexibility, and scalability. This doctoral thesis investigates the development of multi-walled carbon nanotube (MWCNT)-based polymer composites for flexible and conductive sensors, highlighting the impacts of magnetic patterning, matrix selection, and material blending for optimising their electrical and sensing properties. The study demonstrated that applying static magnetic fields in low-viscosity matrices, such as polydimethylsiloxane (PDMS) and Polyurethane (PU), significantly improved MWCNT alignment and positioning, reducing electrical percolation threshold and enhancing conductivity. Adding magnetite further refined particle alignment, indicating that magnetic patterning is an effective approach to optimise conductive pathways using lower MWCNT concentrations. A significant limitation of this technique was observed in high-viscosity matrices like thermoplastics, where particle migration was significantly hindered, suggesting that matrix viscosity is a crucial factor for successful magnetic patterning. Furthermore, an optimised composite consisting of 5 wt.% MWCNTs and 25 wt.% thermoplastic elastomer (TPE) in a polypropylene (PP) matrix showed promising performance for smart textile and flexible electronics applications, providing low electrical resistivity and good mechanical flexibility. Overall, this research makes significant contributions to the field of flexible sensors by demonstrating novel strategies for developing high-performance MWCNT-based composites. Future work should focus on improving the scalability of the manufacturing process to enable mass production of these innovative sensors, exploring alternative matrices, enhancing long-term stability and investigating multifunctional sensor systems.

Keywords: Magnetite, MWCNT, sensors, polymer composites, flexible sensors.

Resumo

A crescente procura por sensores para tecnologias emergentes, incluindo dispositivos vestíveis, têxteis inteligentes e eletrónica flexível, tem impulsionado o desenvolvimento de compósitos inovadores com alta condutividade, flexibilidade mecânica e escalabilidade. Esta tese de doutoramento explora o desenvolvimento de compósitos poliméricos à base de MWCNT para sensores flexíveis e condutores, destacando a importância da padronização magnética, seleção da matriz polimérica e mistura de materiais na otimização das propriedades elétricas e sensoriais. O conjunto dos estudos demonstram que a aplicação de campos magnéticos estáticos em matrizes de baixa viscosidade, como polidimetilsiloxano e poliuretano, melhorou significativamente o alinhamento e a posicionamento dos MWCNT, resultando numa diminuição do limite de percolação elétrica e numa maior condutividade dos compósitos. A adição de magnetite melhorou ainda mais o controlo sobre o posicionamento das partículas, indicando que a padronização magnética é uma abordagem eficaz para o desenvolvimento de elétrodos condutores com baixas concentrações de MWCNT. Foi também identificada uma limitação na aplicação desta técnica em matrizes de alta viscosidade, tal como em termoplásticos, onde a migração das partículas foi significativamente prejudicada, sugerindo que a viscosidade da matriz é um fator crítico para a utilização efetiva da padronização magnética. Adicionalmente, foi desenvolvido um compósito otimizado, composto por 5% em peso de MWCNT e 25% em peso de elastómero termoplástico numa matriz de polipropileno. Este compósito apresentou um desempenho promissor para aplicações em têxteis inteligentes e eletrónica flexível, fornecendo baixa resistividade elétrica e flexibilidade mecânica. No geral, esta investigação contribui significativamente para a área dos sensores flexíveis, ao demonstrar novas estratégias para o desenvolvimento de compósitos à base de MWCNT com elevado desempenho. Trabalhos futuros devem focar-se na escalabilidade do processo de fabrico, permitindo a produção em massa deste tipo de sensores inovadores, exploração de matrizes alternativas, melhoria da estabilidade a longo prazo e investigação de sistemas de sensores multifuncionais.

Palavras-chave: Magnetite, MWCNT, sensores, compósitos poliméricos, sensores flexíveis.

Table of contents

List of Acronyms

AC - Alternated current

Al_4C_3 - Aluminium carbide

Au - Gold

BSED - Backscattering Electron Detector

CB - Carbon black

CCVD - Catalytic Chemical Vapor Deposition

CF - Carbon fibres

CNTs - Carbon nanotubes

CPCs - Conductive polymer composites

CVD - Chemical vapor deposition

DSC - Differential Scanning Calorimetry

EDS - Energy Dispersive Spectroscopy

EMI - Electromagnetic interference

ESD - Electrostatic discharge

Fe - Iron

FeCo - Iron Cobalt

Fe_3O_4 - Magnetite particles

G' - Storage modulus

G" - Loss modulus

GNPs - Graphene nanoplatelets

Hc - Coercivity

LDPE - Low-Density Polyethylene

MFI - Melt Flow Index

Micro CT - Micro Computed Tomography

MPa - Megapascal (unit of pressure)

Mr - Retentivity

Ms - Saturation magnetisation

MWCNTs - Multi-walled carbon nanotubes

OM - Optical microscopy

PBAT- Polybutylene adipate terephthalate

PBE - Polybutylene terephthalate

PC – Polycarbonate

PDMS - Polydimethylsiloxane

PE - Polyethylene

PEDOT - Poly(3,4-ethylenedioxythiophene): polystyrene sulfonate

PET - Polyethylene terephthalate

PP - Polypropylene

PU - Polyurethane

Rm - Maximum load

Ru – Ruthenium

S-CPCs - Segregated conductive polymer composites

SE - Secondary electron

SEBS - Styrene-Ethylene-Butylene-Styrene

SEM - Scanning Electron Microscopy

SmCo - Samarium Cobalt

SR - Silicone rubber

SWCNTs - Single-walled carbon nanotubes

TENG- Triboelectric nanogenerator

Tg - Glass transition temperature

TGA - Thermogravimetric analysis

TPE - Thermoplastic elastomer

TPEs - Thermoplastic elastomers

TPU - Thermoplastic polyurethane

VGCNFs - Vapor-grown carbon nanofibres

wt.% - Weight percent

Ω - Ohm

Ω.m - Ohm meter

List of Figures

List of Tables

Chapter 1: Introduction

This first chapter presents the research's motivation, scope and objectives, delineating the thesis structure. It describes the research context and its industrial impact, aligning the study with the mission of CeNTI (Centre for Nanotechnology and Advanced Materials) to bridge fundamental research and industrial application. Addressing challenges in electrical conductivity, material cost, and processing, this thesis explores innovative fabrication techniques, magnetic alignment, and material optimisation to develop high-performance, scalable, and adaptable materials. With a focus on practical applications, this research demonstrates solutions relevant to the healthcare, soft robotics, and wearable electronics industries, contributing to the development of functional and scalable flexible sensors.

1.1. Motivation and objectives

Polymer composites enhanced with carbon-based conductive fillers, such as carbon nanotubes (CNTs), are promising materials for flexible sensors. CNTs offer exceptional electrical and mechanical properties, making them ideal for advanced composites [1], essential for developing flexible and wearable sensors in healthcare, robotics, and smart textiles, where they can monitor physiological parameters and enhance mechanical sensing [2]. Growing applications drive the demand for advanced materials, motivating the development of flexible, electrically conductive sensors using Multi-Walled Carbon Nanotubes (MWCNT)-polymer composites to address key challenges and opportunities. Firstly, there is a growing need for lightweight, durable, and high-performance materials [3]. Traditional rigid electronic systems are often unsuitable for applications requiring flexibility and resilience under mechanical deformation [4–6], a capability critical for human-interactive robots, such as assistive healthcare or collaborative industrial robots [7]. Secondly, MWCNT-based polymer composites offer scalability and cost-effectiveness for sensor applications [8]. Compared to traditional sensors relying on expensive and complex manufacturing processes that limit widespread adoption in low-cost applications [9,10], MWCNT composites can be produced using scalable techniques like solution mixing and melt blending. Furthermore, the low filler content required for high electrical conductivity in MWCNT composites reduces material costs, making these sensors more accessible for diverse applications.

With this motivation in mind, the research work developed in this thesis focused on the specific objectives summarised below:

1) **To investigate the influence of MWCNT arrangement on composite conductivity and electrical percolation threshold;**

Optimising the arrangement of MWCNTs within the polymer matrix is of major importance for tailoring the electrical percolation threshold. This optimisation enables the development of more efficient and commercially viable flexible sensors through reductions in material costs and required filler content.

2) **To evaluate the impact of polymer matrix viscosity on particle arrangement and conductivity under magnetic fields in thermosets;**

The viscosity of the polymer matrix strongly governs the ability of filler particles to move, orient, and form conductive pathways under a magnetic field. Understanding these interactions is essential for designing composite systems that deliver reliable performance.

3) **To optimise thermoplastic material combinations to enhance composite properties;**

Blending or layering thermoplastic materials, such as thermoplastic elastomer (TPE) and polypropylene (PP), can mitigate the individual limitations of single-component systems. This approach aims to improve mechanical strength and electrical performance while leveraging thermoplastic recyclability for sustainable, large-scale production.

4) **To investigate magnetic field-assisted particle alignment in thermoplastics;**

Thermoplastic processing poses unique challenges, as viscosity, temperature, and process time add complexity beyond those encountered in thermoset-based composites. One key objective of this thesis is to investigate how magnetic field-assisted alignment can be adapted and optimised for thermoplastic matrices, ultimately seeking to enhance filler orientation and improve the electrical properties of the resulting composite.

5) **To compare thermosets and thermoplastics as polymeric matrices for conductive composite applications;**

Examining the differences between thermoset and thermoplastic materials (including processing methods, end-use performance, and recyclability) allows for more informed decisions in flexible electronics development. A thorough comparison of these pathways provides insights into how best to balance cost, mechanical robustness, and sustainability for various market applications, ultimately guiding the design of more efficient and eco-friendly sensor solutions.

To address the proposed objectives, this PhD research investigates the development of flexible and conductive sensors based on MWCNT-polymer composites, focusing on innovative fabrication techniques, material combinations, and the application of magnetic fields to enhance their electrical, mechanical, and sensing properties. Following a comprehensive review of flexible sensors and conductive polymer composites (CPCs) (Chapter 2), the research explores sensor fabrication with low electrical percolation thresholds

using magnetic patterning (Chapters 3 and 4). Chapter 3 introduces a novel method employing static magnetic fields to align MWCNTs within a Polydimethylsiloxane (PDMS) matrix, achieving low percolation thresholds. Chapter 4 incorporates magnetite to enhance magnetic responsiveness and control, demonstrating application in a soft robotic gripper. The research then focuses on developing bi-component flexible conductive electrodes for smart textiles (Chapter 5), combining MWCNTs with TPE for conductivity and flexibility in textile-laminated sensors. Chapter 6 investigates magnetic manipulation of magnetite/MWCNT particles in TPE composites, addressing challenges of particle migration and demonstrating magnetic field control of particle orientation and sensor positioning. The thesis concludes (Chapter 7) by summarising key achievements, addressing limitations in translating techniques from thermosets to thermoplastics and proposing future research directions, including exploring new materials and developing multifunctional sensors and durability/scalability tests. This research contributes to developing high-performance, scalable, and adaptable materials for flexible sensors with applications in soft robotics, wearable electronics, and smart textiles.

The focus of the thesis chapters is illustrated in Figure 1.1.

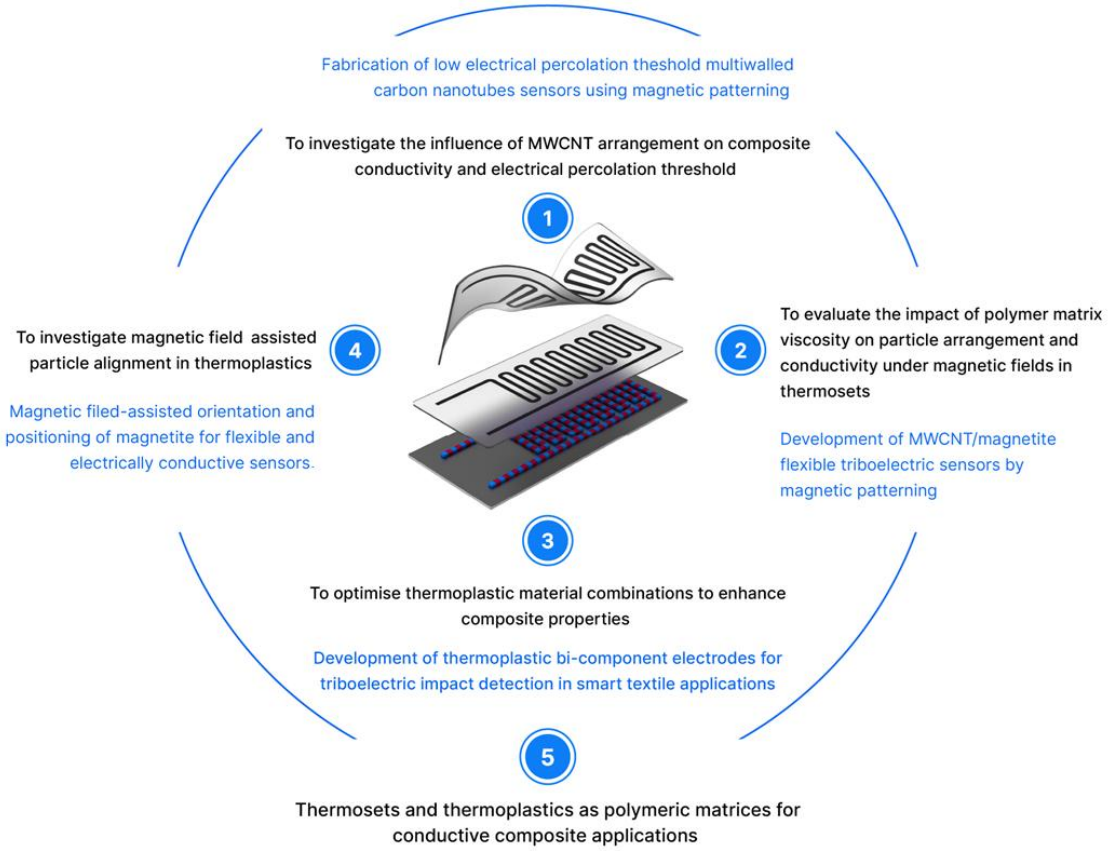

Figure 1.1 Outline of the thesis.

1.2. Industrial impact

This PhD thesis, conducted at CeNTI (Centre for Nanotechnology and Advanced Materials), directly supports the organisation's mission to bridge fundamental research and industrial application. As a non-profit technological interface centre (CTI) specialising in technology transfer, CeNTI helps industries innovate by introducing advanced products, processes, and services tailored to market needs, leveraging its expertise in nanotechnology, advanced materials, and smart systems.

This thesis aligns with CeNTI's objectives by exploring fundamental research with a clear industrial focus. Each chapter integrates practical applications, demonstrating the potential benefits of these developments for industrial use. The studies on MWCNT-based polymer composites address challenges relevant to healthcare, robotics, and wearable electronics, focusing on improving material electrical, mechanical, and sensing properties.

For instance, the work on low electrical percolation threshold composites advances the understanding of MWCNT behaviour under magnetic fields and offers scalable and cost-effective solutions for producing conductive composites directly relevant to industries seeking efficient materials for flexible sensors. Similarly, developing flexible, conductive bi-component filaments for smart textiles provides a clear path for industrial implementation in wearable electronics and adaptive clothing. These innovations demonstrate how fundamental research can yield tangible industrial outcomes, offering solutions that combine functionality, scalability, and sustainability.

CeNTI's role in facilitating industrial innovation is reflected in the thesis's collaborative, industry-focused approach. By considering industrial needs from the outset, this research exemplifies how CTIs like CeNTI can accelerate the translation of cutting-edge research into real-world applications. This synergy highlights the importance of integrating academic research with practical, industry-driven objectives, fostering the development of innovative, market-relevant products and technologies.

1.3. References

[1] Fenta, E. W., & Mebratie, B. A. (2024). Advancements in carbon nanotube-polymer composites: Enhancing properties and applications through advanced manufacturing techniques. Heliyon, 10(16).

[2] Shao, W., et al. (2023). Carbon-based textile sensors for physiological-signal monitoring. Materials, 16(11), 3932.

[3] Zhang, W., & Xu, J. (2022). Advanced lightweight materials for automobiles: A review. Materials & Design, 221, 110994.

[4] Lee, J.-H., Cho, K., & Kim, J.-K. (2024). Age of flexible electronics: Emerging trends in soft multifunctional sensors. Advanced Materials, 36(16), 2310505.

[5] Vaghasiya, J. V., Mayorga-Martinez, C. C., & Pumera, M. (2023). Wearable sensors for telehealth based on emerging materials and nanoarchitectonics. npj Flexible Electronics, 7(1), 26.

[6] Yang, G., Pang, G., Pang, Z., Gu, Y., Mäntysalo, M., & Yang, H. (2018). Non-invasive flexible and stretchable wearable sensors with nano-based enhancement for chronic disease care. IEEE Reviews in Biomedical Engineering, 12, 34–71.

[7] Yang, J. C., Mun, J., Kwon, S. Y., Park, S., Bao, Z., & Park, S. (2019). Electronic skin: Recent progress and future prospects for skin-attachable devices for health monitoring, robotics, and prosthetics. Advanced Materials, 31(48), 1904765.

[8] Mohd Nurazzi, N., et al. (2021). Fabrication, functionalization, and application of carbon nanotube-reinforced polymer composite: An overview. Polymers, 13(7), 1047.

[9] Abdulkarem, M., Samsudin, K., Rokhani, F. Z., & Rasid, M. F. A. (2020). Wireless sensor network for structural health monitoring: A contemporary review of technologies, challenges, and future direction. Structural Health Monitoring, 19(3), 693–735.

[10] Basu, A. K., Tatiya, S., Bhatt, G., & Bhattacharya, S. (2019). Fabrication processes for sensors for automotive applications: A review. Sensors for Automotive and Aerospace Applications, 123–142.

Chapter 2: State of the art

This chapter presents a comprehensive review of the state of the art in conductive composites for flexible sensors, establishing the grounds for this research. The chapter explores the materials, mechanisms, and fabrication techniques for developing advanced composites with tailored electrical and mechanical properties. Particular attention is given to incorporating conductive fillers, such as CNTs, into polymer matrices and strategies to optimise filler dispersion, percolation thresholds, and overall electrical performance. Furthermore, the chapter examines the underlying mechanisms of electrical conductivity in composite materials and highlights innovative approaches to enhance these properties, including segregated networks, filler alignment, and hybrid systems. This review provides the technical and scientific framework for the research contributions detailed in subsequent chapters, stressing the transformative role of conductive composites in materials science and engineering.

2. Introduction

Flexible electronics have evolved significantly, driven initially by the need for flexible silicon in space applications. The emergence of conductive polymers, organic semiconductors, and amorphous silicon enabled bending, stretching, and folding, leading to applications like solar cells and wearable health monitors. The subsequent introduction of nanomaterials like CNTs and graphene further revolutionised the field by enhancing conductivity, flexibility, and performance, enabling flexible sensors, displays, and energy harvesters that conform to irregular surfaces and withstand mechanical deformation, proving invaluable in healthcare, robotics, and wearable technologies [1].

Flexible sensors enable many applications of flexible electronics, becoming transformative tools across several industries. Their conformability, associated with sensitivity and reliability, is essential for applications like real-time health monitoring, robotic feedback systems, and adaptive wearables. In healthcare, they enable continuous vital sign monitoring for early diagnosis and personalised interventions. In robotics, they enhance tactile sensing for seamless interaction with the environment. Wearables support advanced functionalities like activity tracking and integrated energy harvesting, contributing to self-powered, adaptable systems. Current flexible sensor research focuses on improving materials and fabrication for superior stretchability, durability, and biocompatibility. Therefore, polymers and elastomers are essential for seamless integration with dynamic surfaces like skin or soft robotic frameworks. However, challenges remain in scaling manufacturing, ensuring long-term reliability, and developing sustainable materials. Overcoming these obstacles is fundamental for realising the full potential of flexible electronics [1].

2.1. Flexible and electrically conductive sensors

The development of flexible, electrically conductive sensors based on MWCNT polymer composites has the potential to significantly impact various industries, with their scalability and cost-effectiveness making them attractive for mass-market applications [1–3].

Figure 2.1 illustrates the evolution of flexible sensors from 2000 to 2022, highlighting advancements in materials, design, and applications. Initial efforts

concentrated on mechanical sensing for robotics, while subsequent innovations introduced wearable technologies using advanced materials such as yarn-based piezoresistive sensors and organic semiconductors. Over time, flexible sensors have become increasingly specialised, with expanding applications in health monitoring, robotic skin, and user interfaces. Recent advancements emphasise multifunctionality, durability, and healthcare applications, featuring breakthroughs in ultra-thin, stretchable designs and smart materials like MXene for next-generation wearable devices. This timeline reflects a consistent progression toward highly integrated, versatile and flexible sensor systems [4].

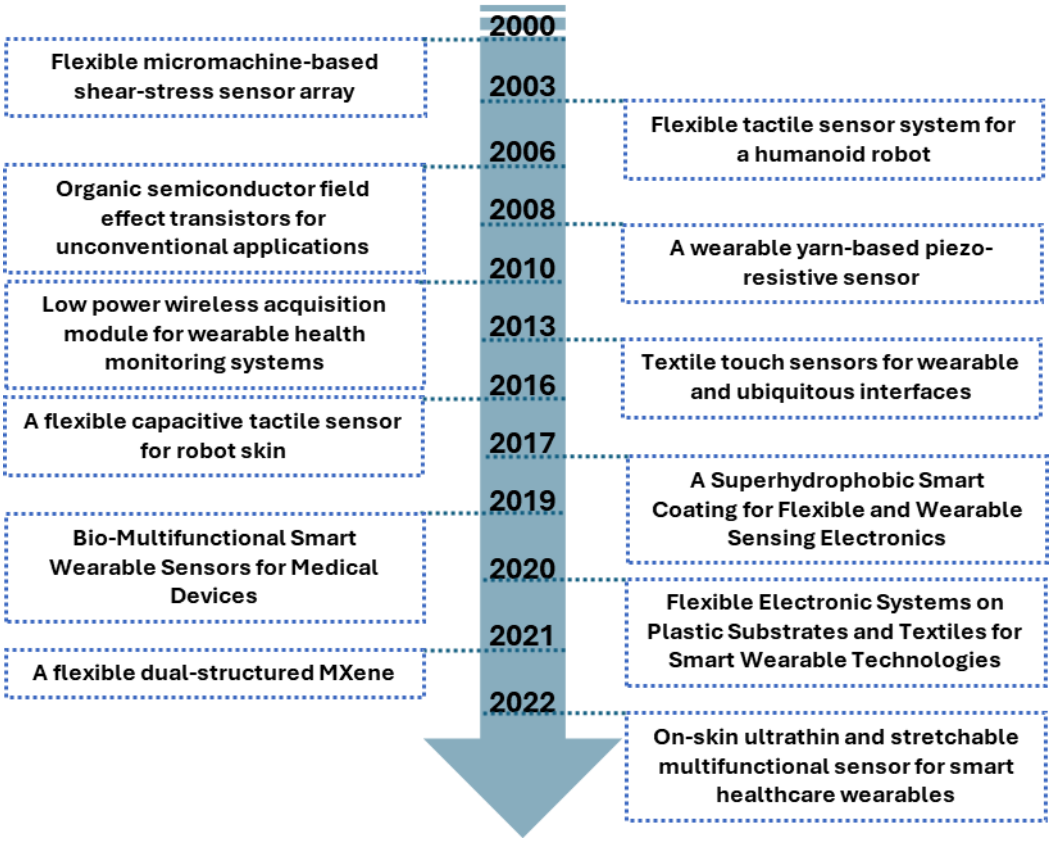

Figure 2.1- Timeline of the major milestones in the development of flexible sensors in the smart wearable field. Adapted from [4].

Sensor technology relies on three essential components that can be seamlessly integrated into flexible structures or polymeric substrates: electrodes, sensing layers, and transduction electronics [2,5]. Electrodes act as the interface between the sensing layer and the electronics and require high electrical conductivity, mechanical flexibility, and strong substrate adhesion. In direct contact with external stimuli, the sensing layer is engineered for high sensitivity,

minimal hysteresis, and a strong signal-to-noise ratio, often incorporating advanced materials like nanostructures and conductive composites. Then, the transduction electronics amplify and convert these signals into readable data, ensuring accuracy and reliability. This seamless integration of components enables flexible sensors to operate through several distinct mechanisms, including piezoresistive, triboelectric, piezoelectric, and capacitive effects [5–9].

The piezoresistive effect detects changes in electrical resistance due to mechanical deformation (compression, tension, or bending). This mechanism measures resistance variations caused by the rearrangement of conductive pathways, often formed by conductive fillers like CNTs or graphene within a polymer matrix, making piezoresistive sensors well-suited for precise strain or pressure monitoring. As an example of the development of piezoresistive sensors, Wang *et al.* [10] constructed self-segregated structures to form dense conductive CNT networks in a PDMS matrix. This innovation enhanced electrical conductivity and piezoresistive sensing performance, showing a gauge factor 7.4 times higher than conventional samples. The sensor also demonstrated improved compression modulus and strength, making it suitable for wearable applications. Similarly, Shao *et al.* [11] utilised photolithography to create micropillar arrays coated with gold. The sensor's sensitivity could be fine-tuned by adjusting the gaps between the pillars, ranging from 0.03 kPa^{-1} to 17 kPa^{-1}. This design showcased promising applications for tactile and pressure sensing. Mai *et al.* [12] developed ultra-stretchable CNT/Ecoflex composite sensors with mechanical properties mimicking human skin. The sensor could withstand up to 200% strain while maintaining a linear electromechanical response, offering high durability for wearable real-time monitoring. Additionally, as shown in Figure 2.2, Feng *et al.* [13] proposed a flexible integrated sensor system designed to simultaneously detect bending strain and pressure, addressing the challenge of discriminating different stimuli. The system combines a bending strain sensor fabricated from graphite wires using a low-cost laser-sintering process with a composite pressure sensor based on PDMS-expandable microspheres and silver nanowires (AgNWs). The strain sensor exhibited a gauge factor of 9.54 and excellent cycling stability, while the pressure sensor demonstrated tunable sensitivity and an adjustable working range. This integrated system successfully monitored motion and discriminated independent signals from strain and pressure sensors without

crosstalk, showcasing its potential in wearable electronics and motion monitoring applications

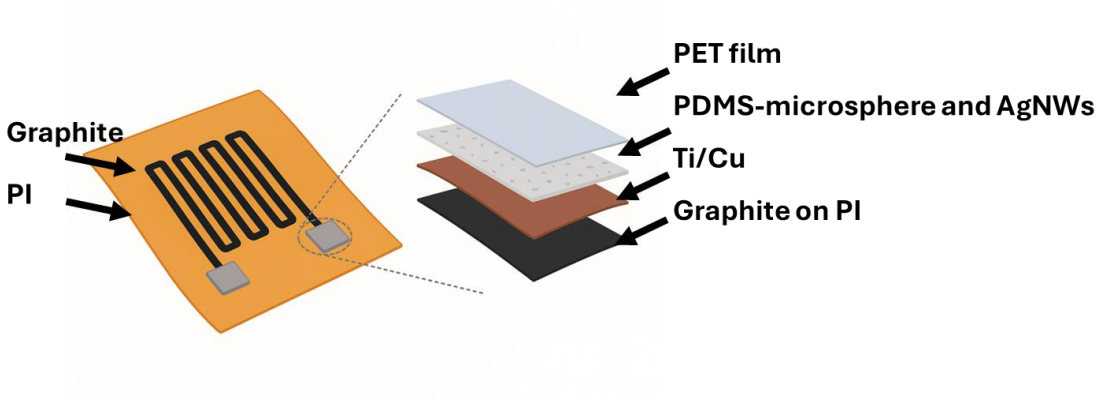

Figure 2.2- Flexible piezoresistive strain and pressure sensor system. Adapted from [13].

On the other hand, Triboelectric sensors generate electrical signals through the triboelectric effect, which occurs when two materials with differing electron affinities contact and separate, inducing charge transfer [4,5,14–16]. During contact, opposite charges accumulate on the material surfaces. Subsequent separation under mechanical force induces electron flow through an external circuit, converting mechanical energy into electricity. This principle enables highly sensitive detection of even subtle mechanical stimuli, such as gentle touches or vibrations [17,18]. Figure 2.3 illustrates the diverse applications of triboelectric nanogenerator (TENG)-based sensors for monitoring physiological and motion signals [19]. These self-powered sensors convert mechanical energy into electrical signals, enabling healthcare, fitness, and motion analysis applications. They detect respiration by monitoring airflow and chest/abdominal movements, track heartbeats and pulse waves for cardiovascular health insights, and detect muscle activity for diagnostics and rehabilitation [19–22]. TENG sensors also monitor joint flexion, extension, and posture during physical activities. They also analyse gait patterns, steps, and movement speed during running or walking, demonstrating their versatility and practicality in wearable and portable applications [23–24].

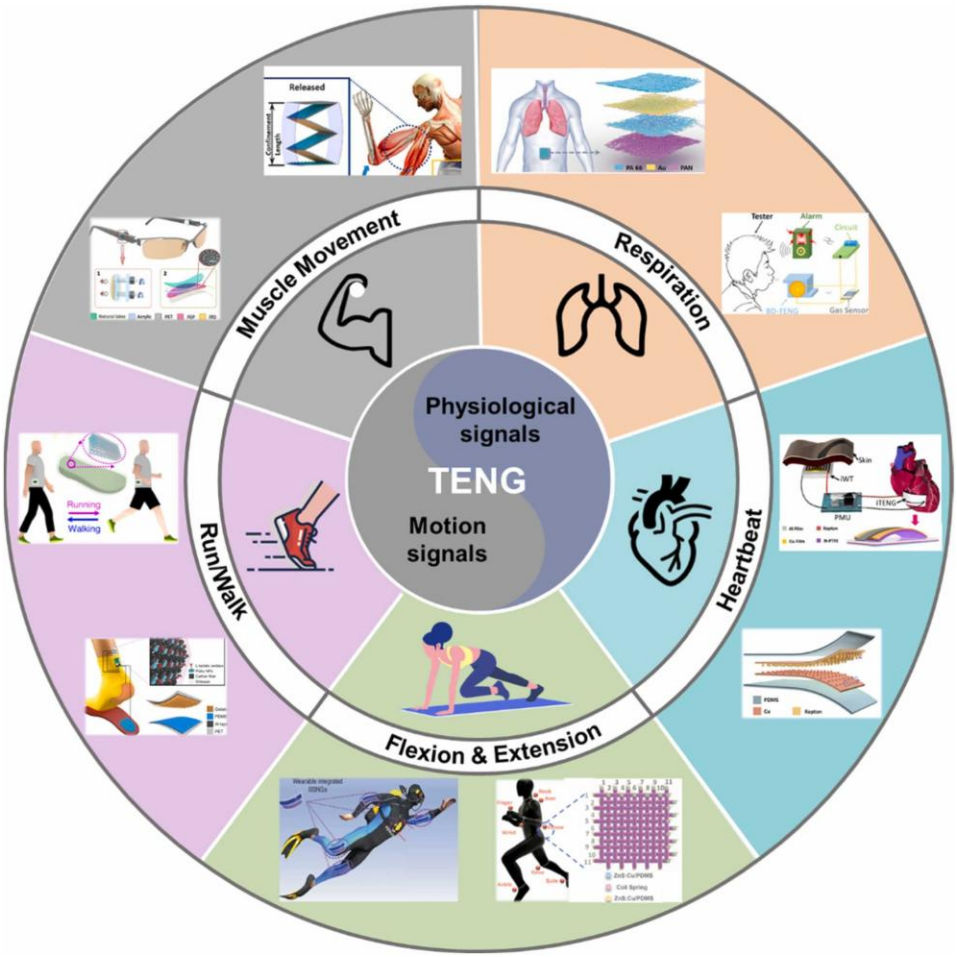

Figure 2.3- An overview of self-powered triboelectric sensor applications. Reprinted with permission from [19]. Copyright © 2024 Elsevier.

Regarding the recent developments of triboelectric sensors, Zheng *et al.* [25] developed a highly sensitive and durable triboelectric sensor (HSDTS) using dual regulation strategies involving surface morphology and functional group modifications on amino-functionalised gelatin (positive layer) and fluorinated MXene (negative layer). The HSDTS demonstrated a sensitivity of 1.06 V kPa^{-1} and maintained stable performance over 10,000 cycles and six months, showcasing potential applications in tactile sensing and Morse code transmission. Similarly, Ding *et al.* [26] designed a bamboo-based triboelectric nanogenerator (B-TENG) for energy harvesting and pressure sensing. Utilising bamboo and PDMS as triboelectric materials, the B-TENG achieved an open-circuit voltage of 169.75 V and a maximum power output of 217.38 μW, exhibiting excellent environmental adaptability and durability suitable for sustainable energy and sensing applications. Nuthalapati *et al.* [27] developed a wearable TENG for haptic applications using an MWCNT/PDMS composite. This device achieved an

open-circuit voltage of 249 V and a power density of 2.81 W/m², demonstrating stable, high-performance energy harvesting capabilities suitable for powering LEDs, small electronics, and wearable haptic systems. In another study, Qu *et al.* [28] presented an all-in-one strain-triboelectric sensor using environmentally friendly ionic hydrogels for wearable sensing and underwater soft robotic grasping. This sensor demonstrated excellent tensile properties, durability, and sensitivity, with a gauge factor of 4.30 and stable performance across 1000 cycles.

The seamless integration of conductive materials in polymeric matrixes, including hydrogels and conductive polymer networks, has emerged as a key factor in enhancing the functionality and adaptability of triboelectric sensors. These materials offer a valuable combination of mechanical and electrical properties and enable the development of flexible, durable, and environmentally friendly devices suitable for diverse applications.

2.2. Polymeric materials for the development of flexible conductive polymer composites (CPCs)

In polymer science, thermosets and thermoplastics are two distinct polymer categories. Thermoplastics are notable for their ability to be melted and remoulded multiple times without undergoing significant chemical alteration. This behaviour is attributed to their linear or branched polymer chains that soften upon heating to their melting point and solidify upon cooling. In some specific conditions, they can be reheated and reshaped repeatedly without material degradation, making them highly versatile for recycling and reprocessing. Common thermoplastics include polyethylene (PE), PP and polycarbonate (PC), finding applications in industries ranging from packaging and consumer goods to automotive and construction [5,29]. Conversely, thermosets are polymers that cannot be remelted or reshaped once cured or set through a chemical reaction. This curing process involves a reaction that typically occurs during the mixing of the resin with a hardener, leading to an irreversible formation of a tightly cross-linked network. This network can impart thermosets with enhanced heat resistance, mechanical strength, and dimensional stability over thermoplastics. Representative materials in this category include epoxy, phenolic resins, unsaturated polyester resins, PDMS and PU, which are used in high-performance

applications such as aerospace components, electronic devices, and automotive parts that must withstand extreme conditions [29].

Understanding the distinct behaviours and processing methods of thermosets and thermoplastics is important for selecting the right material for the application. This knowledge ensures that performance requirements are met while considering the environmental and economic implications, thereby optimising functionality and sustainability in polymer applications [30].

One of the advantages of polymers is that they can undergo internal rotations around their single bonds, enabling conformational changes within their molecular chains. This intrinsic flexibility provides a vast potential to customise polymer properties and functionalities through targeted modifications of their molecular structures. Among these, thermosets like PDMS and Ecoflex and thermoplastics such as Polyethylene terephthalate (PET) are widely used substrates in flexible electronic devices [31]. Additionally, TPE could offer remarkable versatility for flexible electronics applications, as they can be precisely engineered to achieve the desired level of flexibility, making them suitable for a wide array of applications. However, it is essential to highlight the key differences in the properties of PDMS, Ecoflex, and TPEs that must be considered before selecting them as a polymer matrix for sensor applications.

PDMS is a silicone-based thermoset polymer recognised for its exceptional properties, making it highly valuable in materials science, particularly for technological and medical applications. Its biocompatibility is essential for developing medical devices and implants, ensuring safe interaction with biological systems without adverse immune reactions. PDMS's chemical inertness allows it to maintain stability in harsh environments, including exposure to water, solvents, and a wide pH range. Its optical transparency across a broad wavelength range, from ultraviolet to infrared, supports its use in optical and microfluidic devices. The polymer's thermal stability, up to 200 °C, is essential for applications exposed to fluctuating temperatures [32]. There are also several works where PDMS was used as the polymer matrix to develop electrical conductive composites (Figure 2.4). In the work of Wang *et al*. [33], a 3D conductive network of reduced graphene oxide (rGO) within a PDMS matrix was developed. The sensor showcased high sensitivity, stability, and stretchability, demonstrating the potential for large-scale body motion detection and

temperature monitoring, suggesting applications in healthcare. Shao *et al*. [34] focused on creating highly stretchable and conductive elastomers by embedding MWCNTs in a PDMS matrix to improve electrical conductivity and mechanical properties. The innovative preparation technique allowed the composite to maintain electrical conductivity under deformation, positioning it as a promising material for flexible electronics. Shrestha *et al*. [35] developed a novel ink formulation for creating compliant electrodes on hydrophobic PDMS surfaces, addressing the challenge of ink coating and adhesion. The electrodes were suitable for wearable sensors, soft actuators, and microfluidic devices. Li *et al.* [36] also presented a PDMS-Ag nanosheet composite electrode with low electrical resistance, stable electrical properties under strain, and excellent durability over numerous cycles.

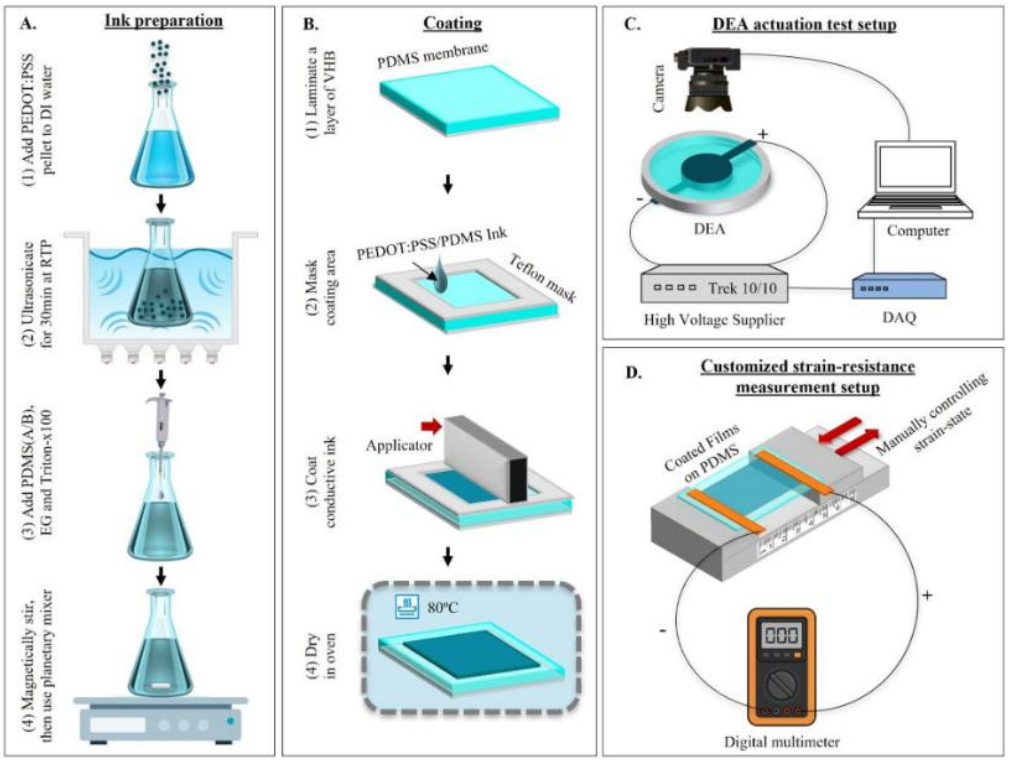

a)

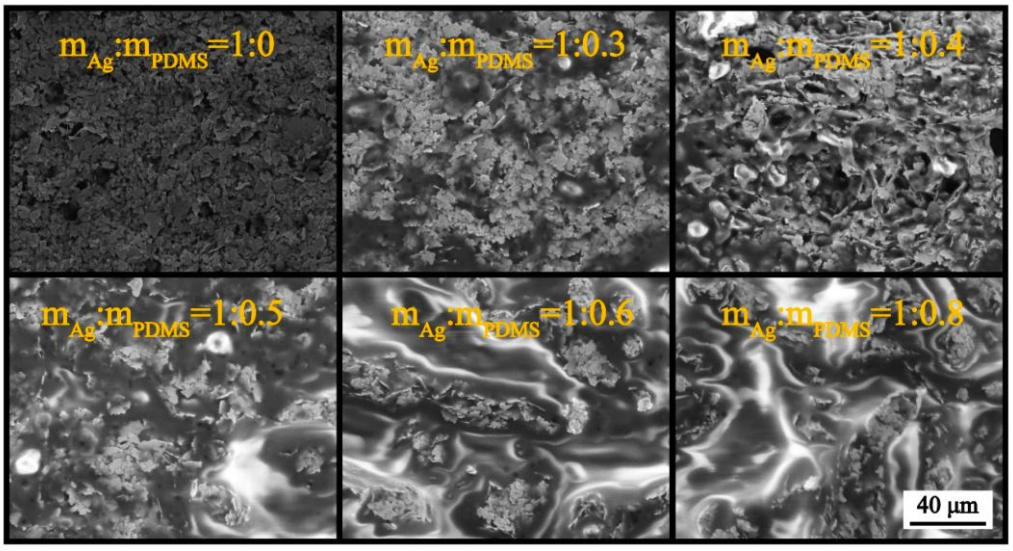

b)

Figure 2.4- a) Development of electrically conductive PDMS, steps on processing it: A. Ink preparation, B Coating, C DEA actuating test and D strain measurement [35]; and b) development of PDMS-Ag conductive composite. Reprinted from [36] under CC BY 4.0 license.

Ecoflex is another flexible thermoset and platinum-catalysed silicone rubber with a lot of potential for wearable electronics, sensors, and medical devices. Its interesting flexibility and tear resistance, with works reporting an elastic modulus of 83.4 kPa and a 535% maximum tensile strain before fracture [37], allows

devices to maintain functionality under mechanical deformation, such as stretching, bending and twisting, which is essential for wearable applications. Moreover, its skin-safe technology makes it suitable for prolonged skin contact, broadening the scope of applications in health monitoring and therapeutic devices [37]. To impart electrical conductivity to Ecoflex, conductive fillers such as CNTs, graphene, silver nanoparticles, or conductive polymers are embedded within the silicone matrix. The choice of filler depends on the desired electrical conductivity level, mechanical properties, and application requirements. The dispersion of conductive fillers within the Ecoflex matrix is an important factor in achieving an optimal balance between conductivity and flexibility [12].

Some examples of Ecoflex-based conductive composites include the work of Devaraj *et al.* [38], which introduced capacitive pressure/force sensing arrays made from carbon black and elastic conductive thin films, highlighting a straightforward fabrication method for integration into soft robotics. The sensors were made entirely from elastomers without rigid components, detecting very light loads and demonstrating high sensitivity and repeatability. This suggests broad applicability in robotics for enhancing tactile capabilities without compromising flexibility. In another work, Kim *et al*. [39] investigated the piezoresistive effects under extreme strain through bi-layer structures of CNTs and Ecoflex composites. Adding conductive and non-conductive fillers improved piezoresistive sensitivity and mechanical stability, showing resilience in bi-layer structures under strains where single-layer composites would fail. Fortunato *et al.* [40] developed low-pressure sensors from ecoflex foam and graphene nanoplatelets (GNPs), targeting applications in smart clothing and soft robotics. These lightweight, cost-effective sensors set a new sensitivity benchmark for detecting minimal pressures, highlighting the promise of elastomeric nanocomposites in flexible electronics. Xu *et al.* [41] presented high-performance dielectric elastomer actuators with a novel layer-by-layer structure of MWCNTs and Ecoflex; this study achieved substantial improvements in the actuated strain at low electric fields. The strategic layering enhanced the dielectric constant while maintaining low loss and modulus, showcasing a significant step forward in dielectric elastomer actuators technology. Additionally, Wen *et al. [*42] developed a seamless multimode sensor capable of decoupling pressure and strain stimuli, highlighting the integration of a structure with resistive and capacitive components for motion

recognition. Combining high sensor accuracy with machine learning algorithms, this sensor's manufacturing process could impact various fields, emphasising the synergy of material science, sensor design, and data analysis in wearable technology advancements (Figure 2.5).

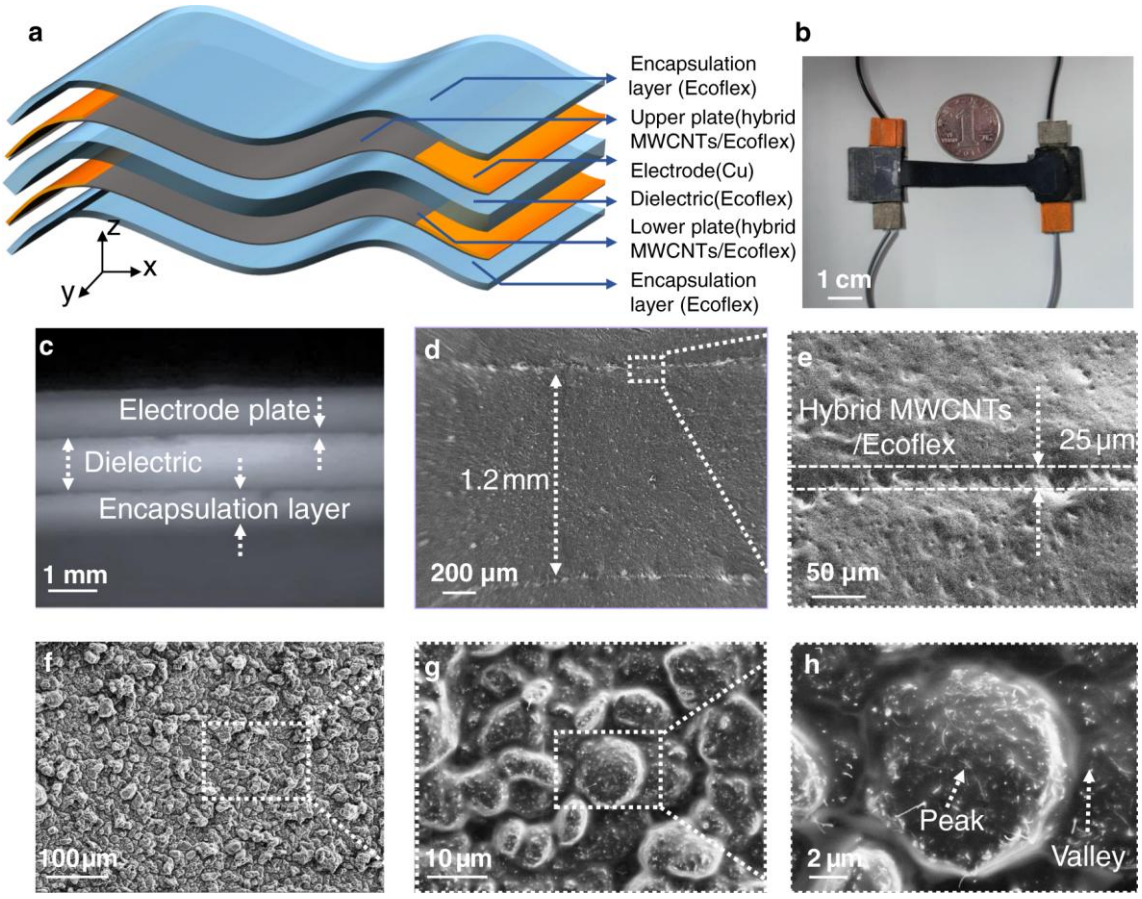

Figure 2.5- a) Exploded view of the SRCSM sensor. b) Photograph of the integrated sensor. c–e) Cross-sectional photograph and SEM images of the developed sensor. f–h) SEM surface topography of the developed sensor. Reprinted from [42] under CC BY 4.0 license.

TPEs can be an interesting material for flexible sensors since they combine the flexibility of elastomers with the processing simplicity of thermoplastics, making them ideal for innovative applications across various industries. Like traditional rubber, TPEs can stretch and recover their original shape, yet they offer the added benefit of being easily moulded and recycled. This combination presents a compelling alternative to conventional silicone-based materials, providing both functional versatility and environmental advantages through recyclability [43]. TPE stand apart from other thermoplastics due to their exceptional elasticity and flexibility, making them ideal for applications requiring durability and resilience. Notably, 3D printed TPE have demonstrated remarkable performance, achieving extraordinary stretchability of up to 5921.3%, a tensile

strength of 5.22 MPa, and a tensile modulus of 1.7 MPa [44]. Furthermore, their compatibility with standard thermoplastic manufacturing methods, such as injection moulding and extrusion, enhances their appeal by enabling efficient and cost-effective production processes [43]. TPEs can be classified into several primary categories; some examples are the following: styrene thermoplastic elastomers, multiblock copolymers, hard polymer-elastomer blends, graft copolymers, ionomers, and core-shell structures (Figure 2.6 a). Their diverse properties result from the detailed and closely integrated polymeric phases, generally featuring at least one elastomeric phase alongside a hard phase. The production methods for TPEs vary with their type; for example, styrene thermoplastic elastomers are produced via anionic polymerisation, while multiblock copolymers are created from condensation reactions of prepolymers [45]. The unique attributes of TPEs, covering a wide spectrum, are shaped by the ratio of hard to soft phases, the selection of polymers for the hard phase, and the qualities of the elastomer phase. Modifying these phase ratios enables the customisation of TPEs' hardness and performance properties, making them adaptable to diverse uses (Figure 2.6 b)). TPEs find applications in numerous sectors, contributing to products as varied as footwear, automotive parts, wire insulation, adhesives, and sealants. Their versatility is further enhanced by compounding with other materials, which allows for modifying TPEs to meet particular needs, such as improved impact resistance or flexibility [45].

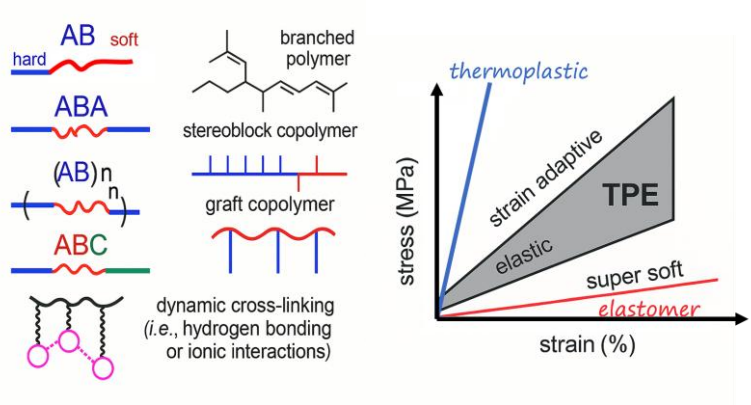

a) b)

Figure 2.6- a) Examples of polyolefin architecture that may serve as TPEs. b) Idealized illustration of stress-strain properties of polymers. Adapted from [43].

TPEs have already been used in flexible electronics; for example, Zhou *et al.* [46] used a TPE to fabricate coaxial fibre conductors, as demonstrated in

Figure 2.7. PEDOT/PSS blended with PBP is the core encased within TPE sheaths. The process involved coaxial wet-spinning followed by a drying phase inducing buckling in the conductive core. The fabrication method yielded fibres with less than 4% resistance change under a 680% strain, showcasing mechanical and electrical stability. This stability is attributed to the hierarchical buckling and the PBP's plasticising effect on PEDOT/PSS, enhancing conductivity and flexibility. Bian *et al*. [47] developed porous conductive composites through solvent etching of polybutylene adipate terephthalate (PBAT) from POE/PBAT/CNT ternary nanocomposites, leaving a lightweight, flexible structure with suspended CNTs. Dichloromethane selectively dissolved PBAT, generating a porous network. The resulting composites significantly improved ductility, elasticity, and electrical conductivity due to the exposed CNT network. Eutionnat-Diffo *et al.* [48] addressed the fabrication of conductive monofilaments for 3D printing via a two-step melt process and one-step extrusion of LDPE/PBE blends with CNT and carbon black fillers, aiming to achieve flexible, highly conductive polymer blends. The co-continuity of the thermoplastic and elastomer phases was essential for maintaining material flexibility. The selective localisation of fillers (carbon black in LDPE and CNTs at the LDPE/PBE interface) improved the electrical conductivity and mechanical properties. Cetin *et al.* [49] explored solvent casting and compression moulding to incorporate carbon black (CB) and vapor-grown carbon nanofibres (VGCNFs) into a styrene ethylene butylene styrene (SEBS) matrix, aiming to develop flexible nanocomposites for piezoresistive strain sensors. They highlighted the importance of filler type and concentration in achieving optimal electrical and mechanical performance. Hybrid filler systems (CB+VGCNFs) exhibited superior sensitivity, attributed to synergistic effects enhancing conductive pathways. Amirkhosravi *et al.* [50] also introduced a scalable dusting technique to fabricate conductive elastomer composites by coating thermoplastic polyurethane (TPU) granules with CNTs and moulding them into films. This process created composites with segregated conductive networks at ultra-low filler contents. They enhanced electrical conductivity and mechanical flexibility, particularly with larger TPU granules, by maintaining low filler content and exploiting the segregated network structure.

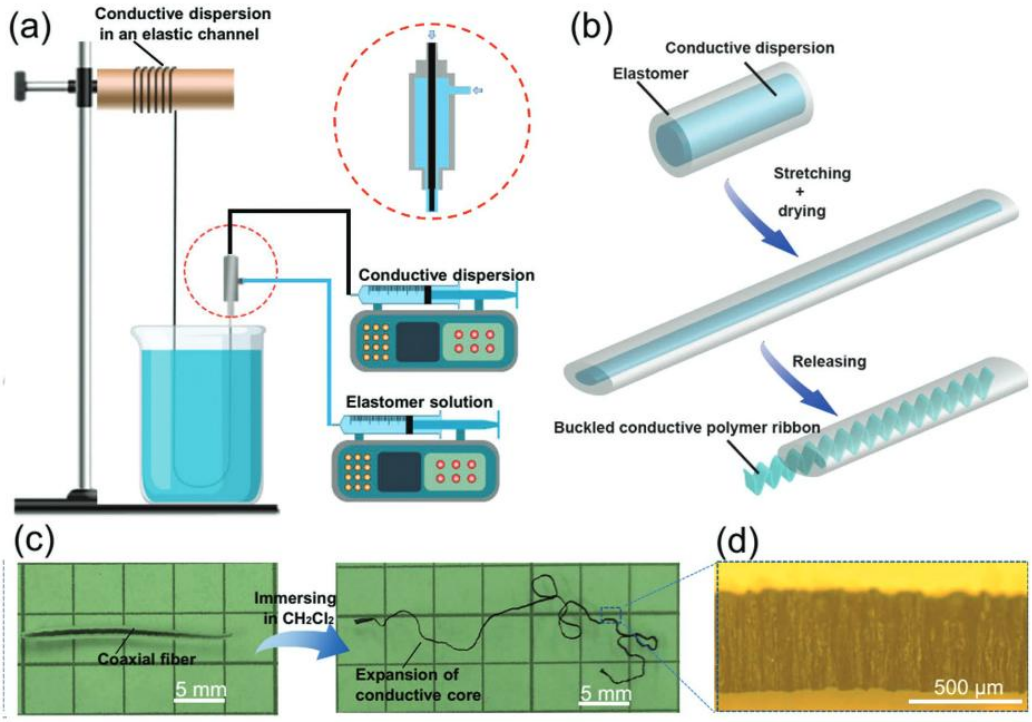

Figure 2.7- Self-buckled conductive ribbon in a thermoplastic elastomer (TPE) channel. a) Schematic illustration showing the coaxial wet-spinning process for encapsulating the conductive dispersion in an elastic TPE channel. b) Schematic presenting how pre strain then buckling strategy was applied to obtain a folded conductive polymer ribbon in a TPE channel. c) A 2 cm coaxial fibre expanded into a 5 cm after immersing it in DCM for 5 min due to the removal of TPE sheath and relaxation of the conductive core. d) Optical image of the conductive core after immersing in DCM, showing buckled structure on the surface. Reprinted with permission from [46].

The previously described works highlight that a thorough understanding of polymer types is essential for selecting and modifying polymers to meet specific mechanical and chemical requirements. Additionally, incorporating conductive fillers into these polymer matrices is a strategic approach to enhance the electrical conductivity of composites, which is vital for sensor functionality. Key factors such as the fillers' shape, size, concentration, and interaction between the filler and polymer significantly impact the composite's overall conductivity. Therefore, a deeper understanding of these variables is essential for designing advanced materials tailored to the electrical needs of flexible electronics, smart textiles, and soft robotics.

2.3. Mechanisms of electrical conductivity in CPCs

The electrical conductivity of materials is an essential factor in determining their functionality and suitability for various applications. As shown in Figure 2.8,

materials can range from highly conductive to insulating, each serving distinct purposes. For instance, highly conductive materials are ideal for metal replacements and conductive adhesives, while conductive composites are suitable for sensors and electromagnetic interference (EMI) shielding. On the other hand, materials with electrostatic dissipative properties are vital in environments where static electricity poses a risk, such as in fuel tanks or electronic device housings. These materials safely dissipate charge, preventing static build-up, which can lead to dangerous sparks or damage to sensitive electronic components [51]. In other scenarios, highly insulating composites are important for ensuring safety and reliability, particularly in high-voltage applications, where preventing electrical leaks and protecting users from electric shocks is essential [52].

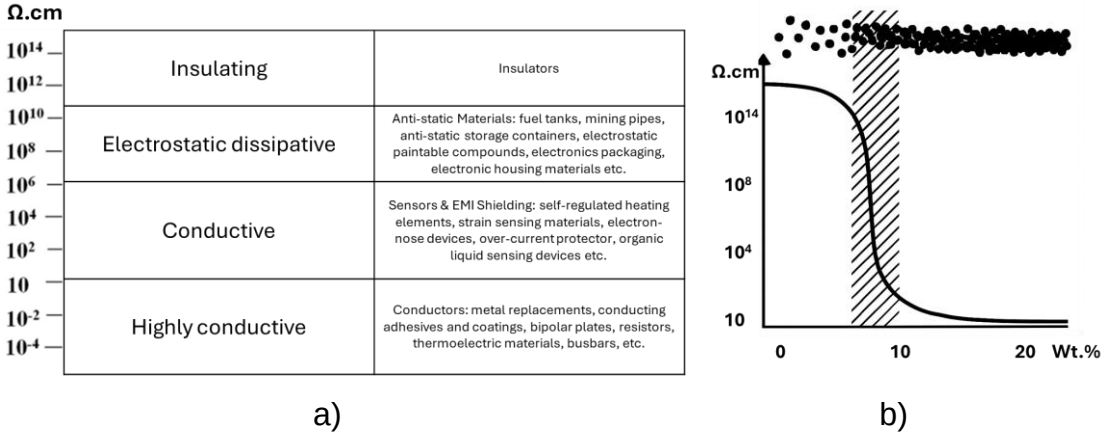

Figure 2.8- a) Electrical resistivity according to the application, adapted from [52], b) illustrative example of the electrical percolation network, adapted from [53].

One of the main functionalities of CPCs is their enhanced electrical conductivity, achieved by integrating conductive fillers such as CNTs, graphene, and metal nanoparticles into polymer matrices. This integration facilitates electron mobility within materials that are inherently insulating. The core mechanism driving electrical conductivity in CPCs involves establishing a percolative network of conductive fillers within the polymer matrix. This network is essential for electron movement across the composite, enabling electrical conduction. The effectiveness of this network, and thus the composite's conductivity, relies on surpassing a critical filler concentration, termed the percolation threshold. Below this threshold, the material remains insulating.

However, crossing it results in a substantial increase in conductivity due to the formation of a continuous pathway for electrons [54].

The percolation threshold is influenced by factors including filler type, size, shape, and distribution within the polymer. Fillers with a high aspect ratio, such as CNTs, are particularly effective in reducing the percolation threshold, thanks to their structure facilitating network formation at reduced concentrations. Equally important is the dispersion of these fillers, which should ideally be uniform to optimise network efficiency. Yet, challenges like filler agglomeration and weak polymer-filler adhesion can hinder dispersion, necessitating strategies such as compatibilisers or surface treatments to ensure a homogeneous filler distribution [54]. In addition to percolative conduction, tunnelling conduction enhances CPCs' electrical properties. This mechanism allows electrons to move between closely positioned fillers, providing an alternate conduction route, especially at filler concentrations around or below the percolation threshold [54]. To predict the behaviour of electrical conductivity in CPCs, as a function of the filler concentration, the power law, which is a mathematical model derived from percolation theory, can be used. The model states that the conductivity increases dramatically as the filler concentration approaches the percolation threshold, emphasising the non-linear nature of this relationship. This model aids in quantifying the critical concentration at which an infinite conductive cluster appears, thereby providing a theoretical framework for optimising the composite's electrical and mechanical performance by manipulating filler content and distribution [54].

The power law can be mathematically expressed as [55]:

$$\sigma \propto (\Phi - \Phi c)^t$$

Where σ is the electrical conductivity, Φ is the volume fraction, Φc is the critical concentration at which an infinite cluster appears in the composite, and t is the critical exponent that depends only on the dimensions of the system [55]. The critical exponent value is an important factor that indicates the lattice dimensionality of the filler. A t value close to 1.5 means that the electrical conductivity is due to the contact between agglomerates whose shape is close to spherical. A higher value of t (close to 3) indicates that the conductivity is imparted by the contact between individual fibres [54]. The percolation threshold Φc also

depends on the type of additives. For the case of MWCNT the following equation represents *Φc*:

$$\Phi c = \frac{D^2}{2L\delta Max}$$

where *D* is the MWCNT outer diameter, *L* is their length and *δMax* is related with the maximum interaction range between two adjacent MWCNT [55].

CNTs are large cylindrical molecules with a hexagonal carbon atom arrangement. The CNTs morphology can be equivalent to rolling up a single sheet of graphene (single walled carbon nanotubes, SWCNTs) or rolling up multiple sheets of graphene (multi walled carbon nanotubes, MWCNTs) [56,57]. Their properties consist of high surface area, stiffness, tensile strength, thermal and electrical conductivities, with Young's modulus reaching approximately 1 TPa, tensile strength ranging from 13 to 53 GPa, thermal conductivity between 400-700 $W.m^{-1}.K^{-1}$ for single-walled carbon nanotubes (SWCNTs) and 300-3000 $W.m^{-1}.K^{-1}$ for MWCNTs, and electrical current densities up to 10^9 $A.cm^{-2}$ [56]. And they can be fabricated using different techniques, such as, arc discharge, chemical vapor deposition (CVD), and laser ablation [57,58]. Due to their excellent properties, the transportation industry (automobile, aeronautics, maritime), energy industry (lithium-ion batteries, flow batteries and super-capacitors), electronics industry (electronic packaging, EMI shielding) and sports goods are using them. However, the growth of the CNTs market can be affected by factors such as production cost, processing difficulties, and the availability of substitutes [59]. For the electronics industry, the price could be decreased by reducing the electrical percolation threshold of the developed structures, through the arrangement of the CNTs in the polymer matrix [60].

2.4. Low electrical percolation threshold composites

There are multiple strategies for lowering the electrical percolation threshold in conductive polymer composites, enhancing their conductivity with minimal filler content. High aspect ratio fillers are one of the most effective approaches due to their extended structures, which facilitate the formation of conductive networks across the polymer matrix at lower concentrations [61]. Beyond this, other

techniques can decrease the percolation threshold and improve the material's performance, such as segregated networks, filler alignment, and hybrid filler systems.

The concept of segregated networks consists of designing composites where conductive fillers form an arranged network within the matrix, significantly reducing the percolation threshold. This strategy involves creating a continuous path for electron flow that requires less filler material by exploiting the phase separation between the polymer and the filler. Some examples of using segregated networks to reduce the electrical percolation threshold can be found in the review of Pang *et al.* [52]. This work demonstrates that contrary to traditional CPCs, which often necessitate high filler loadings to achieve desired conductive properties, segregated conductive polymer composites (s-CPCs) are distinguished by their conductive fillers primarily localised at the interfaces between polymeric granules (Figure 2.9). This strategic arrangement results in s-CPCs exhibiting ultralow percolation thresholds significantly enhanced electrical conductivity, and improved mechanical properties at lower filler loadings. Such materials can be highly promising for applications necessitating high-performance anti-static capabilities, EMI shielding, and sensitive sensing mechanisms. The review further explains the factors influencing the performance of s-CPCs, including the impact of conductive fillers, host polymers, and the various fabrication methods employed. Some important parameters are the type, aspect ratio, and dispersion methods of conductive fillers. Another aspect is the polymer matrix's molecular weight and chemical interaction with these fillers. Finally, the specific fabrication techniques and processing parameters, with influencing factors such as temperature and pressure, are all pinpointed as key determinants in optimising s-CPC structures and their resultant properties. Despite the clear advantages and promising applications of s-CPCs, challenges remain, particularly concerning the distribution of fillers, optimisation of the filler-polymer interface, and scalability of production methods.

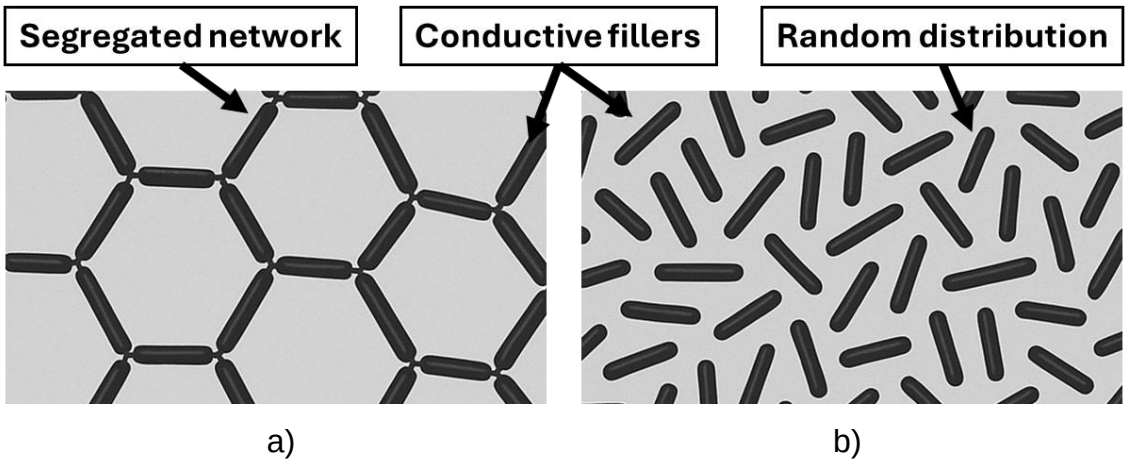

Figure 2.9- Schematic illustration of a) the segregated and b) random distribution conductive network in CPC. Adapted from [52].

A more concrete example investigated the main differences between randomly distributed conductive polymer composites using chlorinated polyethylene (CPE) and MWCNTs, achieved through solution mixing, and a 3D segregated structure created via direct hot-pressing. The researchers found that the 3D segregated structure facilitates easier construction of conductive paths and results in a significantly lower percolation threshold than the randomly distributed structure. Specifically, the percolation threshold for the randomly distributed structure was 4.81 wt.%, while it was only 1.09 wt.% for the 3D segregated structure. This suggests a more efficient conductivity in the 3D segregated structure with less filler content required. Regarding flame retardance, adding MWCNTs enhanced this property in both composites, with the randomly distributed structure achieving slightly higher limiting oxygen indices than the 3D segregated structure. Mechanical testing indicated that while both structures benefited from adding MWCNTs, the randomly distributed structure exhibited more significant improvements in mechanical properties such as tensile strength and modulus. Rheological evaluations supported these findings, showing stronger interactions between MWCNTs and the CPE matrix in the randomly distributed structure, which correlates with better mechanical performance. Therefore, the work provided insights that are important for the manufacturing and application of CPCs, suggesting that the choice between a randomly distributed structure and a 3D segregated structure should be based on the specific application requirements, such as the case of electrical conductivity, mechanical strength, and flame retardancy [62].

In the last years, the alignment of CNTs in a polymer matrix has been investigated using different processing methods: shear flow extrusion, mechanical shear stretching, melt spinning, electro-spinning, magnetic field, liquid crystalline phase, and ex-situ alignment of CNTs [63]. The alignment of the CNTs requires a driving torque to change their orientation. The driving torque can be generated by applying external force fields or induced by constraints of the surrounding medium, such as using polymer beads that force the contact between CNTs [64]. In their work, Goh *et al.* [65] describe the mechanisms of alignment and orientation of carbon nanotubes in polymeric matrixes. Of all the described techniques, three techniques could be suitable for implementation in the melt spinning process: mechanical alignment, electrical alignment, and magnetic alignment or positioning. The mechanical alignment can be induced by shear force. Since CNTs have a high aspect ratio, the shear force during the extrusion process can cause the parallel alignment of the CNTs. This alignment mechanism was studied by Pötschke *et al.* [66]. They conclude that for composite fibres made of 2 wt.% MWCNT/PC, the high draw ratios induced the parallel alignment of the MWCNT. However, the electrical properties decreased compared with non aligned fibres due to the lower number of contacts between particles. The electrical and magnetic field alignment can also rearrange CNTs inside the polymeric matrix. Electric fields have proven effective in aligning CNTs in both alternated current (AC) [67–72] and direct current (DC) [73,74]. The orientation efficiency of electric field alignment depends on the material viscosity, voltage, and frequency. Typically, higher efficiency can be achieved using a low viscosity material and applying high electrical voltage and frequency. One disadvantage of using a DC electric field for aligning CNTs is that when in suspension, CNTs tend to migrate and accumulate at the electrodes, causing their non-uniform distribution. Therefore, an AC electric field is typically used because it provides better CNTs distribution and requires lower voltage than a DC electric field. The CNT response to an applied electric field can be characterised by alignment and migration [75]. Alignment describes the orienting of a CNT with its long axis parallel to the electric field direction, which happens due to the highly anisotropic electric polarizability of CNTs. The electric field then induces a torque that forces the CNT to align parallel to the electric field direction. On the other hand, with migration, the particles tend to accumulate in a particular

location, usually near the electrodes [76]. The effect of the electric forces on MWCNT was explored by Gupta *et al.* [77], who produced PVDF/MWCNT samples under AC and DC electrical fields and compared the sample's electrical conductivities. From their conclusions represented in Figure 2.10, it was possible to understand that when they applied an AC electric field to the sample, the particles aligned parallel to the direction of the electric field. The CNTs arranged themselves evenly on the polymeric matrix and parallelled with each other. However, the increase in conductivity was smaller than in the samples where DC current was used. For these samples, the CNTs accumulated in specific parts of the polymeric matrix and created conductive paths between electrodes, which increased the electrical conductivity four times compared with the random alignment samples. It was also interesting to notice that the polymeric sample was damaged with increased current, decreasing the electrical conductivity compared to a lower electrical current. From this study, it was possible to understand that the accumulation of CNTs in specific parts of the sample, creating thick conductive paths, increases the electrical conductivity since there is a higher surface area of CNTs interacting with each other.

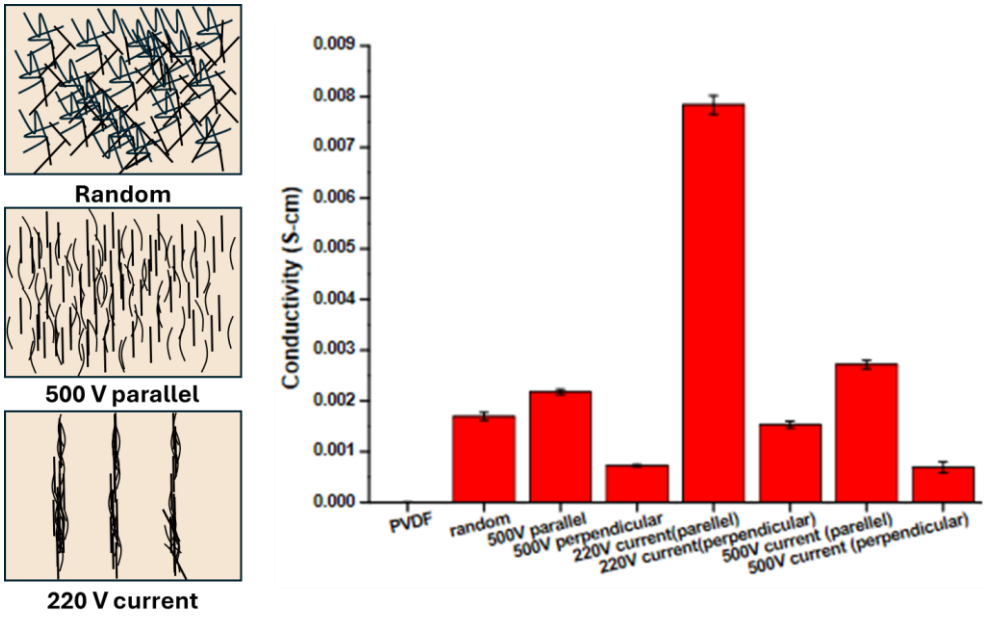

Figure 2.10- Effects of electric field alignment and electric current alignment on the electrical conductivity of PVDF/MWCNT composites. Adapted from [77].

Another electromagnetic force that can arrange MWCNT in polymeric matrixes is the magnetic field. It can be applied as AC magnetic fields or static magnetic fields. Similarly to the electric field, the AC magnetic field induces

parallel alignment in the MWCNT, and the static magnetic field attracts the particles to the regions with stronger magnetic flux density [65]. There are several theories for the magnetic field effect on CNTs. One of them is that the movement of the electrons circling the circumference of the nanotubes results in a large orbital magnetic moment, explaining the anisotropic susceptibility of CNTs. This anisotropic susceptibility is responsible for the magnetic field–induced torque acting on the CNTs in a magnetic field [77]. Other theories are related to vacancies in the CNT structure that induce ferromagnetic behaviour [78]. Another possible cause is the CNTs production route, due to the catalyst materials (such as ferromagnetic Fe, FeCo and diamagnetic Re) used in CVD methods that are usually attached to the nanotubes, they can influence the magnetic response of the samples [79]. Like the electric field, strong magnetic fields can effectively position and align MWCNT inside polymeric matrixes [80,81]. However, the strong magnetic field can cause coil overheating problems, damaging the electromagnets [82]. An active cooling system for the coils is needed to generate large magnetic fields. Functionalising CNTs with magnetic particles enhances their magnetic responsiveness, facilitating their alignment and enabling the use of lower magnetic fields. This was demonstrated in the work of Ariu *et al.* [83]. The study shows that an external magnetic field has great potential for positioning and aligning CNTs. The produced epoxy/MWCNT blends were exposed to a magnetic DC field with a flux density of 0.5 T until gel time. Several metal plating methodologies, including nickel, cobalt, and nickel-iron plating, were investigated to increase the magnetic sensitivity of the nanotubes. The magnetic characterisation indicated cobalt-plated nanotubes as the most suitable candidate for magnetic alignment due to their high magnetic sensitivity. Another possible approach is to directly mix the MWCNT with particles with magnetic properties, which will be further explored in this thesis.

Combining different conductive fillers is another approach to achieving low percolation thresholds. Distinct sizes, shapes, or aspect ratios can lead to a synergistic effect where the percolation threshold is lower than that achievable with any individual filler type. This approach benefits from the complementary properties of the fillers, such as combining high aspect ratio fillers with smaller conductive particles that can fill the spaces between larger fillers, thus enhancing the overall connectivity of the conductive network. Tang *et al*. [84] created a novel

analytical model based on excluded-volume theory to demonstrate this. As demonstrated in Figure 2.11, this model explores the impact of the dimensions of the CNTs and graphene and their interactions, allowing the authors to predict the synergistic percolation threshold in CPCs containing both CNTs and graphene. The model suggested that the fillers' aspect and content ratios must be considered for stronger percolation synergism. The predictions made by this model were validated against experimental data, showing good agreement. Additionally, parametric studies illustrated the optimisation of the total percolation threshold, revealing that higher filler aspect ratios and proper content ratios were beneficial. The study concludes that the developed model could effectively predict the nonlinear synergistic percolation effect in CPCs with CNTs and graphene. In another study, reported by Motaghi *et al.* [85], the enhancement of electrical properties in polystyrene composites by adding carbon fibres (CF) and CB was explored. The experimental results revealed that hybrid composites with CF and CB achieved higher conductivity and lower percolation thresholds than those with CF alone, except at the highest CF/CB ratio due to increased fibre breakage. The research concluded that the strategic combination of CF and CB fillers can significantly improve the electrical performance of polymer composites, offering a potential alternative to metals in applications requiring lightweight, corrosion-resistant materials with good electrical conductivity.

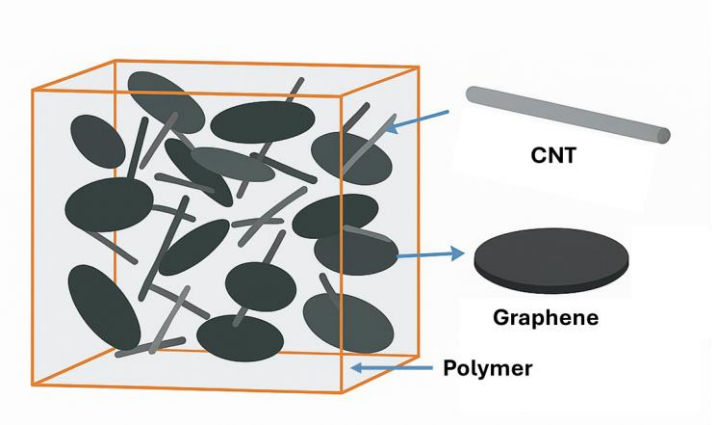

Figure 2.11- Schematic showing of hybrid 3D random CPCs containing 1D CNTs and 2D graphene nanosheets. Adapter from [84].

2.5. References

[1] Costa, J. C., Spina, F., Lugoda, P., Garcia-Garcia, L., Roggen, D., & Münzenrieder, N. (2019). Flexible sensors—from materials to applications. Technologies, 7(2), 35.

[2] Liu, C., Huang, N., Xu, F., Tong, J., Chen, Z., Gui, X., & Lao, C. (2018). 3D printing technologies for flexible tactile sensors toward wearable electronics and electronic skin. Polymers, 10(6), 629.

[3] Han, S. T., Zhou, Y., Zhang, Z., Zhu, D., Wang, H., Xu, J., & Roy, V. A. L. (2017). An overview of the development of flexible sensors. Advanced Materials, 29(33), 1700375.

[4] Yin, Y., Guo, C., Li, H., Yang, H., Xiong, F., & Chen, D. (2022). The progress of research into flexible sensors in the field of smart wearables. Sensors, 22(14), 5089.

[5] McGrath, M. J., & Scanaill, C. N. (2013). Sensing and sensor fundamentals. In Sensor Technologies: Healthcare, Wellness, and Environmental Applications (pp. 15–50). Springer.

[6] Liang, A., Stewart, R., & Bryan-Kinns, N. (2019). Analysis of sensitivity, linearity, hysteresis, responsiveness, and fatigue of textile knit stretch sensors. Sensors, 19(16), 3618.

[7] Luo, Y., Huang, X., Tang, Y., Gao, L., Xu, Q., Zhang, J., ... & Wang, X. (2023). Technology roadmap for flexible sensors. ACS Nano, 17(6), 5211–5295.

[8] Dos Santos, A., Fortunato, E., Martins, R., Águas, H., & Igreja, R. (2020). Transduction mechanisms, micro-structuring techniques, and applications of electronic skin pressure sensors: A review of recent advances. Sensors, 20(16), 4407.

[9] Elnemr, Y. E., Abu-libdeh, A., Carlo, G., & Raj, A. (2023). Multi-transduction-mechanism technology: An emerging approach to enhance sensor performance. Sensors, 23(9), 4457.

[10] Wang, M., Li, Y., Liu, Y., Wang, J., Dong, L., Sun, L., ... & Wang, Z. (2017). Enhanced electrical conductivity and piezoresistive sensing in multi-wall carbon nanotubes/polydimethylsiloxane nanocomposites via the construction of a self-segregated structure. Nanoscale, 9(31), 11017–11026.

[11] Shao, Q., Niu, Z., Hirtz, T., Lü, L., Chen, X., & Dong, L. (2014). High-performance and tailorable pressure sensor based on ultrathin conductive polymer film. Small, 10(8), 1466–1472.

[12] Mai, H., Mutlu, R., Tawk, C., Alici, G., & Sencadas, V. (2019). Ultra-stretchable MWCNT-Ecoflex piezoresistive sensors for human motion detection applications. Composite Science and Technology, 173, 118–124.

[13] Feng, R., Liu, L., Dong, Z., Zhang, P., Xie, Y., Zhang, Y., & Cui, Y. (2021). A flexible integrated bending strain and pressure sensor system for motion monitoring. Sensors, 21(12), 3969.

[14] Elnemr, Y. E., Abu-libdeh, A., Carlo, G., & Raj, A. (2023). Approach to enhance sensor performance. Manuscript in preparation.

[15] Luo, Y., Huang, X., Tang, Y., Gao, L., Xu, Q., Zhang, J., ... & Wang, X. (2023). Technology roadmap for flexible sensors. ACS Nano, 17(6), 5211–5295.

[16] Huang, P., Liu, X., Wang, W., & Zhang, T. (2021). Textile-based triboelectric nanogenerators for wearable self-powered microsystems. Micromachines, 12(2), 158.

[17] Fan, F.-R., Tian, Z.-Q., & Wang, Z. L. (2012). Flexible triboelectric generator. Nano Energy, 1(2), 328–334.

[18] Wang, X., Dong, L., Zhang, H., Yu, R., Pan, C., & Wang, Z. L. (2016). Self-powered high-resolution and pressure-sensitive triboelectric sensor matrix for real-time tactile mapping. Advanced Materials, 28(15), 2896–2903.

[19] Ou-Yang, W., Zhang, H., Zhao, Y., Zhang, D., Zhao, Z., & Wang, Z. L. (2024). Recent advances in triboelectric nanogenerator-based self-powered sensors for monitoring human body signals. Nano Energy, 120, 109151.

[20] Wang, Y., Yang, Y., & Wang, Z. L. (2017). Triboelectric nanogenerators as flexible power sources. npj Flexible Electronics, 1(1), 10.

[21] Zheng, Q., Zou, Y., Zhang, Y., Liu, Z., Shi, B., Wang, X., ... & Wang, Z. L. (2016). In vivo self-powered wireless cardiac monitoring via implantable triboelectric nanogenerator. ACS Nano, 10(7), 6510–6518.

[22] Ouyang, H., Tian, J., Sun, G., Zou, Y., Liu, Z., Li, H., ... & Wang, Z. L. (2017). Self-powered pulse sensor for antidiastole of cardiovascular disease. Advanced Materials, 29(40), 1703456.

[23] Lin, Z., Chen, J., Li, X., Zhou, Z., Meng, K., Wei, W., & Wang, Z. L. (2019). A triboelectric nanogenerator-based smart insole for multifunctional gait monitoring. Advanced Materials Technologies, 4(2), 1800360.

[24] Huang, Y.-J., & Chung, C.-K. (2023). Design and fabrication of polymer triboelectric nanogenerators for self-powered insole applications. Polymers, 15(20), 4035.

[25] Zheng, C., Yang, W., Zhang, L., Liu, F., Zhang, X., Yang, H., & Chen, C. (2023). A triboelectric sensor with highly sensitive and durable: Dual regulation strategy based on surface morphology and functional groups on negative/positive tribolayers. Chemical Engineering Journal, 477, 147071.

[26] Ding, Z., Zou, M., Yao, P., & Fan, L. (2022). A triboelectric nanogenerator for mechanical energy harvesting and as self-powered pressure sensor. Microelectronic Engineering, 257, 111725.

[27] Nuthalapati, S., Singh, S., Ghosh, S., Das, S., Banerjee, R., & Goswami, P. (2024). Wearable high-performance MWCNTs/PDMS nanocomposite-based triboelectric nanogenerators for haptic applications. IEEE Journal of Flexible Electronics.

[28] Qu, J., Ren, Y., He, T., Zhai, X., Wu, C., Cheng, X., & Sun, L. (2023). All-in-one strain-triboelectric sensors based on environment-friendly ionic hydrogel for wearable sensing and underwater soft robotic grasping. Nano Energy, 111, 108387.

[29] Pascault, J.-P., & Williams, R. J. J. (2012). Overview of thermosets: structure, properties and processing for advanced applications. In Thermosets (pp. 3–27). Elsevier.

[30] Bîrca, A., Gherasim, O., Grumezescu, V., & Grumezescu, A. M. (2019). Introduction in thermoplastic and thermosetting polymers. In Materials for Biomedical Engineering: Thermoset and Thermoplastic Polymers (pp. 1–28). Elsevier.

[31] Gong, M., Zhang, L., & Wan, P. (2020). Polymer nanocomposite meshes for flexible electronic devices. Progress in Polymer Science, 107, 101279.

[32] Tan, X., & Rodrigue, D. (2019). A review on porous polymeric membrane preparation. Part II: Production techniques with polyethylene, polydimethylsiloxane, polypropylene, polyimide, and polytetrafluoroethylene. Polymers, 11, 1310.

[33] Wang, X., Zheng, Z., Li, Z., Li, C., Liu, Y., & Wang, J. (2022). PDMS-based conductive elastomeric composite with 3D reduced graphene oxide conductive network for flexible strain sensor. Composites Part A: Applied Science and Manufacturing, 161, 107113.

[34] Shao, J., Yu, L., Skov, A. L., & Daugaard, A. E. (2020). Highly stretchable conductive MWCNT-PDMS composite with self-enhanced conductivity. Journal of Materials Chemistry C, 8(38), 13389–13395.

[35] Shrestha, M., Depari, L., Shakerzadeh, M., Shivakumar, R., & Teo, E. H. T. (2023). Ink-based transparent compliant electrode for direct coating on untreated hydrophobic PDMS surface. Sensors and Actuators Reports, 5, 100162.

[36] Li, C., Huang, K., Yuan, T., Cong, T., Fan, Z., & Pan, L. (2022). Fabrication and conductive mechanism analysis of stretchable electrodes based on PDMS-Ag nanosheet composite with low resistance, stability, and durability. Nanomaterials, 12(15), 2526.

[37] Herren, B., Saha, M. C., Altan, M. C., & Liu, Y. (2020). Development of ultrastretchable and skin-attachable nanocomposites for human motion monitoring via embedded 3D printing. Composites Part B: Engineering, 200, 108224.

[38] Devaraj, H., Ponnusamy, V., Ragupathy, S., Balasubramani, P., & Balamurugan, K. (2019). Highly elastic and flexible multi-layered carbon

black/elastomer composite-based capacitive sensor arrays for soft robotics. Measurement and Sensors, 2–4, 100004.

[39] Kim, W. J., Nam, K. W., Kang, B. H., & Park, S. H. (2023). Piezoresistive effect of conductive and non-conductive fillers in bi-layer hybrid CNT composites under extreme strain. Materials, 16(18), 6335.

[40] Fortunato, M., Bellagamba, I., Tamburrano, A., & Sarto, M. S. (2020). Flexible Ecoflex®/graphene nanoplatelet foams for highly sensitive low-pressure sensors. Sensors, 20(16), 4406.

[41] Xu, Z., Luo, Y., Liu, Y., Zhang, C., Hu, Z., Zhang, L., & Sun, Z. (2019). High actuated performance MWCNT/Ecoflex dielectric elastomer actuators based on layer-by-layer structure. Composites Part A: Applied Science and Manufacturing, 125, 105527.

[42] Wen, L., Liu, Y., Zhang, Q., Zhao, S., Xu, Y., Liang, T., ... & Zhang, C. (2022). Wearable multimode sensor with a seamless integrated structure for recognition of different joint motion states with the assistance of a deep learning algorithm. Microsystems & Nanoengineering, 8(1), 358.

[43] Zanchin, G., & Leone, G. (2021). Polyolefin thermoplastic elastomers from polymerization catalysis: Advantages, pitfalls, and future challenges. Progress in Polymer Science, 113, 101342.

[44] Bayati, A., Akbari, R., Hossaini, M., & Ashrafee, S. (2024). 3D printed elastomers with superior stretchability and mechanical integrity by parametric optimization of extrusion process using Taguchi method. Materials Research Express.

[45] Holden, G. (2017). Thermoplastic elastomers. In Science and Technology of Rubber (pp. 455–491). Elsevier.

[46] Zhou, J., Tian, G., Jin, G., Xin, Y., Tao, R., & Lubineau, G. (2020). Buckled conductive polymer ribbons in elastomer channels as stretchable fiber conductor. Advanced Functional Materials, 30(5), 907316.

[47] Bian, Y., & Li, Y. (2022). Porous conductive elastomeric composites with carbon nanotubes suspended in the narrow pores from co-continuous polymer blend nanocomposites. Composites Science and Technology, 218, 109116.

[48] Eutionnat-Diffo, P. A., Cayla, A., Chen, Y., Guan, J., Nierstrasz, V., & Campagne, C. (2020). Development of flexible and conductive immiscible thermoplastic/elastomer monofilament for smart textiles applications using 3D printing. Polymers, 12(10), 2300.

[49] Cetin, M. S., & Karahan Toprakci, H. A. (2021). Flexible electronics from hybrid nanocomposites and their application as piezoresistive strain sensors. Composites Part B: Engineering, 224, 109199.

[50] Amirkhosravi, M., Yue, L., & Manas-Zloczower, I. (2020). Dusting thermoplastic polyurethane granules with carbon nanotubes toward highly

stretchable conductive elastomer composites. ACS Applied Polymer Materials, 2(9), 4037–4044.

[51] Vieira, L. S., Ferreira, D. S., Lima, A. G. B., Borges, J. M. N., & do Nascimento, R. F. (2022). A review concerning the main factors that interfere in the electrical percolation threshold content of polymeric antistatic packaging with carbon fillers as antistatic agent. Nano Select, 3(2), 248–260.

[52] Pang, H., Xu, L., Yan, D. X., & Li, Z. M. (2014). Conductive polymer composites with segregated structures. Progress in Polymer Science, 39(11), 1908–1933.

[53] Kupke, M., Wentzel, H.-P., & Schulte, K. (1998). Electrically conductive glass fibre reinforced epoxy resin. Materials Research Innovations, 2(3), 164–169.

[54] Katheria, A., Nayak, J., & Das, N. C. (2022). A journey of thermoplastic elastomer nanocomposites for electromagnetic shielding applications: From bench to transitional research. Materials Advances, 3(6), 2670–2691.

[55] Costa, P., Silva, J., Sencadas, V., Simoes, R., Viana, J. C., & Lanceros-Méndez, S. (2013). Mechanical, electrical and electro-mechanical properties of thermoplastic elastomer styrene-butadiene-styrene/multiwall carbon nanotubes composites. Journal of Materials Science, 48(3), 1172–1179.

[56] Maniecki, T., Rydz, D., Marciniak, M., & Kubiak, P. (2018). Carbon nanotubes: Properties, synthesis, and application. Fibre Chemistry, 50(4), 297–300.

[57] Roslan, M. S., Kassim, M. M., Adi, A. S., & Hamzah, H. H. (2019). Growth of wall-controlled MWCNTs by magnetic field-assisted arc discharge plasma. Journal of Saudi Chemical Society, 23(2), 171–181.

[58] Saifuddin, N., Raziah, A. Z., & Junizah, A. R. (2013). Carbon nanotubes: A review on structure and their interaction with proteins. Journal of Chemistry, 2013, 1–18.

[59] Carbon Nanotubes (CNT) Market by Type, End-use Industry. (2021). Retrieved from https://www.globenewswire.com/en/news-release/2021/05/31/2238713/28124/en/Carbon-Nanotubes-CNT-Market-by-Type-End-use-Industry-Method-and-Region-Global-Forecast-to-2026.html

[60] Dong, S., Wu, X., Wang, E., & Wang, X. (2020). Reduced percolation threshold of multi-walled carbon nanotubes/polymer composites by filling aligned ferromagnetic particles. Journal of Intelligent Material Systems and Structures, 31(2), 187–197.

[61] Haghgoo, M., Ansari, R., Hassanzadeh-Aghdam, M. K., & Nankali, M. (2019). Analytical formulation for electrical conductivity and percolation threshold of epoxy multiscale nanocomposites reinforced with chopped carbon fibers and wavy carbon nanotubes considering tunneling resistivity. Composites Part A: Applied Science and Manufacturing, 126, 105616.

[62] Mao, Z., Zhou, Z., Zhang, J., & Wang, T. (2022). Comparison between randomly distributed structure and 3D segregated structure in chlorinated polyethylene/MWCNT composites: Electrical conductivity, mechanical property, flame resistance and rheological property. Composites Science and Technology, 221, 109338.

[63] Xie, X.-L., Mai, Y.-W., & Zhou, X.-P. (2005). Dispersion and alignment of carbon nanotubes in polymer matrix: A review. Materials Science and Engineering R: Reports, 49(4), 89–112.

[64] Shrivastava, N. K., & Khatua, B. B. (2011). Development of electrical conductivity with minimum possible percolation threshold in multi-wall carbon nanotube/polystyrene composites. Carbon, 49(13), 4571–4579.

[65] Goh, G. L., Agarwala, S., & Yeong, W. Y. (2019). Directed and on-demand alignment of carbon nanotube: A review toward 3D printing of electronics. Advanced Materials Interfaces, 6(4), 1–18.

[66] Pötschke, P., Brünig, H., Janke, A., Fischer, D., & Jehnichen, D. (2005). Orientation of multiwalled carbon nanotubes in composites with polycarbonate by melt spinning. Polymer, 46(23), 10355–10363.

[67] Park, C., Wilkinson, J., Banda, S., Ounaies, Z., Wise, K. E., Sauti, G., ... & Harrison, J. S. (2006). Aligned single-wall carbon nanotube polymer composites using an electric field. Journal of Polymer Science Part B: Polymer Physics, 44(12), 1751–1762.

[68] Zhang, R.-P., Zhu, Y.-F., Ma, C., & Liang, J. (2009). Alignment of carbon nanotubes in poly (methyl methacrylate) composites induced by electric field. Journal of Nanosci. and Nanotechnology, 9(5), 2887–2893.

[69] Yamamoto, K., Akita, S., & Nakayama, Y. (1998). Orientation and purification of carbon nanotubes using AC electrophoresis. Journal of Physics D: Applied Physics, 31(8), L34.

[70] Oliva-Avilés, A. I., Avilés, F., Sosa, V., Oliva, A. I., & Gamboa, F. (2012). Dynamics of carbon nanotube alignment by electric fields. Nanotechnology, 23(46), 465710.

[71] Kumar, M. S., Datar, R., Viswanathan, K., & Venugopal, G. (2004). Influence of electric field type on the assembly of single-walled carbon nanotubes. Chemical Physics Letters, 383(3–4), 235–239.

[72] Gao, J., He, Y., & Gong, X. (2018). Effect of electric field-induced alignment and dispersion of functionalized carbon nanotubes on properties of natural rubber. Results in Physics, 9, 493–499.

[73] Monti, M., Natali, M., Torre, L., & Kenny, J. M. (2012). The alignment of single-walled carbon nanotubes in an epoxy resin by applying a DC electric field. Carbon, 50(7), 2453–2464.

[74] Chapkin, W. A., Zhu, Y.-F., Song, C., Wu, S., Zhu, L., & Liang, J. (2016). Real-time assessment of carbon nanotube alignment in a polymer matrix under an applied electric field via polarized Raman spectroscopy. Polymer Testing, 56, 29–35.

[75] Zhu, Y.-F., Ma, C., Zhang, W., Zhang, R.-P., Koratkar, N., & Liang, J. (2009). Alignment of multiwalled carbon nanotubes in bulk epoxy composites via electric field. Journal of Applied Physics, 105(5), 054319.

[76] Oliva-Avilés, A. I., Avilés, F., Sosa, V., & Seidel, G. D. (2014). Dielectrophoretic modeling of the dynamic carbon nanotube network formation in viscous media under alternating current electric fields. Carbon, 69, 342–354.

[77] Fujiwara, M., Oki, E., Hamada, M., Tanimoto, Y., Mukouda, I., & Shimomura, Y. (2001). Magnetic orientation and magnetic properties of a single carbon nanotube. The Journal of Physical Chemistry A, 105(18), 4383–4386.

[78] Ma, Y., Lehtinen, P. O., Foster, A. S., & Nieminen, R. M. (2004). Magnetic properties of vacancies in graphene and single-walled carbon nanotubes. New Journal of Physics, 6, 68.

[79] Lipert, K., Ritschel, M., Leonhardt, A., Krupskaya, Y., Büchner, B., & Klingeler, R. (2010). Magnetic properties of carbon nanotubes with and without catalyst. Journal of Physics: Conference Series, 200(7), 072061.

[80] Piao, G., Lim, D. S., Kim, J. S., Kim, J. K., & Kim, H. D. (2007). Alignment and micropatterning of carbon nanotubes in polymer composites using modulated magnetic field. Polymer Journal, 39(6), 589–592.

[81] Kazemikia, K., Bonabi, F., Asadpoorchallo, A., & Shokrzadeh, M. (2016). Influence of the concentration of carbon nanotubes on electrical conductivity of magnetically aligned MWCNT-polypyrrole composites. Bulletin of Materials Science, 39(2), 457–462.

[82] Rudnev, V. I. (2006). Systematic analysis of induction coil failures. Heat Treating Progress, 6, 19.

[83] Ariu, G., Hamerton, I., & Ivanov, D. (2016). Positioning and aligning CNTs by external magnetic field to assist localised epoxy cure. Open Physics, 14(1), 508–516.

[84] Tang, Z. H., Wang, D. Y., Li, Y. Q., Huang, P., & Fu, S. Y. (2022). Modeling the synergistic electrical percolation effect of carbon nanotube/graphene/polymer composites. Composites Science and Technology, 225, 109496.

[85] Motaghi, A., Hrymak, A., & Motlagh, G. H. (2015). Electrical conductivity and percolation threshold of hybrid carbon/polymer composites. Journal of Applied Polymer Science, 132(13), 1–9.

Chapter 3: Fabrication of low electrical percolation threshold multi-walled carbon nanotubes sensors using magnetic patterning

This chapter addresses the thesis's first objective: investigate the influence of MWCNT arrangement on composite conductivity and electrical percolation threshold. Achieving low electrical percolation thresholds is a key challenge in developing conductive polymer composites. A novel fabrication method was developed to address this, employing static magnetic fields to precisely pattern MWCNTs within a PDMS polymer matrix. This approach demonstrated that controlling the distribution of conductive particles through magnetic field-driven alignment can effectively lower the required MWCNT weight fraction needed to achieve desired electrical properties, resulting in enhanced conductivity and reduced production cost and complexity.

This chapter is based on the article published in the Special Issue Smart Composites: Design, Manufacturing and Integration of Applied Sciences, with reference: Esteves, D. S., Durães, N., Pedroso, R., Melo, A., Paiva, M. C., & Sequeiros, E. W. (2023). Fabrication of Low Electrical Percolation Threshold Multi-Walled Carbon Nanotube Sensors Using Magnetic Patterning. Applied Sciences, 13(3), 1437. https://doi.org/10.3390/app13031437

Abstract

Soft robotics is an expanding area with multiple applications, however building low-cost, soft and flexible robots requires the development of sensors that can be directly integrated into the soft robotics fabrication applications. Thus, the motivation of this work was the design of a low-cost fabrication process of flexible sensors that can detect touch and deformation. The fabrication process proposed uses a flexible polymer nanocomposite with permanent magnets strategically placed where the conductive electrodes should be. The nanocomposite is based on PDMS and MWCNT. The MWCNT contains ferromagnetic impurities remaining from the synthesis process, which can be used for magnetic manipulation. Several electrode geometries were successfully simulated and tested. The magnetic patterning was simulated, allowing the fabrication of conductive patterns within the composite. This fabrication process allowed the reduction of the electrical resistivity of the nanocomposites as compared to the composites with homogeneous MWCNT dispersion. It also allowed the fabrication of piezoresistive and triboelectric sensors, at MWCNT concentration as low as 0.5 wt.%. The fabrication process proposed is flexible, allows the development of sensors for soft robotics, as well as monitoring large and unconventional areas, and may be adapted to different mould shapes and polymers, at low cost.

Keywords: MWCNT; ferromagnetic; flexible sensors; smart composites; self-sensing;

3.1. Introduction

The fabrication of low electrical percolation threshold polymer nanocomposites aims to reduce the weight fraction of electrically conductive nanomaterial necessary to achieve a given level of electrical resistivity of the nanocomposite [1]. There are several strategies to achieve a lower electrical percolation threshold in nanocomposites [2]. Most methods consist in aligning the conductive nanoparticles [3], or constraining the location of CNTs such as the utilisation of polymer beads during *in situ* polymerization, forcing the contact between CNTs [4], or the migration to the interface of immiscible polymers [5]. Concerning nanocomposites with aligned nanoparticles, McNally *et al.* [6]

demonstrated that mechanical deformation induced a decrease in nanoparticle contacts, thus decreasing the electrical conductivity of the composite. The use of immiscible polymers to force the nanoparticle's location at the interface does not allow the control of their position within the nanocomposite. Conversely, magnetic forces may induce the contact between conductive nanoparticles with a ferromagnetic response, making it possible to control their location in the polymer matrix, thus allowing the fabrication of conductive patterns that can be used as sensor electrodes.

The magnetic field can be generated using electromagnets or permanent magnets. During the fabrication process, the strong magnetic field can lead to coil overheating problems that may damage the electromagnets [7], thus making the use of permanent magnets more attractive. The latter is more straightforward to use, however, the magnetic field density can be lower. The effective use of lower magnetic fields may be possible by functionalising CNTs with magnetic nanoparticles or using metal plating techniques, as reported by Ariu *et al.* [8]. Several metal plating methodologies were investigated in their work, including nickel, cobalt, and nickel-iron plating. Still, this is an unnecessary extra step when the MWCNT can already provide a magnetic response.

The magnetic response of CNTs has been interpreted using different theories. M. Fujiwara *et al.* [9] interprets it as resulting from the movement of the electrons circling the circumference of the CNTs producing a significant orbital magnetic moment, explaining the anisotropic susceptibility. Other theories are related to vacancies in the CNT structure that induce ferromagnetic behaviour [10]. CNTs produced by the Catalytic Chemical Vapor Deposition (CCVD) method present significant contamination by the catalyst materials used in their fabrication process, which are typically encapsulated in the CNTs, and will undoubtedly be the primary source of their magnetic response [11].

The precise control of the location of the MWCNT in the polymer matrix may lower the electrical percolation threshold and help sensor fabrication. This technique can be used for an application as piezoresistive sensors [12], triboelectric sensors and generators [13–15], capacitive sensors [16], temperature sensors [17], heating bands [18], etc. The present work explores the use of permanent magnets to fabricate low electrical percolation threshold samples by controlling the position of the MWCNT inside PDMS. To detect

physical contact and mechanical deformation, the nanocomposites were tested for application as triboelectric and piezoresistive sensors. In the future, this fabrication technique can produce multisensory devices in the same substrate, which may be applicable in soft robotics and wearables [19].

3.2. Materials and Methods

The workflow adopted in this work is shown in Figure 3.1, covering three main topics: the characterisation of the MWCNT and its nanocomposites, numerical simulations of the magnetic interactions, and sensor fabrication and testing. The characterisation of the MWCNT and its nanocomposites focused on the study of the MWCNT magnetic properties and the influence of the application of magnetic fields upon the electrical percolation threshold of MWCNT/PDMS nanocomposites prepared at different concentrations. Then, the numerical simulations helped to select the best magnet configurations to create linear patterns. The evaluation of the interactions between individual magnets allowed the simulation of more complex sensor electrode patterns. Linear and zig-zag patterns were simulated; however other designs may be simulated according to the application requirements. Finally, the performance of the fabricated sensors was evaluated, both as a piezoresistive sensor to detect deformation and as a triboelectric sensor to detect contact and release.

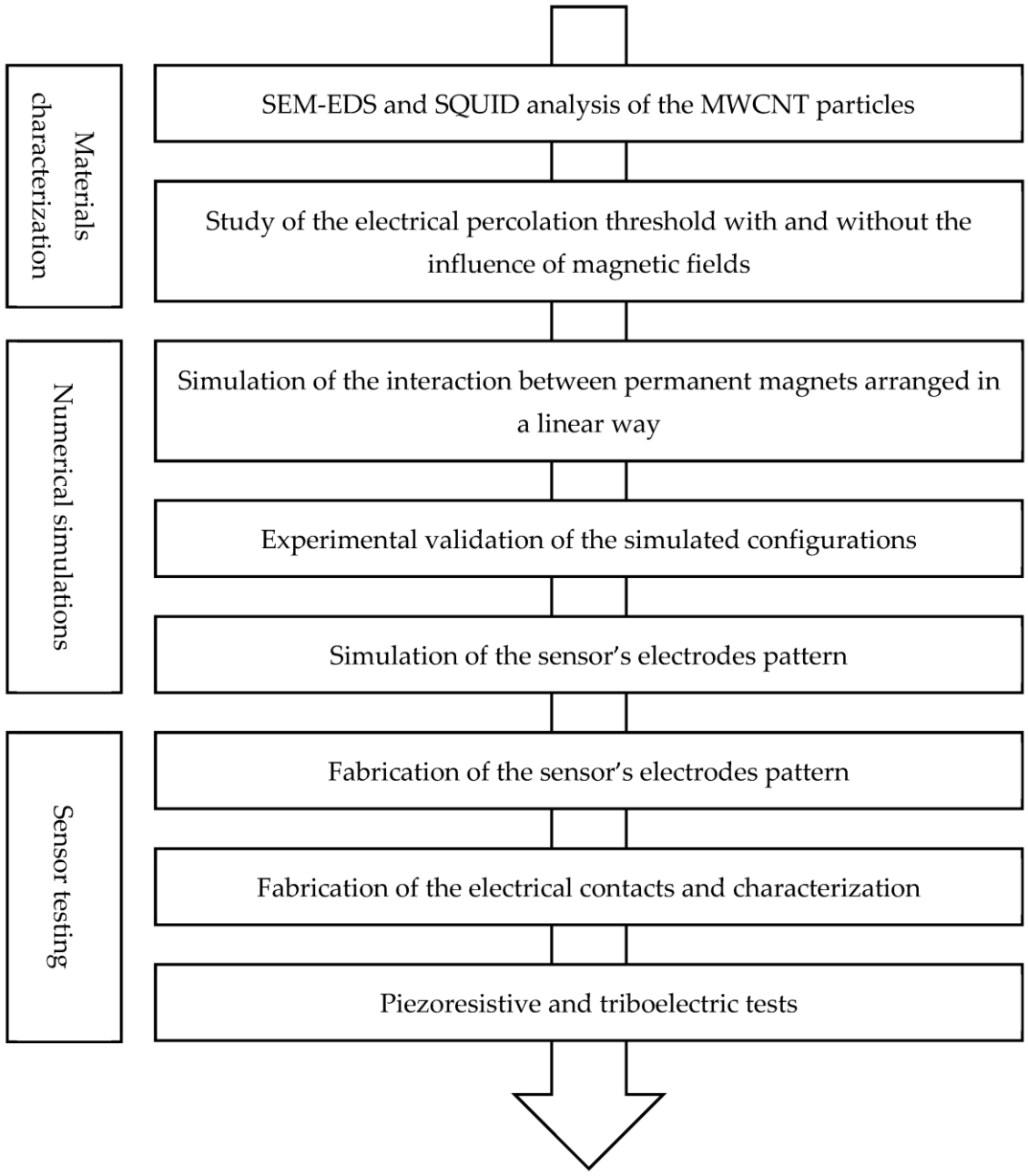

Figure 3.1- Overview of the workflow carried out

3.2.1 Materials

The MWCNTs were supplied by Nanocyl (NC7000, Sambreville, Belgium). The Nanotubes were analysed by scanning electron microscopy/energy dispersive spectroscopy (SEM/EDS) (FEI, Quanta 400FEG) to observe the morphology and obtain the elemental analysis to identify the catalyst attached to the MWCNT. The PDMS and the curing agent (SYLGARD™ 184 Silicone Elastomer Kit) were supplied by Dow Corning Co. Ltd. The neodymium magnets

were bought at K&J magnetics. The magnets used for the rectangular pattern were N42SH magnets with dimensions of 25.2x19.1x19.1 mm, and for the other patterns N42 magnets were used with dimensions of 0.5x0.5x0.5 cm.

3.2.2. Numerical simulation and fabrication processes

The fabricated patterns were simulated using the Ansys Maxwell software to study the magnetic interactions between permanent magnets. In the first stage, three different patterns were studied. The first pattern consisted of the use of permanent magnets in an alternating configuration; the second pattern consisted of the utilisation of permanent magnets in a design where the surface of the magnets had the same polarity; and finally, the third pattern consisted of a Halbach array.

After observing that the MWCNT response under a static magnetic field compares to the ANSYS simulation, the three different electrode patterns were simulated (rectangle, zig-zag shape, and parallel lines). These three patterns were implemented using permanent magnets in a configuration of alternated polarity to allow the formation of continuous patterns.

The magnetic patterns were fabricated in the laboratory to confirm the simulation results. Tests were carried out to characterise: 1) the electrical percolation threshold of the nanocomposites, 2) the magnetic patterns produced and 3) the fabrication of the sensor's electrodes. The samples prepared for each study were rectangular with the following dimensions and MWCNT concentrations: for test 1) 2x1x0.5 cm, with MWCNT concentration in the range 0.01 - 5 wt.%; for test 2) 2x1x0.5 cm and MWCNT concentration of 0.1 wt.%; for test 3) 4x2x0.2 cm with MWCNT concentration of 0.5 and 1 wt.%.

The fabrication process of all the MWCNT/PDMS nanocomposites is schematically illustrated in Figure 3.2. First, the MWCNT were dispersed into the PDMS under constant manual stirring for 2 minutes. Then, the curing agent, in a 1:10 ratio, was added to the MWCNT/PDMS mixture and manually stirred for another 2 minutes. Then, the mixtures obtained were placed in rectangular laser cut acrylic moulds, on top of the magnetic patterns, for 15 hours. The samples were cured during 15 hours to make sure that the PDMS was solid enough to prevent the movement of the MWCNT before the final curing process. The final

curing process was done in an oven at 110 °C for 30 minutes without magnetic fields. If the curing process is too fast there is not enough time for the particles to settle in the right position, affecting the patterning quality.

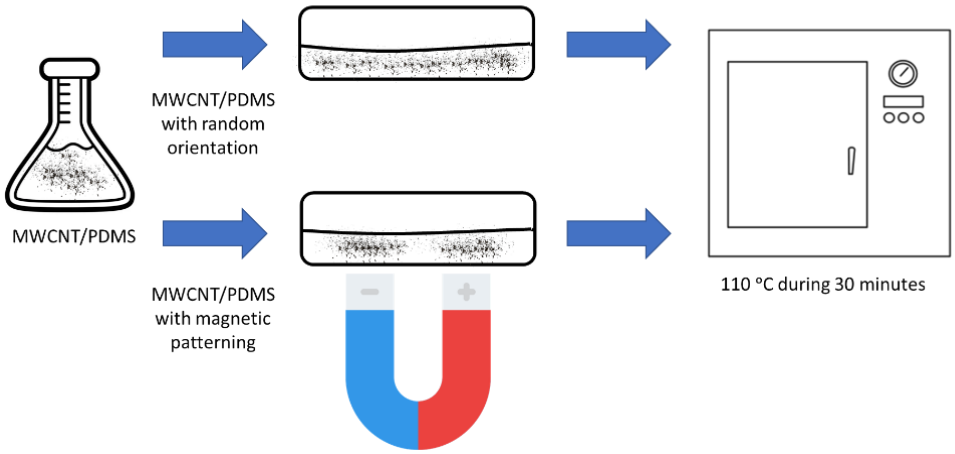

Figure 3.2- Fabrication process of the composite sensors under magnetic field.

The electrical contacts were fabricated by cutting a thin layer of MWCNT/PDMS on opposite sides of the sample and by placing silver conductive epoxy (MG Chemicals 8331S Silver Conductive Epoxy) on the MWCNT surface. After curing the conductive epoxy, the electrical contacts were covered with copper tape to facilitate the connection to the measurement equipment.

3.2.3. Experimental tests

The magnetic properties of the MWCNT were analysed using a SQUID magnetometer (Quantum Design at IFIMUP-IN). The magnetisation as a function of the applied magnetic field (M(H)) was performed at temperatures 300, 320, 340, 360, and 380 K for a maximum applied magnetic field of 50 kOe.

The electrical resistivity of the fabricated nanocomposite samples was measured by the two-point electrical resistance measurement technique (Keithley Instruments 6487). Seven samples were analysed for each nanocomposite prepared. The morphological characterisation of the samples was performed using a Digital Microscope (Leica DVM6). The three-point bending tests were carried out on a Shimadzu AGX-V at 150 mm/min speed and with applied forces between 6 and 9 N.

The nanocomposite samples prepared with different magnetic patterning were characterised as piezoresistive and triboelectric sensors using a setup similar to the three-point bending test, as shown in Figure 3.3.

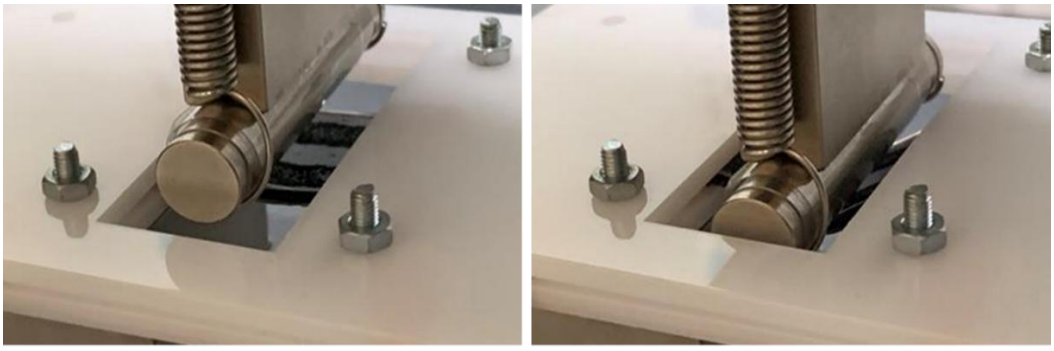

Figure 3.3- Bending tests with an applied force of 6.6 N, a) press and b) release motion.

The piezoresistive sensors were characterised using a Keithley DMM7510 7 ½ Digital Multimeter, where both sample electrodes were connected to the multimeter terminals. For the triboelectric characterisation, the exact high speed digital multimeter was used; however, the open circuit output voltage was measured instead of electrical resistance. The triboelectric effect was measured in single electrode configuration mode. One probe was connected to the sample, and the other was connected to the electrical ground, measuring the flow of the accumulated charge between the sample and the electrical ground.

3.3. Results

3.3.1. Characterization of the magnetic properties of MWCNT and MWCNT/PDMS nanocomposite

To better understand the magnetic properties of the MWCNT particles, SEM EDS was performed on the MWCNT. This test was useful to analyse the elemental composition and search for contaminants remaining from the fabrication process. Figure 3.4 presents an SEM backscattered electron image of the MWCNT, showing contrasting particles identified by EDS as based on aluminium. The fabrication of the NC7000 MWCNT uses alumina substrate for the iron catalyst, which under the MWCNT synthesis conditions (high temperature environment with carbon rich gas) may reduce to aluminium carbide, Al_4C_3 [20].

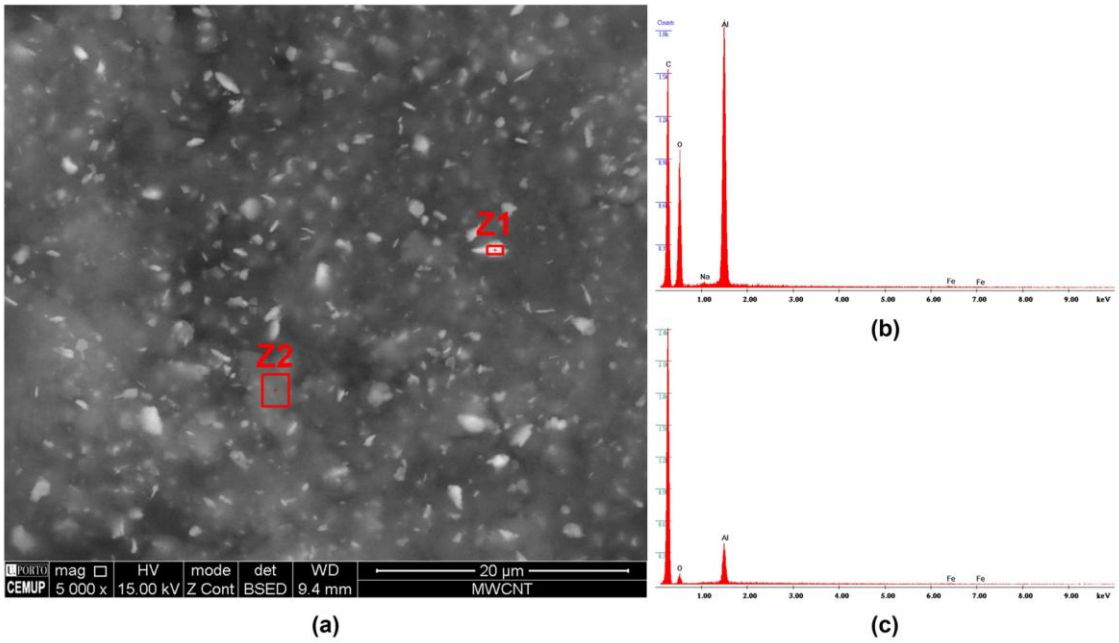

Figure 3.4- Detection of particles based on aluminium and iron as some of the impurities of the CCVD fabrication process of the MWCNT NC 7000. a) SEM image and regions where the SEM EDS was performed. b) regions with higher amounts of aluminium oxide impurities, and c) regions with lower impurities.

The SQUID analysis presented in Figure 3.5, showed that the MWCNT and the MWCNT/PDMS present both ferromagnetism and diamagnetism. By analysing the magnetisation curve for the MWCNT it is noticeable that the ferromagnetic properties dominate at lower fields (between -6000 and 6000 Oe) and the diamagnetism dominates at higher fields. This behaviour could be associated with the ferromagnetic saturation, since the diamagnetism keeps changing linearly with the magnetic field. The diamagnetic property could be associated with the different materials, it could be due to the magnetic properties of MWCNT, or the catalysts (alumina or Al_4C_3). The ferromagnetic response could be related to the presence of iron, a ferromagnetic material that was also identified by SEM EDS.

Similar behaviour was also reported by Ellis *et al*. [21] where the authors measured the magnetic properties of MWCNT and concluded that in their specific case, the particles showed a combination of diamagnetism and ferromagnetism. They concluded that the diamagnetism arose from the multi-walled nanotubes, and the ferromagnetism was due to the presence of iron nanoparticles derived from the fabrication process.

Another example is the work of Zoladz *et al*., 2020 [22], which reported that CNTs grown from alumina by CVD show significant ferromagnetic properties, even though the catalyst materials showed diamagnetic properties.

By analysing Figure 3.5 b) in detail, it is possible to notice a dominant ferromagnetic effect [23]. The measured coercivity (Hc), retentivity (Mr) and saturation magnetisation (Ms) of the MWCNT particles at 300 K were 84.8 Oe, 0.2 emu/g, and 1.1 emu/g, respectively. The results demonstrate that the magnetic properties of the MWCNT are invariant in the temperature range studied, from 300 to 380 K.

As expected, when compared with the particles, the lower concentration of the MWCNT (5 wt.%) and the polymeric nature of PDMS decrease the overall ferromagnetic properties in the nanocomposite. Analysing Figure 3.5 d) it is presented a ferromagnetic curve. The measured coercivity (Hc), retentivity (Mr) and saturation magnetisation (Ms) of the nanocomposite at 300 K were 93.02 Oe, 0.004 emu/g, and 0.03 emu/g, respectively. Similar to the MWCNT particles, the 5 wt.% MWCNT/PDMS also show a dominant ferromagnetic effect at lower fields (between -6000 and 6000 Oe) and a dominant diamagnetic behaviour at fields between 6000 and 50000 Oe.

It is also noticeable that the nanocomposite has a stronger diamagnetic behaviour than the MWCNT particles. This increase in the diamagnetic behaviour could be associated with the PDMS matrix. In the work of Hamidi *et al*. [24] it was possible to observe a similar behaviour. When the authors tested samples with and without the PDMS matrix, a dominant diamagnetism was also present for higher fields.

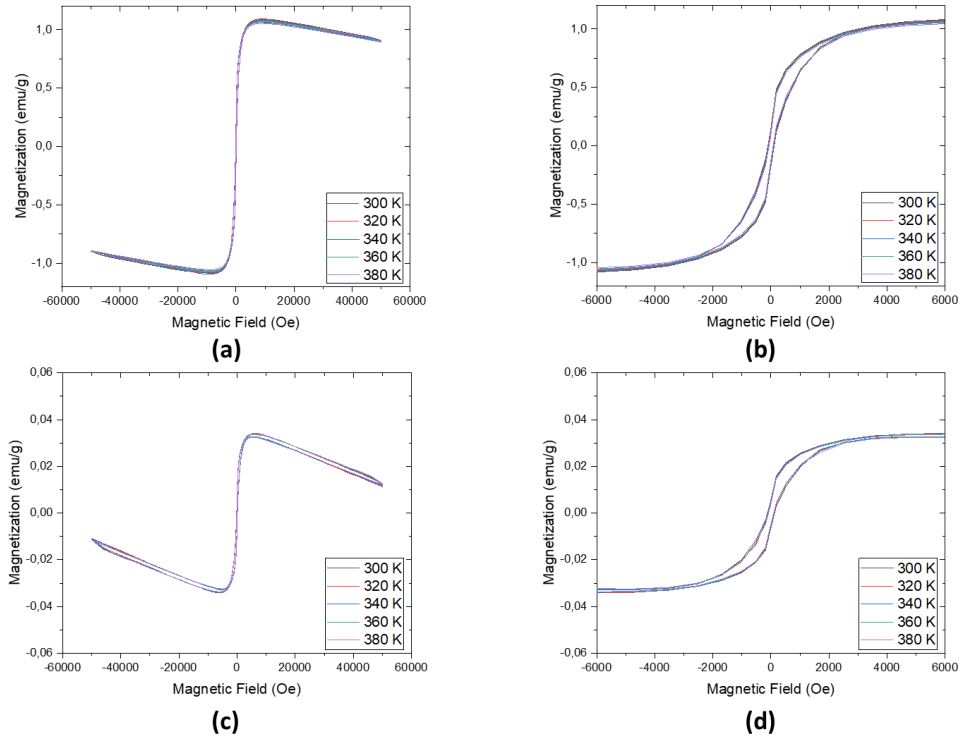

Figure 3.5- Magnetisation curve for the MWCNT (a, b), and 5 wt.% MWCNT/PDMS with random distribution (c, d).

3.3.2. Electrical percolation threshold of MWCNT/PDMS under magnetic forces

MWCNT/PDMS nanocomposites were prepared with MWCNT concentrations ranging from 0.01 to 5 wt.% The impact of applying a magnetic field upon the MWCNT distribution in the nanocomposite, and thus on the nanocomposite's electrical conductivity, was evaluated. The electrical resistivity of the samples was determined using the following equation:

$$\rho = R \times A/l \quad (1)$$

where ρ is the electrical resistivity of the nanocomposite sample, R is the electrical resistance between electrodes, A is the cross-sectional area of the sample, and l is the distance between the electrodes.

The nanocomposites' electrical resistivity, prepared with the magnetic field (magnetic orientation) and without magnetic field (random distribution), are presented in Figure 3.6, defining the electrical percolation threshold obtained in each case.

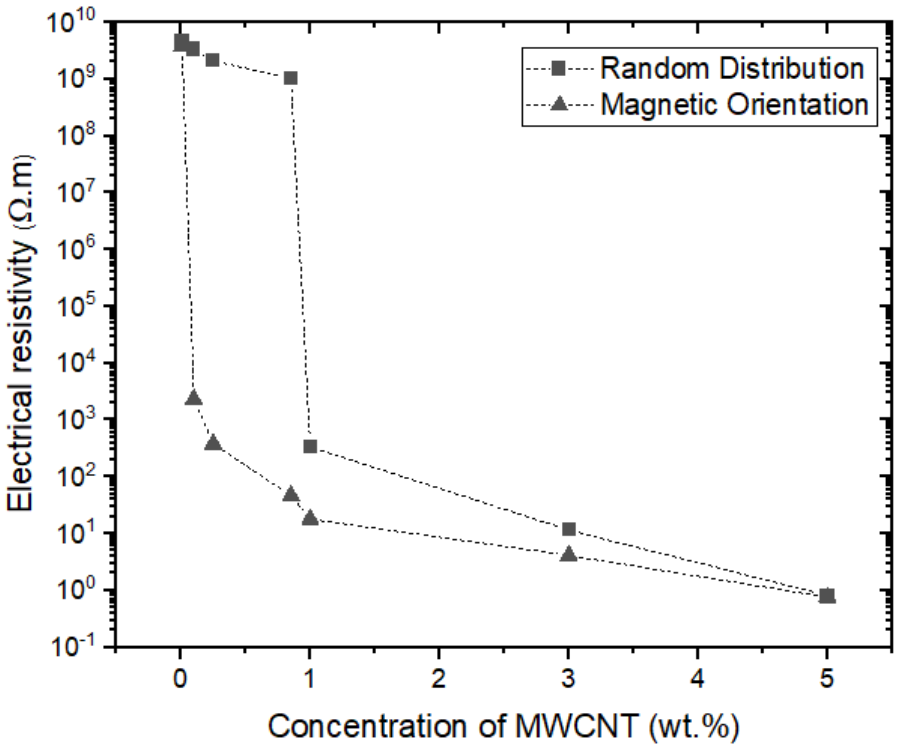

Figure 3.6- Electrical resistivity of MWCNT/PDMS nanocomposites prepared with and without magnetic alignment.

Figure 3.6 depicts the impact of the magnetic field's application on the nanocomposites' electrical resistance. the magnetic field application reduces the MWCNT concentration at the electrical percolation threshold from 0.85 - 1 wt.% to 0.01 - 0.1 wt.% MWCNT. The longitudinal images of the nanocomposites obtained by digital microscopy show the effect of the magnetic field on the nanocomposite morphology as illustrated in Figure 3.7 a) and b). The magnetic field forces the localisation of the nanoparticles near the magnet, increasing the contact between conductive particles. A numerical simulation was performed to predict the localisation of the MWCNT relative to the magnet. The simulation was performed using ANSYS Maxwell software to illustrate the effect of the magnetic field on two stacked permanent magnets. Figure 3.7 c) and d) shows that magnetic flux density is predicted to be greater at the magnet’s edges.

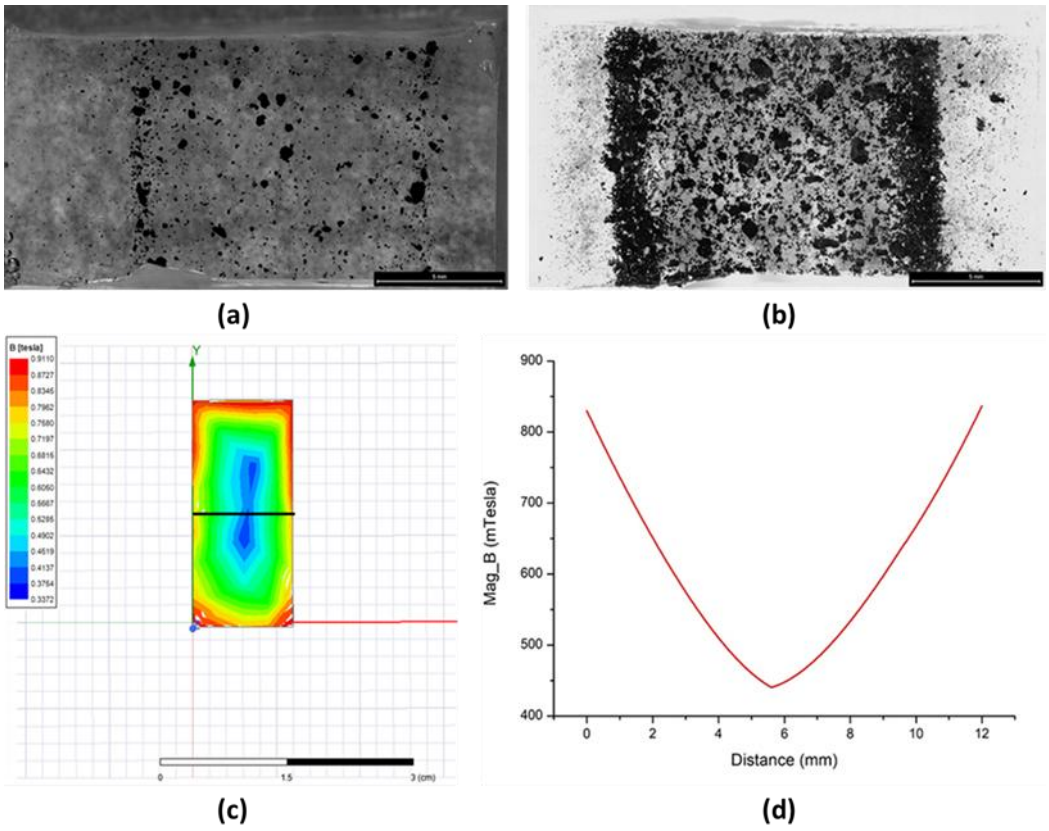

Figure 3.7- Magnetic pattern in MWCNT/PDMS samples with concentrations of a) 0.01 and b) 0.1 wt.% and c) magnetic flux density profile on the surface of a permanent neodymium magnet, with d) magnetic flux density in the region of the black line.

To confirm the magnetic flux variation between the edges and centre of the magnet, the magnetic flux density along the black line drawn in Figure 3.7 c) was calculated and represented in Figure 3.7 d). The magnetic flux density is observed to decrease from the edges to the centre of the magnet, which coincides with the MWCNT localisation on the PDMS matrix, showing that the MWCNT are attracted to the locations with higher magnetic flux.

The curves depicting the electrical percolation threshold for the nanocomposites in Figure 3.6 show that at 5 wt.% MWCNT the nanocomposite's electrical resistivity is similar with and without applying a magnetic field. At this concentration and above, the conductivity of the nanomaterial is so large that its distribution in the nanocomposite does not affect the overall electrical resistivity.

3.3.3. Numerical simulations and MWCNT/PDMS magnetic patterning

To propose low electrical percolation threshold designs for the fabrication of sensors, MWCNT interaction with more than one magnet was simulated. Three different configurations of permanent magnets were studied. The first pattern consisted of the use of permanent magnets in an alternating configuration; the second pattern consisted of the utilisation of permanent magnets in a design where the surface of the magnets had the same polarity; and finally, the third pattern consisted of a Halbach array. The configurations were first simulated using the ANSYS software and then replicated in the laboratory. The magnets were placed under MWCNT/PDMS nanocomposites with a concentration of 0.1 wt.% before the cure of the polymer. Figure 3.8 represents the simulation results for the magnetic field distribution and the magnetic flux lines for the three different configurations.

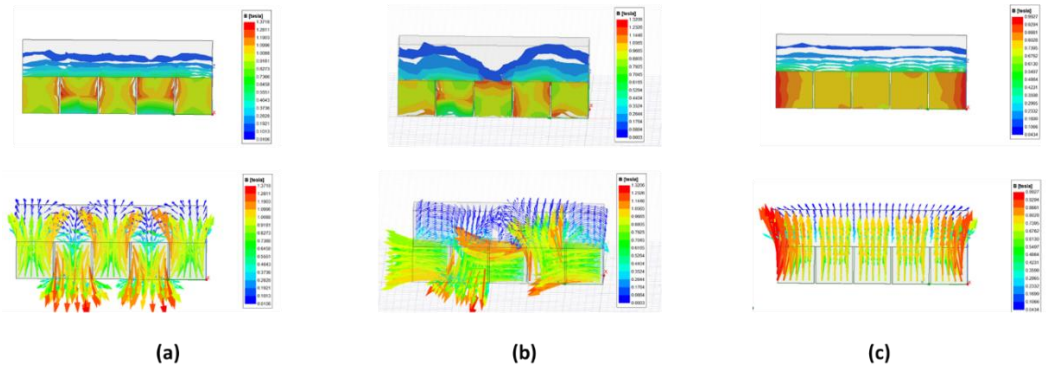

Figure 3.8- Magnet configuration to create linear and discontinuous patterns, using a) alternated polarity, b) Halbach array, and c) same polarity configurations.

Figure 3.9 shows the magnetic patterns achieved using the three magnetic configurations (Figure 3.8 a, b and c), compared with a randomly distributed nanocomposite (Figure 3.9 a). The top line of Figure 3.9 represents the 3D image obtained in the micrographs, while the bottom line shows optical micrographs of the nanocomposites prepared. The 3D images reinforce the location of the MWCNT agglomerates on the polymeric matrix. A comparison of the simulation and experimental results shows the similarity between the MWCNT location and the simulation predictions, the latter showing the density of the magnetic field of permanent neodymium magnets in the air.

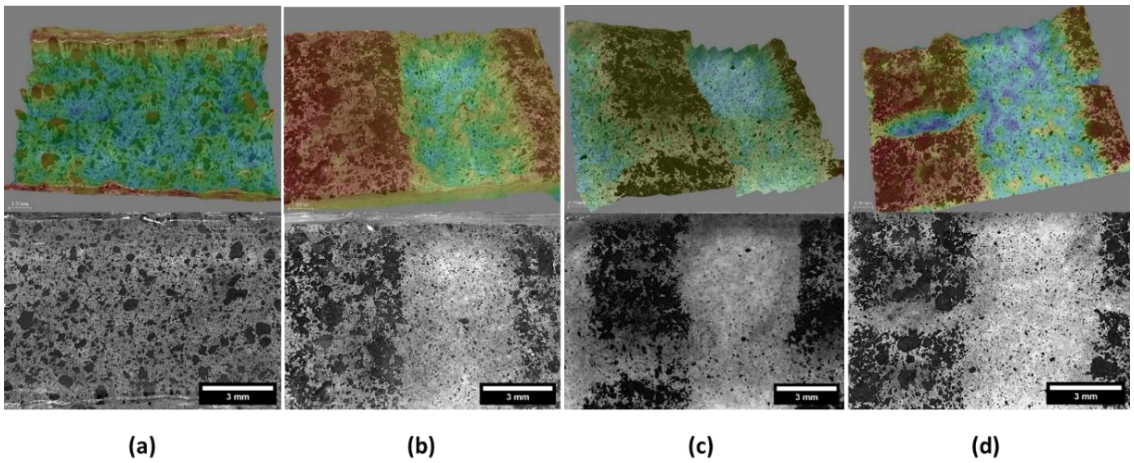

Figure 3.9- Magnetic patterns and 3D reconstruction of the samples a) randomly distributed, b) magnetic pattern with alternate polarity, c) magnetic pattern with Halbach array, and d) magnetic pattern with the same polarity.

As demonstrated in Figure 3.8 and Figure 3.9, the MWCNT localisation replicates the magnetic pattern of the permanent magnets, accumulating in the regions of higher magnetic flux and following the magnetic field patterns of the interaction between multiple permanent magnets. Figure 3.9 b) illustrates the effect of using alternate polarity magnets, showing that it generates a continuous pattern, like continuous lines. Using magnets aligned with the same polarity (Figure 3.9 d) creates discontinuities due to the low magnetic field in the region between the magnets. Finally, the utilisation of Halbach arrays (Figure 3.9 c) also creates discontinuities due to the non-uniform field at the surface of the magnets.

Lastly, sensor electrodes were developed using MWCNT patterns in PDMS generated with permanent magnets. The first step consisted in simulating the patterns using ANSYS software and then replicating the patterns in the laboratory, as shown in Figure 3.10.

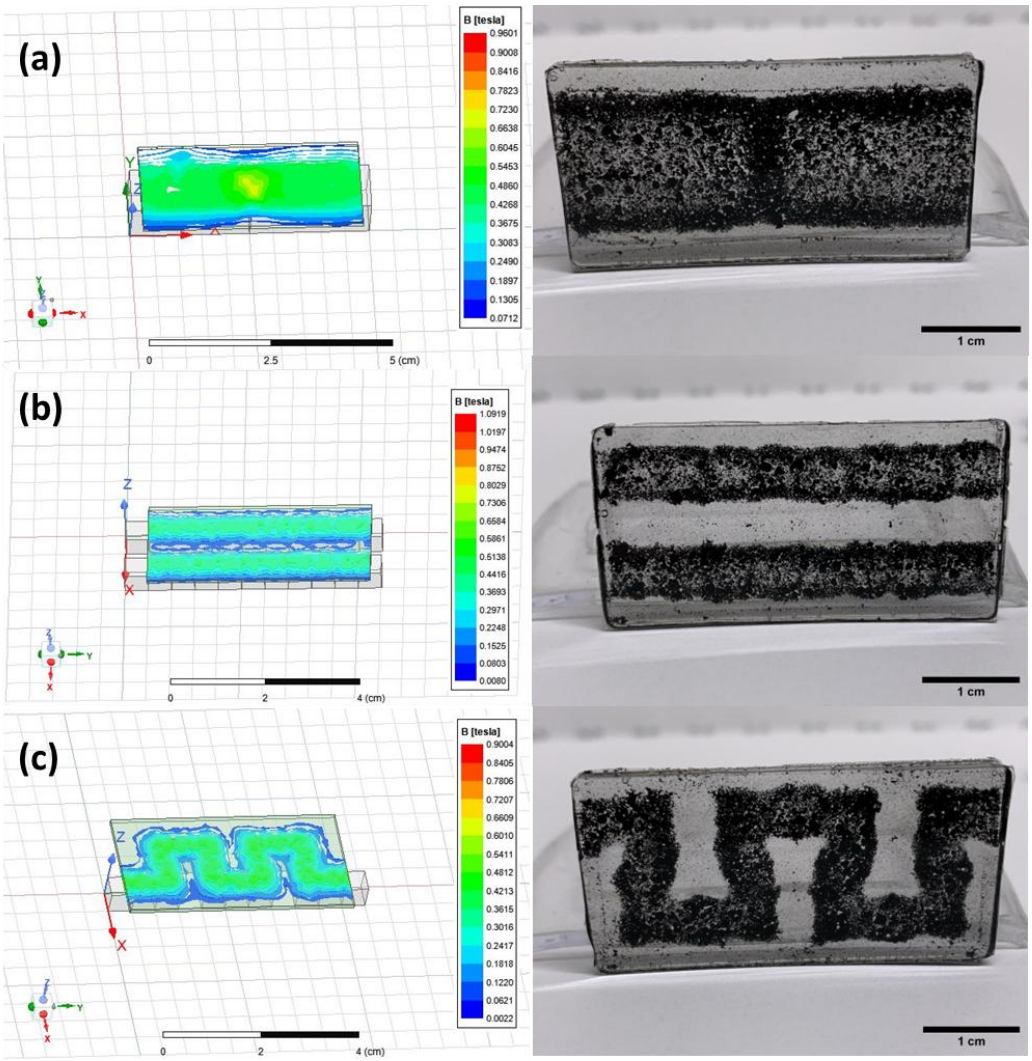

Figure 3.10- Magnetic patterns in Ansys Maxwell and magnetic patterns of MWCNT/PDMS achieved in the laboratory, a) Rectangular ; b) Parallel lines; and c) Zig zag shape.

Figure 3.10 illustrates that, as demonstrated before, the pattern generated by the simulation for the magnetic field intensity is replicated by the MWCNT localisation inside the PDMS matrix. Analysing the electrical resistivity of the nanocomposites prepared with different magnetic patterning, shown in Figure 3.11, it is observed that the random distribution nanocomposite with 0.5 wt.% MWCNT has high electrical resistivity due to a lack of contact between conductive particles. The nanocomposites prepared with magnetic patterning presented lower electrical resistivity compared with randomly distributed nanocomposites, either for 0.5 or 1 wt.% MWCNT concentration. The zig-zag pattern produced higher electrical resistivity nanocomposites than the other patterns, probably due to the increase in length of the electrical conductive path. This increase in resistivity may help to adjust the electrical resistance of a sensor, if needed.

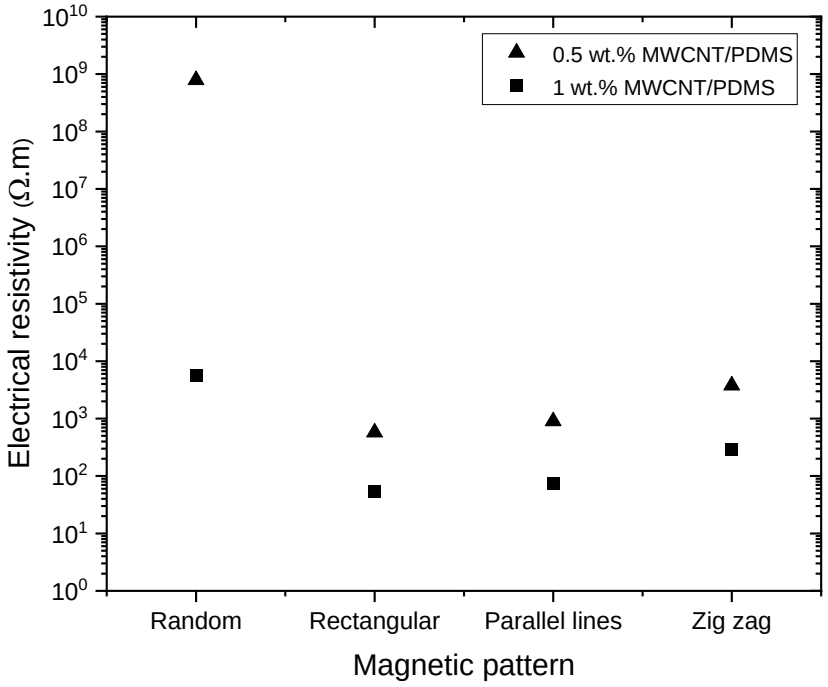

Figure 3.11- Electrical resistivity of the nanocomposites fabricated with different magnetic patterns.

3.3.4. Low electrical percolation threshold piezoresistive sensors

The piezoresistive effect can be used to detect different stimuli. When compression, tension, or bending is applied to these flexible sensors, the location and morphology of the fillers in the sensors change, causing a change in electrical resistance. The magnitude of the piezoresistive effect and the electrical properties vary depending on the filler's dimensions, content, and morphology [18]. The resistance change rate for the piezoresistive sensors is defined in equation 2:

$$\Delta R/R_0 = (R-R_0)/R_0 \quad (2)$$

where R is the measured electrical resistance and R_0 is its initial resistance before the application of force [25].

To evaluate the piezoresistive effect, all the samples were tested during 30 cycles of 3-point-bending. The piezoresistive effect was measured for 0.5 and 1 wt.% concentration of MWCNT and all the magnetic patterns and random

distribution nanocomposites. Figure 3.12 shows that the nanocomposites with random distribution for 0.5 wt.% of MWCNT did not present a piezoresistive response due to their high electrical resistance. Conversely, all the nanocomposites prepared with magnetic patterning presented a piezoresistive response. It was observed that, for an MWCNT concentration of 1 wt.%, the random distribution provides a more unstable response than the magnetically patterned nanocomposites. After analysis of the piezoelectric response obtained for all the magnetically induced patterns, the two parallel lines pattern was selected for dynamic tests.

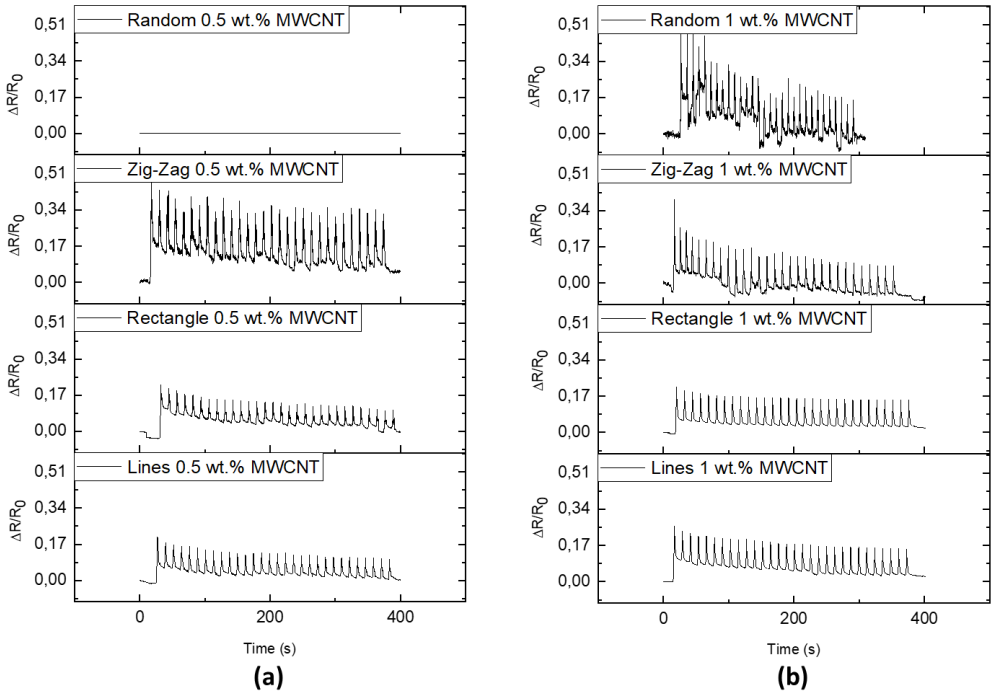

Figure 3.12- Piezoresistive effect for samples with a) 0.5 and b) 1 wt.% of MWCNT with different magnetic patterns, from top to bottom: random, zig-zag, rectangular and parallel lines.

As shown in Figure 3.13, both concentrations are adequate to develop piezoresistive sensors and offer good stability under the application of decreasing and increasing forces. The nanocomposites respond when the force is applied instantaneously, as well as when it is maintained for 10 seconds before release. The samples show good stability since the electrical resistance is similar during the application of decreasing and increasing force. In the future, a deeper analysis of the sensor performance can be carried out, including the evaluation

of the use of pre-strain since the first deformation appears to have a different response compared to the deformations that follow.

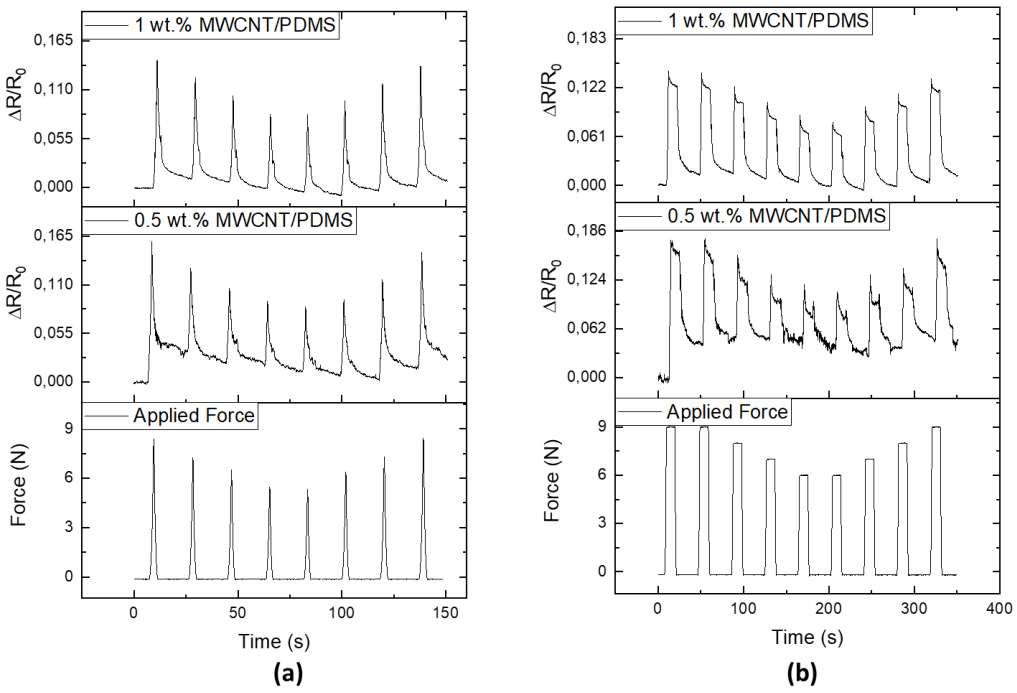

Figure 3.13- Piezoresistive effect for the sample with the parallel lines pattern with 0.5 and 1 wt.% of MWCNT/PDMS. a) unloading-loading peaks, b) unloading-loading delayed peaks.

3.3.5.Low electrical percolation threshold triboelectric sensors

The triboelectric effect is a combination of contact electrification and electrostatic induction; the static polarised charges, resulting from the contact between the two friction surfaces with different charge affinities, are generated on the friction surfaces and cause different surface potentials, inducing charges among the two attached electrodes [26-28]. In this specific case, the PDMS nanocomposites present a high triboelectric charge density. When the mechanical testing equipment touches the surface of the PDMS, the flow of electrons generates a measurable electrical voltage. The same happens at release, but the output voltage measured has an opposite sign since the electrons are leaving the surface of the PDMS [29]. When the materials are in contact, the output voltage is zero since there is no significant exchange of electrons between the materials. Therefore, triboelectric sensors help detect instantaneous contact and release. Even for applied forces lower than 6 N, a generated output voltage

may be detected, indicating that these sensors have a fast response and are pretty sensitive. Figure 3.14 shows that all the nanocomposites generate output voltage under contact and release. The signal is low for the random distribution nanocomposite with 0.5 wt.% due to the low electrical conductivity across the sample. The magnetic patterned nanocomposites and the random distributed nanocomposite with 1 wt.% MWCNT, which have lower electrical resistance, generate a considerable output voltage that may be used to detect instantaneous impact and release.

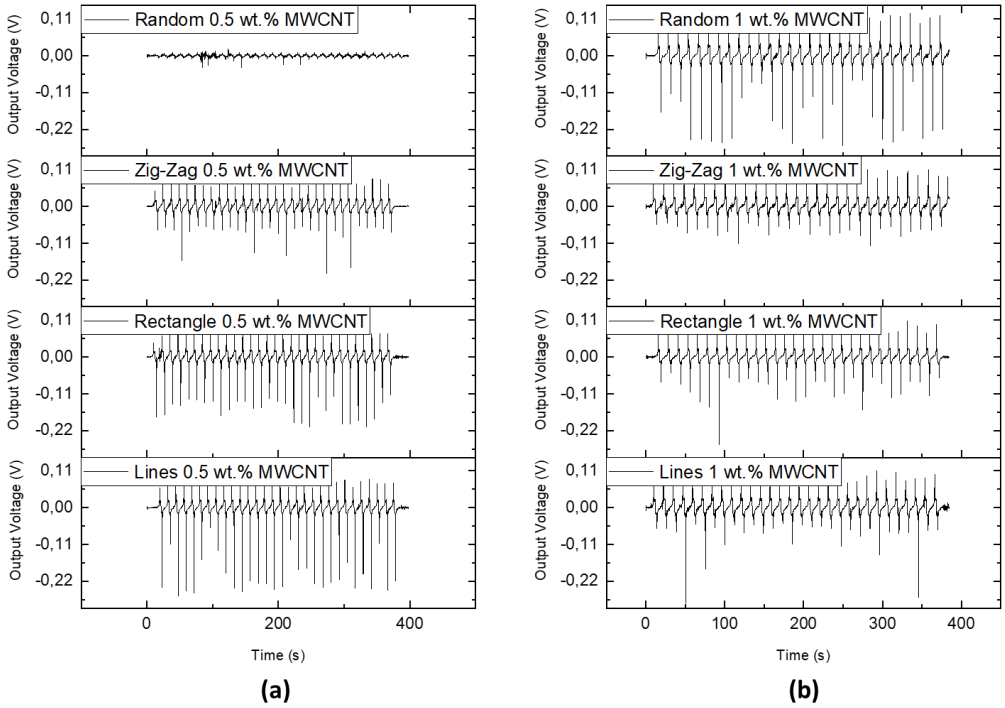

Figure 3.14- Triboelectric effect for nanocomposites with a) 0.5 and b) 1 wt.% of MWCNT with random distribution and with different magnetic patterns (zig-zag, rectangle and parallel lines).

When analysing the triboelectric response of the nanocomposite produced with a magnetic pattern of parallel lines, represented in Figure 3.15, it is observed that the contact and release is detected within different applied force ranges. When the applied force is maintained for 10 seconds, the output voltage is zero due to the lack of interaction between the two surfaces; however, the output voltage is visible at the moment of release.

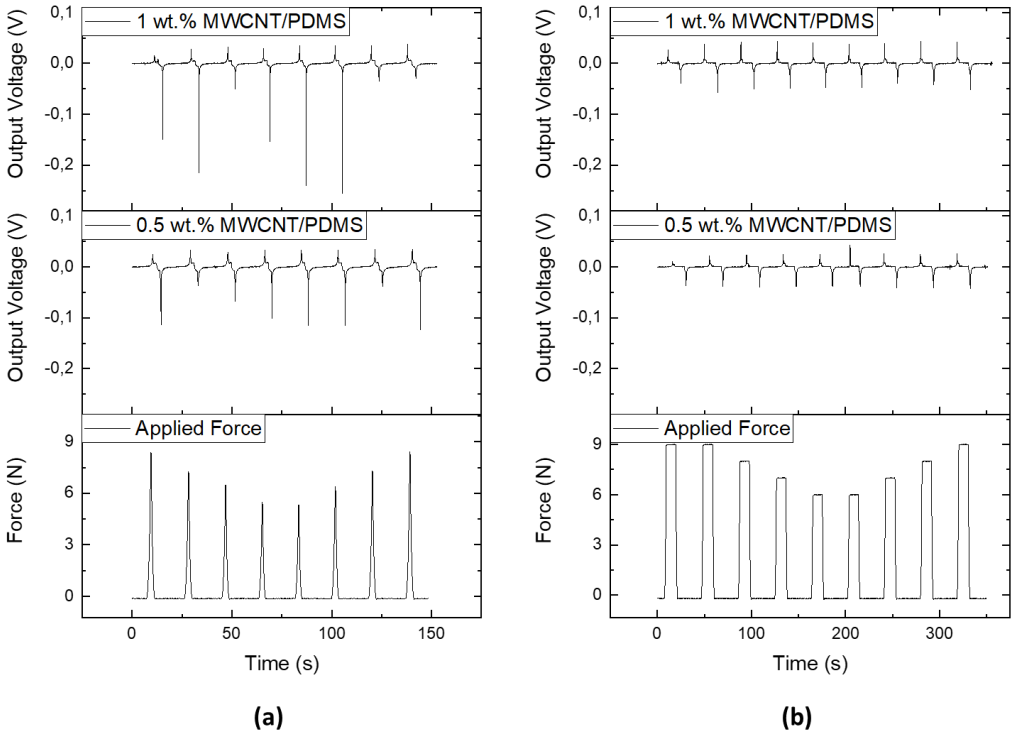

Figure 3.15- Triboelectric effect obtained for the nanocomposites prepared with the parallel line magnetic pattern with 0.5 and 1 wt.% of MWCNT; a) unloading-loading peaks, b) unloading-loading delayed peaks. The bottom images represent the applied force by the testing machine.

The piezoresistive sensors detect the moment the force is applied to the material, as shown in Figure 3.16; however it does not detect the touch if the sensor contacts a surface without deforming the sensor. The triboelectric effect, however, can detect contact without bending the sensor. Therefore, the two sensor types can complement each other by having a high sensitivity to touch due to the triboelectric properties and stable monitoring of the applied force or deformation due to the piezoresistive properties.

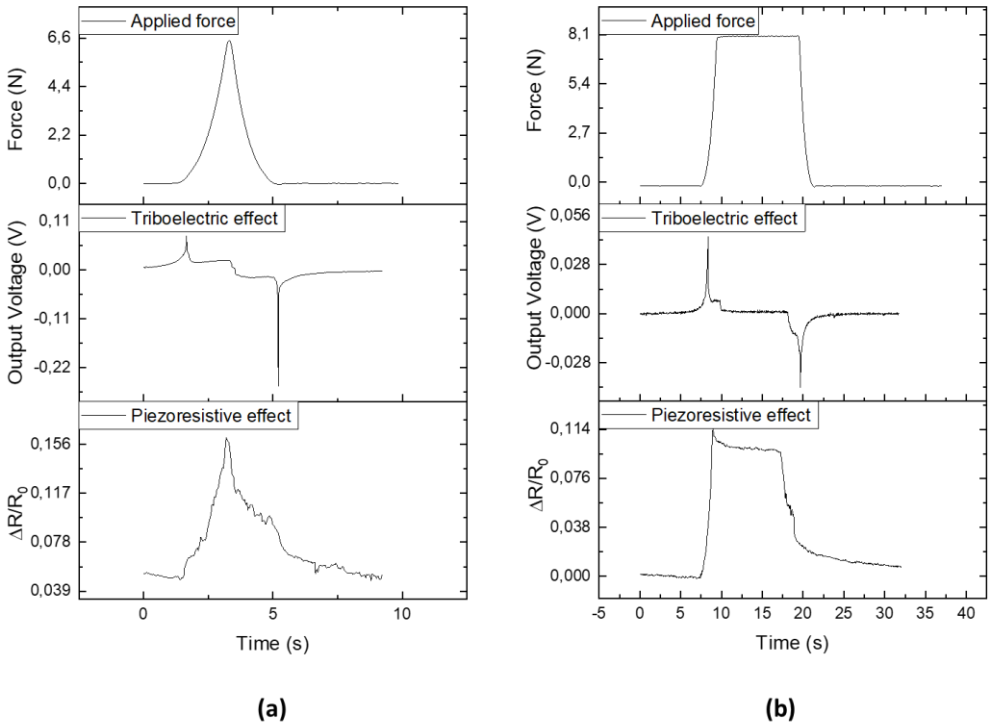

Figure 3.16- Piezoresistive and triboelectric effects under a deformation force for the nanocomposite prepared with the parallel lines magnetic pattern. a) 0.5 wt%. of MWCNT/PDMS under a peak force of 6.6 N b) 1 wt%. of MWCNT/PDMS sample under a force of 8.1 N for 10 seconds.

Figure 3.16 shows in detail the difference between the response of the sensors for fast (Figure 3.16 a) and slow movements (Figure 3.16 b). Analysing the presented results, it is possible to confirm that the triboelectric sensors work well to detect the contact and release of objects on the sensor's surface, independently of the time frame and applied force. The piezoresistive effect works better for monitoring the deformation of the sensor, being capable of monitoring both fast and slow deformations.

3.4. Conclusions

This work reports a new low-cost fabrication technique for developing low electrical percolation threshold sensors based on magnetically oriented MWCNT/PDMS nanocomposites. Compared with randomly distributed MWCNT composites, these sensors originate electrodes with low electrical resistance, suitable for developing flexible piezoresistive and triboelectric sensors.

The MWCNT were observed to present a magnetic response due to impurities remaining from their fabrication process. SEM-EDS analysis detected

the presence of aluminium and iron. SQUID analysis confirmed the ferromagnetic properties of the MWCNT powder. The magnetic response of the MWCNT was used to control their localisation inside a polymer matrix, PDMS, using magnetic fields. The use of magnetic fields to localise the MWCNT decreased the electrical percolation threshold compared to the nanocomposites prepared with a random distribution of the MWCNT, thus reducing the concentration of conductive nanomaterial necessary while creating patterned electrodes that can be used for the fabrication of flexible sensors.

The different interactions between permanent magnets were simulated and tested in the lab, showing that the use of alternated polarity configuration allowed the fabrication of continuous conductive lines of MWCNT. Finally, nanocomposites with three different electrode designs were simulated and fabricated. Although all designs produced electrodes with an adequate response, the pattern obtained with parallel lines was produced and tested for piezoelectric and triboelectric properties. The nanocomposites were tested under bending forces between 6 and 9 N, showing a stable response under fast and slow deformation. The developed sensors proved to be stable for touch detection and deformation under the range of forces.

Future work can include the scale up of this fabrication technique and its extension to using different polymer matrices. A detailed analysis of the stability of the sensors and their application as multi-sensors could be carried out. The fabrication process presented may be used in the near future to develop sensors for soft robotics applications. It may be applied to monitor large and unconventional areas; it can be adapted to different moulds and polymer matrices since it is an adaptable, low-cost solution that does not require expensive equipment or materials.

3.5. References

[1] Liu, H., & Thostenson, E. T. (2018). Conductive nanocomposites for multifunctional sensing applications. In Comprehensive Composite Materials II (pp. 311–331). Elsevier.

[2] Kausar, A., & Taherian, R. (2018). Effect of external fields on electrical conductivity of polymer-based composites. In Electrical Conductivity in Polymer-Based Composites: Experiments, Modelling and Applications (pp. 275–298). Elsevier.

[3] Xie, X.-L., Mai, Y.-W., & Zhou, X.-P. (2005). Dispersion and alignment of carbon nanotubes in polymer matrix: A review. Materials Science and Engineering: R: Reports, 49(4), 89–112.

[4] Shrivastava, N. K., & Khatua, B. B. (2011). Development of electrical conductivity with minimum possible percolation threshold in multi-wall carbon nanotube/polystyrene composites. Carbon, 49(13), 4571–4579.

[5] Salehiyan, R., & Ray, S. S. (2019). Tuning the conductivity of nanocomposites through nanoparticle migration and interface crossing in immiscible polymer blends: A review on fundamental understanding. Macromolecular Materials and Engineering, 304(2), 1800431.

[6] McNally, T., Murphy, W. R., Lew, C. Y., Turner, R. J., Brennan, G. P., & Poetschke, P. (2005). Polyethylene multiwalled carbon nanotube composites. Polymer, 46(19), 8222–8232.

[7] Rudnev, V. I. (2006). Systematic analysis of induction coil failures. Heat Treating Progress, 6, 19.

[8] Ariu, G., Hamerton, I., & Ivanov, D. (2016). Positioning and aligning CNTs by external magnetic field to assist localised epoxy cure. Open Physics, 14(1), 508–516.

[9] Fujiwara, M., Oki, E., Hamada, M., Tanimoto, Y., Mukouda, I., & Shimomura, Y. (2001). Magnetic orientation and magnetic properties of a single carbon nanotube. The Journal of Physical Chemistry A, 105(18), 4383–4386.

[10] Ma, Y., Lehtinen, P. O., Foster, A. S., & Nieminen, R. M. (2004). Magnetic properties of vacancies in graphene and single-walled carbon nanotubes. New Journal of Physics, 6, 68.

[11] Lipert, K., Ritschel, M., Leonhardt, A., Krupskaya, Y., Büchner, B., & Klingeler, R. (2010). Magnetic properties of carbon nanotubes with and without catalyst. Journal of Physics: Conference Series, 200(7), 72061.

[12] Fu, X., Ramos, M., Al-Jumaily, A. M., Meshkinzar, A., & Huang, X. (2019). Stretchable strain sensor facilely fabricated based on multi-wall carbon nanotube composites with excellent performance. Journal of Materials Science, 54(3), 2170–2180.

[13] Zhao, Z., Wu, C., & Zhou, Q. (2021). A self-powered basketball training sensor based on triboelectric nanogenerator. Applied Sciences, 11(8), 3506.

[14] Rasel, M. S., Cho, H. O., Kim, J. W., & Park, J. Y. (2018). A self-powered triboelectric sensor for wide-range pressure detection in wearable application. Journal of Physics: Conference Series, 1052(1), 012029.

[15] Liu, P., Zhu, Z., Liu, L., Han, H., & Wang, J. (2021). Ultra-low CNTs filled high-performance fast self-healing triboelectric nanogenerators for wearable electronics. Composites Science and Technology, 208, 108733.

[16] Yoon, S. G., & Chang, S. T. (2017). Microfluidic capacitive sensors with ionic liquid electrodes and CNT/PDMS nanocomposites for simultaneous sensing of pressure and temperature. Journal of Materials Chemistry C, 5(8), 1910–1919.

[17] Kwon, M., & Hong, Y. (2009). Flexible temperature sensor array of PDMS-encapsulated conductive CNT thin films fabricated by solution process. In 2009 International Semiconductor Device Research Symposium (pp. 1–2).

[18] Jang, S.-H., & Park, Y.-L. (2018). Carbon nanotube-reinforced smart composites for sensing freezing temperature and deicing by self-heating. Nanomaterials and Nanotechnology, 8, 1847980418776473.

[19] Souri, H., Bhattacharyya, D., Yong, W., & Liang, J. (2020). Wearable and stretchable strain sensors: Materials, sensing mechanisms, and applications. Advanced Intelligent Systems, 2(8), 2000039.

[20] Paiva, M. C., Proenca, M. F., Henrique, M. R., Goncalves, F., & Feng, J. (2010). Controlled functionalization of carbon nanotubes by a solvent-free multicomponent approach. ACS Nano, 4(12), 7379–7386.

[21] Ellis, A. V., & Ingham, B. (2006). Magnetic properties of multiwalled carbon nanotubes as a function of acid treatment. Journal of Magnetism and Magnetic Materials, 302(2), 378–381.

[22] Zoladz, F., Shao, R., Srivastava, S., Sayle, D. C., & Sayle, T. X. (2020). Enhanced magnetic properties of aluminum oxide nanopowder reinforced with carbon nanotubes. Journal of Nanoparticle Research, 22(6), 1–9.

[23] Elsi, S., & Pushpanathan, K. (2019). Role of Cu and Mn dopants on d0 ferromagnetism of ZnS nanoparticles. Journal of Materials Science: Materials in Electronics, 30(11), 10792–10807.

[24] Hamidi, S. M., Sobhani, A., Aftabi, A., & Najafi, M. (2015). Optical and magneto-optical properties of aligned Ni nanowires embedded in polydimethylsiloxane. Journal of Magnetism and Magnetic Materials, 374, 139–143.

[25] Huang, K., Liu, X., Li, Y., & Li, J. (2020). Ultrasensitive MWCNT/PDMS composite strain sensor fabricated by laser ablation process. Composites Science and Technology, 192, 108105.

[26] Wu, J., Zheng, Y., & Li, X. (2021). Recent progress in self-powered sensors based on triboelectric nanogenerators. Sensors, 21(21), 7129.

[27] Kao, F.-C., Yeh, T.-H., Tsai, W.-S., & Liu, C.-T. (2022). Self-assisted wound healing using piezoelectric and triboelectric nanogenerators. Science and Technology of Advanced Materials, 23(1), 1–16.

[28] Xu, J., Zou, Y., Nashalian, A., & Chen, J. (2020). Leverage surface chemistry for high-performance triboelectric nanogenerators. Frontiers in Chemistry, 8, 577327.

[29] Hwang, H., Lee, K. Y., Shin, D., Shin, J., Kim, S., & Choi, W. (2018). Metal-free, flexible triboelectric generator based on MWCNT mesh film and PDMS layers. Applied Surface Science, 442, 693–699.

Chapter 4: Development of MWCNT/Magnetite Flexible Triboelectric Sensors by Magnetic Patterning

This chapter addresses the thesis's second objective: evaluate the impact of polymer matrix viscosity on particle arrangement and conductivity under magnetic fields in thermosets. Building upon the findings of Chapter 4, this work explores the synergistic effect of incorporating magnetite particles into the MWCNT/polymer composite to refine magnetic alignment techniques. This combined approach enhances the filler's magnetic responsiveness, improving composite fabrication reproducibility and electrical conductivity. The resulting triboelectric sensors demonstrate potential for detecting mechanical stimuli in flexible electronic applications such as soft robotics, highlighting the importance of synergistic filler optimisation and precise particle control for advancing sensor performance.

This article belongs to the Special Issue Polymer-Based Materials for Sensors II of Polymers with reference: Esteves, D. S., Pereira, M. F. C., Ribeiro, A., Durães, N., Paiva, M. C., & Sequeiros, E. W. (2023). Development of MWCNT/Magnetite Flexible Triboelectric Sensors by Magnetic Patterning. Polymers, 15(13), 2870. https://doi.org/10.3390/polym15132870

Chapter 4: Development of MWCNT/Magnetite Flexible Triboelectric Sensors by Magnetic Patterning

Abstract: The fabrication of low electrical percolation threshold polymer composites aims to reduce the weight fraction of the conductive nanomaterial necessary to achieve a given level of electrical resistivity of the composite. The present work aimed at preparing composites based on MWCNT and magnetite particles in a PU matrix, to study the effect on the electrical resistance of electrodes produced under magnetic fields. Composites with 1 wt.% of MWCNT, 1 wt.% of magnetite and combinations of both were prepared and analysed. The hybrid composites combined MWCNT and magnetite at the weight ratios of 1:1; 1:1/6; 1:1/12; and 1:1/24. The results showed that MWCNT were responsible for the electrical conductivity of the composites since the composites with 1 wt.% magnetite were non-conductive. Combining magnetite particles with MWCNT reduces the electrical resistance of the composite. SQUID analysis showed that MWCNT simultaneously exhibits ferromagnetism and diamagnetism, ferromagnetism being dominant at lower magnetic fields while diamagnetism is dominant at higher fields. Conversely, magnetite particles present a ferromagnetic response much stronger than MWCNT. Finally, optical microscopy (OM) and X-ray micro computed tomography (micro CT) identified the interaction between particles and their location inside the composite. In conclusion, the combination of magnetite and MWCNT in a polymer composite allows the control of the location of these particles using an external magnetic field, decreasing the electrical resistance of the electrodes produced. By adding 1 wt.% of magnetite to 1 wt.% of MWCNT (1:1), the electric resistance of the composites decreased from $9x10^4$ to $5x10^3$ Ω. This approach significantly improved the reproducibility of the electrode's fabrication process, enabling the development of a triboelectric sensor using PU composite and silicone rubber (SR). Finally, the method's bearing was demonstrated by developing an automated robotic soft grip with tendon-driven actuation controlled by the triboelectric sensor. The results indicate that magnetic patterning is a versatile and low-cost approach to manufacturing soft robotics sensors.

Keywords: MWCNT; ferromagnetic; flexible and stretchable sensors; smart composites; sensor fabrication; polymer composites; polymer actuators; soft-robotics

4.1. Introduction

Soft robotics is a new class of intelligent systems with specific properties that differentiate them from traditional rigid devices [1]. Instead of integrating rigid joints and links, where motion is predominantly localised at the joint, soft robots rely on continuum deformations to achieve motion. The control of these soft systems requires continuous monitoring of their state during action [1]. However, traditional sensors have high stiffness compared to the materials used in soft robotics [2-3]. Thus, developing a new class of soft sensors made from low-stiffness materials, such as those found in soft robots, is of tremendous interest. This new class of intelligent systems has the potential to be more adaptable and versatile, enabling robots to navigate complex environments and interact with humans and objects more safely and naturally. The potential applications of soft robotics are broad and range from medical devices to search and rescue operations, industrial automation and even space exploration. Their main advantages compared with traditional rigid devices are related to their flexibility, adaptability, durability and light weight [4-6].

The integration of flexible soft sensors can be particularly useful in soft robotic grippers, an area that has been growing considerably over time and is expected to grow even more by 2030 [7]. Soft robotic grippers significantly impact the close interaction between robots and their surroundings [8]. Safe and dexterous grasping is one of the main requisites for a wider implementation, but one of the major challenges is the accurate control of soft bodies. Therefore, a significant effort in perception has been made with embedded sensory systems [9].

The types of sensors used in soft robotic grippers are mostly proprioceptive sensors (e.g., Hall-effect sensors, encoders, torque sensors, tendon tension sensors, strain sensors) to estimate the position and velocity of the gripper elements or exteroceptive sensors (e.g., piezoelectric sensors, triboelectric sensors, resistive sensors, electromagnetic sensors) to gather information about external objects [10-12].

Regarding the exteroceptive sensors, the triboelectric sensors have been showing great potential due to their flexibility, material compatibility, and simplicity. Triboelectric sensors generate electrical signals through frictional

contact between two dissimilar materials. The interaction between the generated charges is measured through the electrodes and can be used to sense motion, touch or pressure [13-15].

Like triboelectric sensors, many flexible soft robotics sensors require electrodes, which can be made using various conductive materials such as fillers [3,16,17]. MWCNTs have been used as effective fillers in polymer composites because of their high aspect ratio, low density, excellent mechanical strength and high thermal and electrical conductivities [18].

In a previous work [19], the authors reported the development of sensors that were compatible with soft robotics materials. The sensors presented low electrical resistance, using MWCNTs as conductive material and a magnetic patterning technique/method for fabricating electrodes. This magnetic patterning technique has the advantage of decreasing the weight percentage of MWCNTs needed to achieve the same electrical resistance compared to randomly aligned composites [18,20]. However, when the viscosity of the composites increases significantly due to the polymer cross-linking process, the MWCNTs' low magnetic properties (assigned to the residual catalyst remaining in the MWCNT) decrease the quality of the magnetic patterning [21]. The solution to this issue was achieved by using magnetite particles (Fe_3O_4) combined with MWCNTs. The combination of MWCNT/magnetite has been introduced previously, typically involving the synthesis of Fe_3O_4/MWCNT by chemical processes [21-27]. As an example, Dong *et al*. [28] synthesised MWCNT/Fe_3O_4 to increase the electrical and dielectric properties of PI films. The chemical synthesis involves extra steps that can be avoided by physical mixing, facilitating sensor fabrication for soft robotics.

This study explores the fabrication of triboelectric sensors for soft robotics applications, using the physical mixing of MWCNTs and magnetite to decrease the electrical resistance of the sensor's electrodes and facilitate magnetic patterning.

4.2. Materials and Methods

The presented work can be divided into three parts: materials, composites and prototype. The study of the materials consisted in evaluating three relevant

aspects for the application: i) the effect of the addition of particles and nanoparticles on the viscosity of the reactive polyurethane rubber; ii) the differences in the characteristic magnetic properties of MWCNT and magnetite particles; iii) the interaction between the particles in a thermoset PU matrix composite and a static magnetic field applied to the composite during the crosslinking process. The second part involved characterising the magnetic patterns generated on the composites after cross-linking. Optical microscopy and X-ray computed microtomography were used to explore the particle's distribution in detail. The ratio of particles with the electrical resistance of the fabricated electrodes was correlated, and the triboelectric sensors were characterised. Finally, a soft robotic prototype was developed in the last part, consisting of two tendon-driven actuators controlled by a triboelectric sensor.

4.2.1. Materials and characterisation

The MWCNTs were supplied by Nanocyl (NC7000, Sambreville, Belgium). The synthetic magnetite powder, with an average particle dimension of 200 nm and an average density of 4.6 g/cm^3, was supplied by Inoxia (Cranleigh, United Kingdom). The reactive PU rubber and the curing agent (Poly GlassRub 50 - Transparent Polyurethane Rubber) were provided by Feroca (Madrid, Spain). The silicone rubber (Ecoflex 00-50) was supplied by Smooth-on, Inc. (Pennsylvania, USA). The neodymium N42 magnets with 0.5x0.5x0.5 cm^3 were bought at K&J magnetics (Pipersville, USA).

Regarding the characterisation processes, the PU viscosity was measured using a rotational viscometer (Fungilab-Master series smart) with an L2 spindle. The measurement was carried out for 30 minutes for each sample (PU without any additives, 1 wt.% MWCNT in PU, and 1 wt.% MWCNT plus 1 wt.% of magnetite in PU).

The magnetic properties of the MWCNT and magnetite powder were analysed using a superconducting quantum interference device (SQUID) magnetometer (Quantum Design, IFIMUP-IN). The SQUID magnetometers typically allow a fully automated measurement of the magnetisation of a specimen as a function of the magnetic field; the magnetisation as a function of the applied magnetic field (M(H)) was performed at 300 K for a maximum applied magnetic

field of 50 kOe. OM analysis using a Digital Microscope (Leica DM 2500M) characterised the particles and the permanent magnets. The variation of the magnetic response with PU curing time was assessed 20 minutes before and after PU cross-linking under a static magnetic field on composites containing 1 wt.% of MWCNT and 1 % wt.% MWCNT + 1 % wt.% of magnetite.

Finally, to ensure uniformity across the electrodes, the polarities of the magnets should be symmetrical. Therefore, to characterise the magnetic flux density of the magnets, a 3D magnetic characterisation was performed using a portable magnetic field mapper (M3D-2A-Port, Senis). The tested area was 30x30 mm, and the distance between the permanent magnets and the probe was approximately 1 mm.

4.2.2. Composite fabrication and characterisation

After characterising the interaction between the particles and the permanent magnets, six different composites, consisting of MWCNT + magnetite in a PU matrix, were produced using the magnetic patterning process. Two magnet arrays arranged in an alternated polarity configuration generated the magnetic patterns.

The fabrication process of the composites is illustrated in Figure 4.1. Six different composites were prepared. Two composites containing 1 wt.% of the individual particles: 1 wt.% MWCNT/PU and 1 wt.% magnetite/PU. The other four composites were prepared with different ratios of magnetite added to 1 wt.% MWCNT (1:1, 1:1/6, 1:1/12, 1:1/24). The different ratios of magnetite, consist in adding the extra weight percentage of magnetite to 1 wt% of MWCNT. For example, for the sample (1:1), 1 wt.% magnetite is added to 1 wt.% MWCNT, which means that the composite has a total of 2 wt.% of fillers. For the sample (1:1/24), 0.04 wt.% magnetite is added to 1 wt.% MWCNT, which means that the composite has a total of 1.04 wt.% of fillers.

For the fabrication of the composites, the PU rubber was mixed with the particles by hand for 2 minutes, then the mixture was poured into a mould (10 x 3 x 0.3 cm), and then the mould was placed on top of the permanent magnet array. After 16 hours, as described in the PU rubber datasheet, the specimen was de-moulded, and the process was repeated for each prepared sample and

replicas. After de-moulding, a thin layer of PU was cut in both extremities, exposing the electrodes to test the electrical resistance of the electrodes. A thin silver ink (CI 1036, ECM) layer was placed on each electrode and cured at 110 °C for 20 minutes.

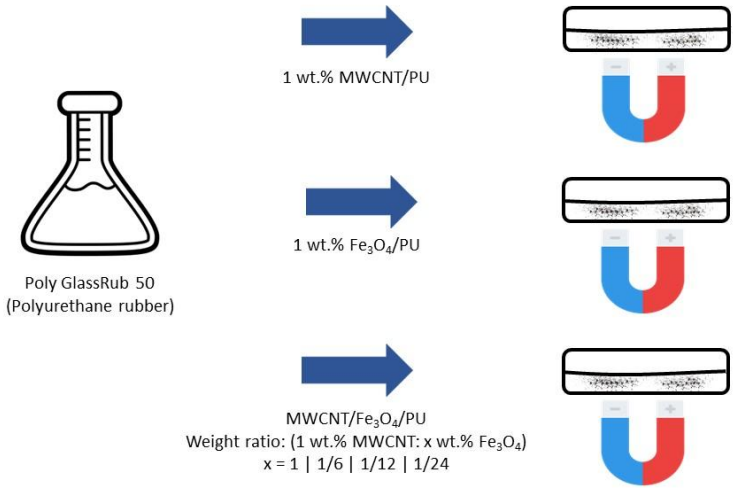

Figure 4.1- Composite materials fabrication process.

The morphological characterisation of the specimens was performed using a Digital Microscope (Leica DM 2500 M). The images were acquired in transmission mode at different magnifications.

The micro CT was performed at the Laboratory of Mineralogy and Petrology of IST (LAMPIST-GEOLAB) to assess the composites' three-dimensional (3-D) microstructural and compositional heterogeneities. Digital radiographs were acquired on a micro CT SkyScan 1172 scanner (Bruker, Massachusetts, USA) using an X-ray cone incident on a rotating specimen. Due to the specimens' reduced size and composition, the experimental conditions were optimised for each specimen using a constant source power (10 W). The following operating conditions were used: source voltage of 60 kV, current of 165 µA, a pixel size resolution of 5-6 µm, and an average of five radiographs per each position. The acquisition was performed by rotating the specimen over 180° with a 0.25° rotational step. Slice reconstructions were obtained with the NRecon 1.6.3 routine, and volumetric visualisation was achieved with DataView and CTvox programs, which integrate the instrument software packages.

The electrical measurements consisted in testing the electrical resistance of each composite's electrode. The dimensions of each electrode were approximately the dimensions of the magnet's arrays (10 x 0.5 cm). The electrical resistance of the fabricated samples was measured by the two-point electrical resistance measurement technique (Keithley 6487, Solon, Ohio). Each electrode of the six samples was tested. Four replicas of each sample were fabricated and tested to study the reproducibility of the fabrication process of the composites (1 wt.% magnetite, 1 wt.% MWCNT, 1:1, 1:1/6, 1:1/12 and 1:1/24).

The triboelectric sensors were characterised using a high-speed digital multimeter (Keithley DMM7510 7 ½ Digital Multimeter, Solon, Ohio), where both electrodes were connected to the multimeter terminals, and the output voltage was measured. Two materials were tested as friction layers, PU and SR. Both materials were pressed against the electrodes several times under controlled conditions in a three-point bending setup. The three-point bending tests were conducted on a Shimadzu AGX-V at 500 mm/min speed with an applied force of 10 N.

4.2.3. Prototype development and testing

The methodology for prototype development is presented in Figure 4.2. Regarding the sensor and actuator fabrication, first, the triboelectric sensor was patterned using 1 wt.% MWCNT plus 1 wt.% of magnetite in PU. Then the triboelectric sensor was placed inside the mould of the actuator, and finally, it was filled with PU rubber. The actuator's mould consisted of a polymeric part produced by 3D printing. The structure also comprises two channels on the sides, where the string moves. The motion is comparable to the movement of a tendon, bending the structure after pulling the sting. The mould presents several folds on the front and back, facilitating the movement of the actuator and decreasing the force needed for the micro servo to pull the strings.

The mould and the prototype were designed with SolidWorks and fabricated using a 3D printing machine (Stratasys Fortus 250mc, Minnesota, USA). The hardware to control the prototype consisted of an Arduino Uno, electrical resistances, LEDs and two micro servo motors (DFRobot SER0006). All the

components were assembled inside the 3D printing prototype structure to test the prototype.

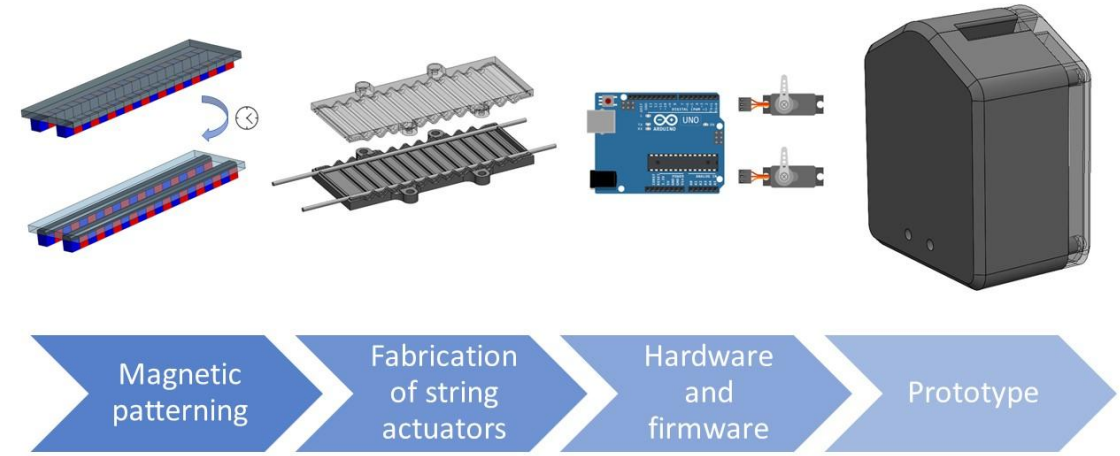

a)

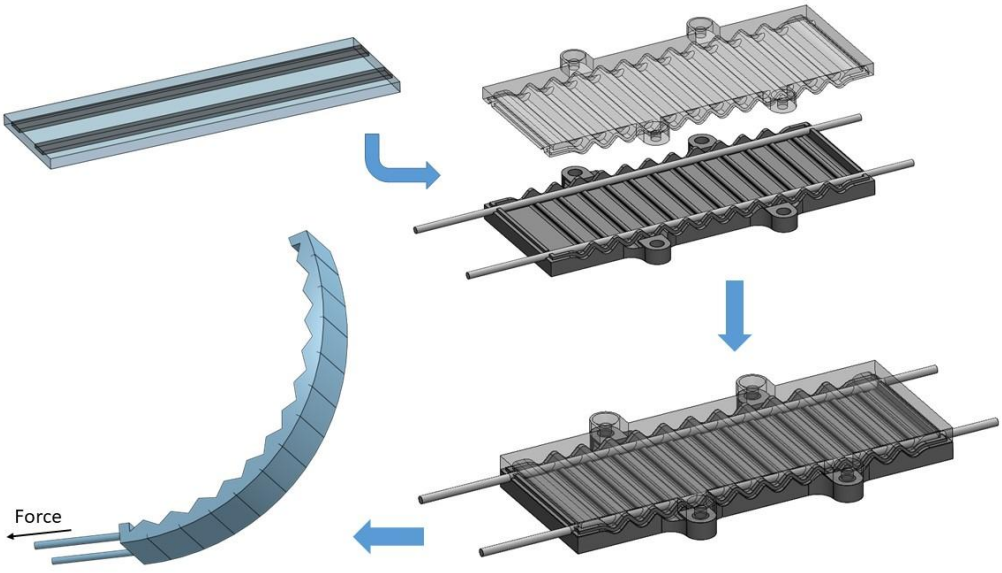

b)

Figure 4.2- a) Methodology for the prototype development and b) development of a tendon-driven actuator with an integrated triboelectric sensor.

4.3. Results and discussion

4.3.1. Materials and characterisation

One of this work's main objectives was to use magnetic patterning to fabricate electrodes to develop MWCNT/PU sensors. However, the pot life of the PU rubber was just 30 minutes, meaning that after mixing the two components the viscosity significantly increases, hampering the mixture's workability and affecting patterning quality. Furthermore, the addition of MWCNT to PU increases the viscosity, as shown in Figure 4.3, from approximately 4000 mPa.s to 12000 mPa.s or higher. Thus, magnetite particles were added to the composite to overcome the increase in viscosity and the low magnetic response of the MWCNT. Increasing the magnetic response of the composite is expected to enhance the velocity of the particles inside the fluid, compensating for the increase in viscosity. Among the various magnetic additives available, magnetite was chosen for its attractive magnetic properties and low cost.

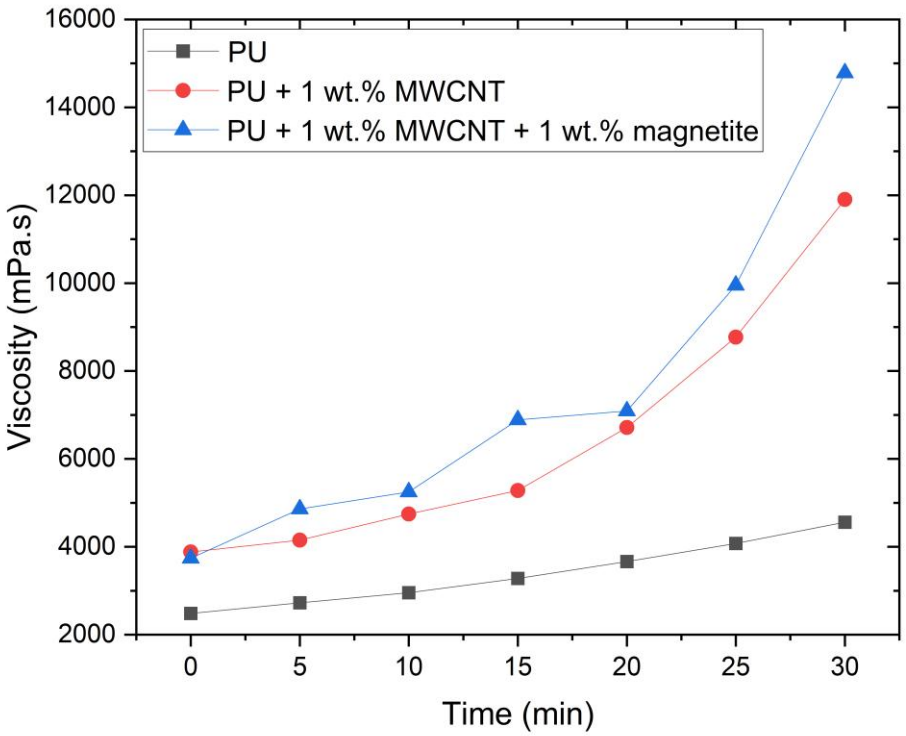

Figure 4.3- Characterization of the viscosity of the PU thermoset over time. The viscosity was analysed for pure PU and PU composites.

The magnetic properties of the individual particles used to prepare the composite, magnetite and MWCNT, were evaluated by SQUID magnetometry analysis. The SQUID analysis (Figure 4.4) shows that the MWCNT presents ferromagnetism and diamagnetism. This behaviour was explored in detail in previous work [19], where the magnetic response of the MWCNT was related to impurities from the fabrication process. Even though the MWCNT presents ferromagnetic properties, the values are relatively low compared to magnetite. The measured coercivity (Hc), retentivity (Mr), and saturation magnetisation (Ms) of the MWCNT at 300 K were 104.4 Oe, 0.2 emu/g, and 1.1 emu/g, respectively. For the magnetite powder, the measured coercivity (Hc), retentivity (Mr), and saturation magnetisation (Ms) at 300 K was 64.0 Oe, 4.6 emu/g and 83.7 emu/g, respectively. Since magnetite has higher magnetic susceptibility than MWCNT, the magnetic attraction between the permanent magnets and the magnetite particles will also be higher [29]. A higher magnetic susceptibility can result in faster movement of the particles towards the permanent magnets inside fluids of similar viscosity. Therefore, when MWCNT and magnetite particles are mixed in a solution, the magnetic patterning quality is expected to increase under a static magnetic field [21,29]. According to McCloskey *et al.* [29] the magnetophoretic mobility in magnetic separation depends on inherent characteristics of the magnetic particles and the medium, such as medium viscosity, particle size, and magnetic susceptibilities of both the medium and the magnetic particles. There are also various forces influencing particle movement in a liquid suspension, including magnetic forces, buoyancy, gravity, and drag forces.

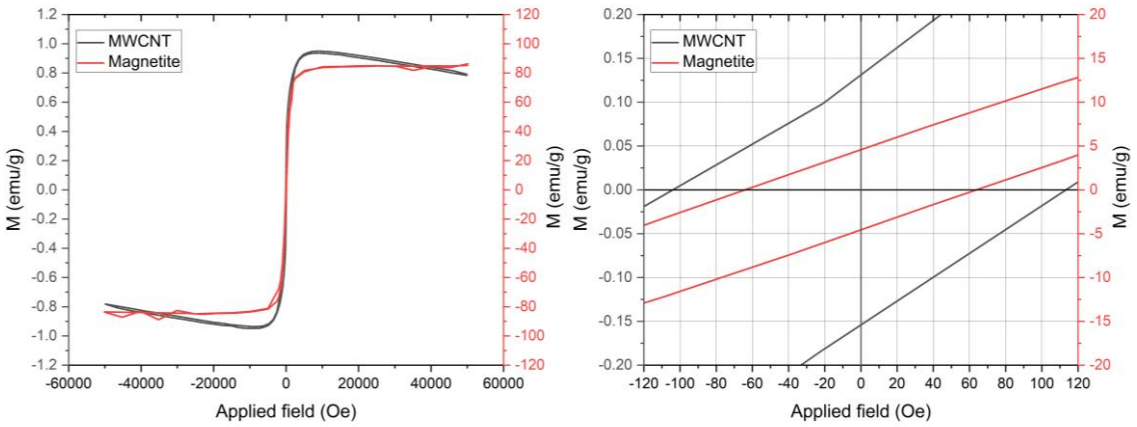

a) b)

Figure 4.4- SQUID analysis of the MWCNT and magnetite particles. a) From -50000 to 50000 Oe. b) From -120 to 120 Oe.

The interaction between the particles (MWCNT and magnetite particles) in a PU solution was assessed by OM analysis, carried out before and after 20 minutes of the cross-linking process under a static magnetic field (Figure 4.5). A comparison of Figure 4.5 a) and b) shows that, in the case of the composite with 1 wt.% MWCNT + 1 wt.% of magnetite, there is an alignment of the particles with the magnetic field lines, creating a “magnetic mesh/net” that drags the MWCNT in the direction of the permanent magnet. However, the composite with MWCNT only shows that the MWCNT are dragged in the direction of the permanent magnet without any perceptive alignment.

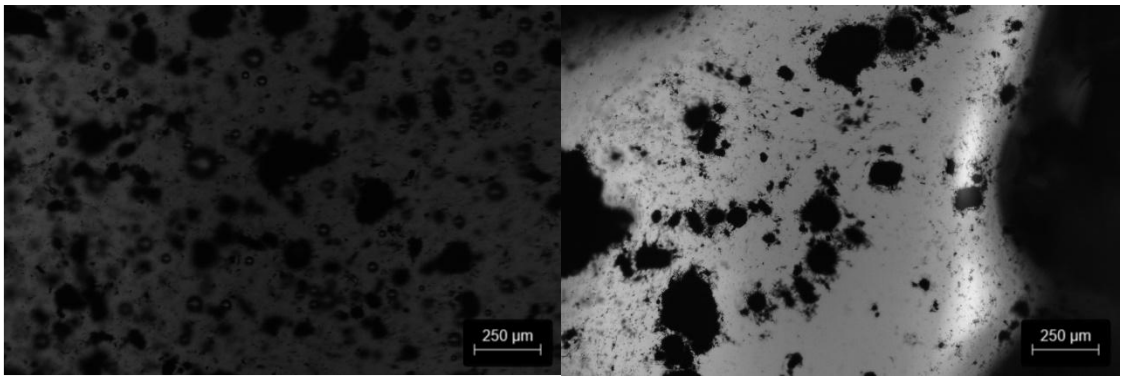

a)

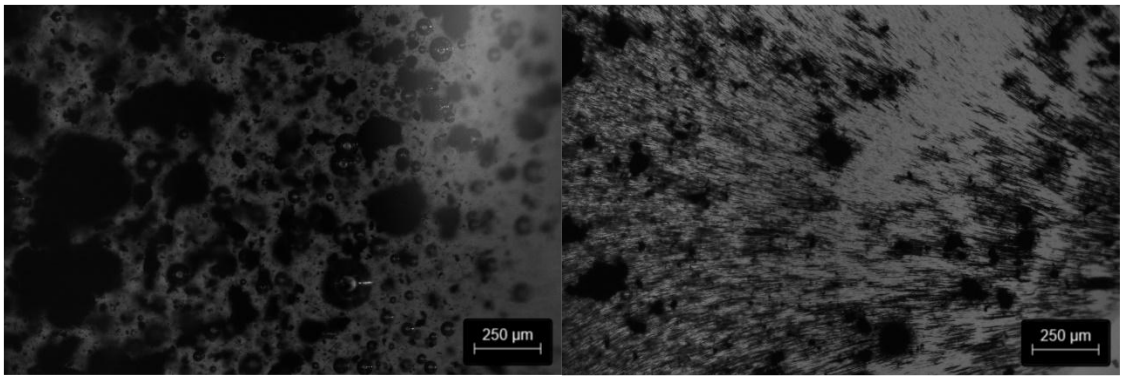

b)

Figure 4.5- OM analysis of the organisation of the particles over time under a static magnetic field. a) 1 wt.% of MWCNT and b) 1 % wt.% MWCNT + 1 % wt.% of magnetite. The images on the left were acquired before crosslinking and on the right 20 minutes after the crosslinking process started, under the applied magnetic field.

Figure 4.6 presents the magnetic characterisation performed on the permanent magnets array (Figure 4.6 a) to produce the magnetic patterns/electrodes. The magnets show a configuration of alternated polarity (Figure 4.6 b) and a magnetic flux density of approximately 260 mT for less than 1 mm between the probe and the magnet's surface. Figure 4.6 c) shows that the magnetic flux density between the north and south poles is quite symmetric since both poles present values around 260 mT, guaranteeing a good uniformity of magnetic field across the location of the electrodes.

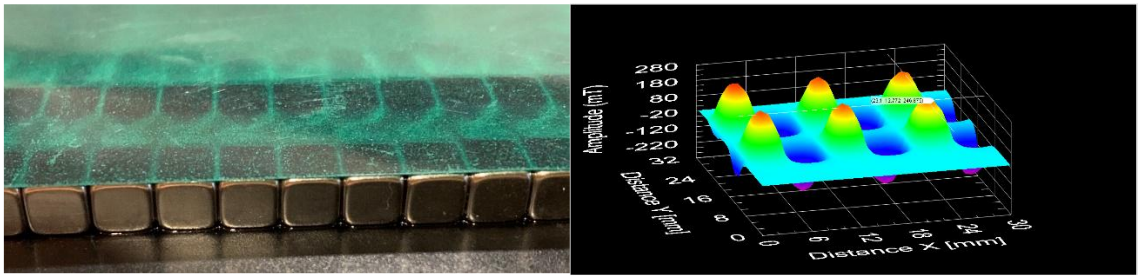

a) b)

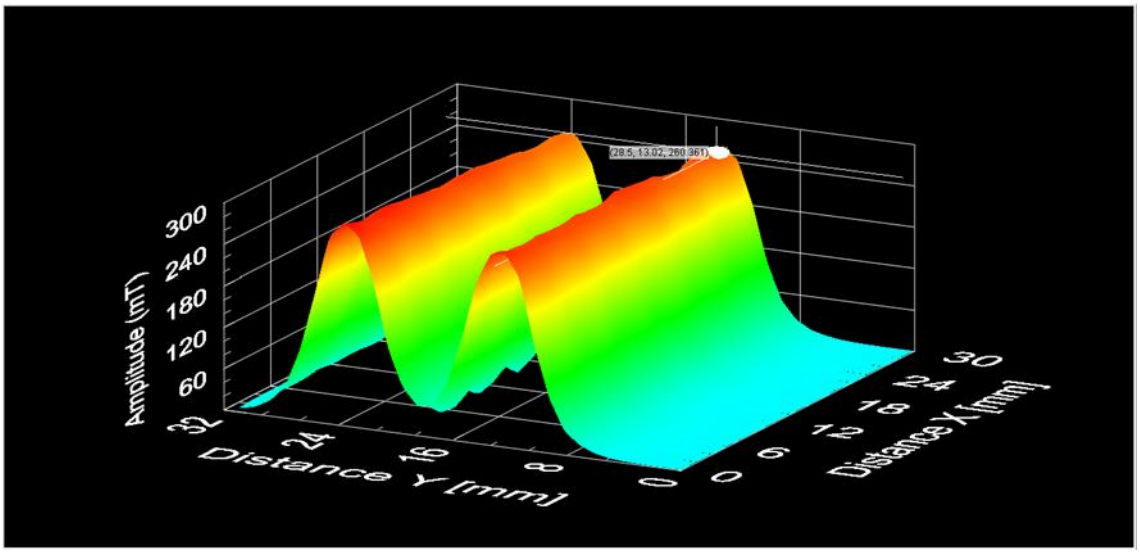

c)

Figure 4.6- Magnetic characterisation of the permanent magnets used for the magnetic patterning of the electrodes. a) Permanent magnets with a magnetic film. b) 3D north pole and south pole distribution in the Z axis. c) 3D symmetry analysis for the north and south poles in the Z axis.

4.3.2. Composite fabrication and characterisation

Figure 4.7 shows the longitudinal images of the magnet patterns (Figure 4.6 a)) created on the produced composite samples. A comparison of Figure 4.7 and Figure 4.6 c) shows a good match of the patterns formed with the applied magnetic field. The major difference between the three composites is the square patterns formed on 1 wt.% magnetite (Figure 4.7 b), which is related to the higher magnetic flux density on the edges of the magnets [19].

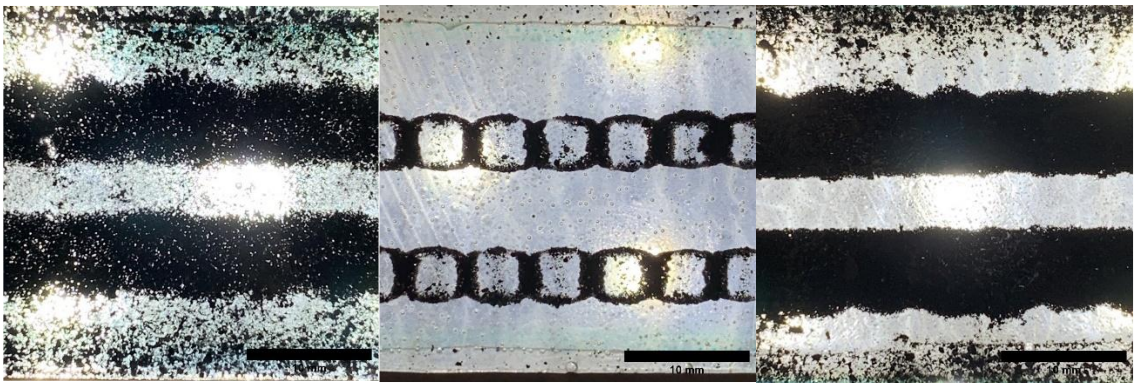

a) b) c)

Figure 4.7- Longitudinal images of the magnetic patterns created on the composite samples produced. a) 1 wt.% MWCNT/PU, b) 1 wt.% magnetite/PU and c) (1 wt.% MWCNT + 1 wt.% magnetite)/PU. (OM, transmission).

The longitudinal view of the samples presented in Figure 4.7, depicts the formation of two parallel patterns along the composites, forming the electrodes. The composite with 1 wt.% MWCNT (Figure 4.7 a)) differs from the other specimens (Figure 4.7 b) e c)), showing the presence of agglomerates of MWCNT between the parallel patterns, as well as apparent porosity inside the electrodes. These differences can be attributed to the small magnetic susceptibility of the MWCNT (Figure 4.4) and the increase in viscosity over time (Figure 4.3), hampering the movement towards the magnets. The composite with 1 wt.% magnetite (Figure 4.7 b) is more transparent due to the fast displacement of the particles with high magnetic susceptibility towards the magnets. Finally, Figure 4.7 c) shows the sample (1 wt.% MWCNT + 1 wt.% magnetite) depicting the two parallel patterns of conductive particles with significantly fewer MWCNT agglomerates between the electrodes and with higher MWCNT density along the electrodes. Thus, adding magnetite to MWCNT increases the composite's overall magnetic properties, dragging the MWCNT along the magnetic field, increasing the pattern quality.

OM cross-section analysis of the composites is presented in Figure 4.8. The images depict the side view (across the thickness) of one electrode of each composite (1 wt.% MWCNT, 1 wt.% magnetite and (1 wt.% MWCNT + 1 wt.% magnetite)). Comparison of Figure 4.8 a), b) and c) confirm that the MWCNT agglomerates do not align along the magnetic field. Instead, the low magnetic susceptibility MWCNT agglomerates are dragged toward the magnets.

Conversely, the composite with 1 wt.% magnetite (Figure 4.8 b)) presents the magnetic particles aligned in the magnetic field direction, and particles accumulate on the location of the permanent magnets. The sample with 1 wt.% MWCNT + 1 wt.% magnetite (Figure 4.8 c)) presents a mixture of both behaviours. The magnetite particles align with the magnetic field, and small agglomerates of MWCNT are dragged toward the magnets.

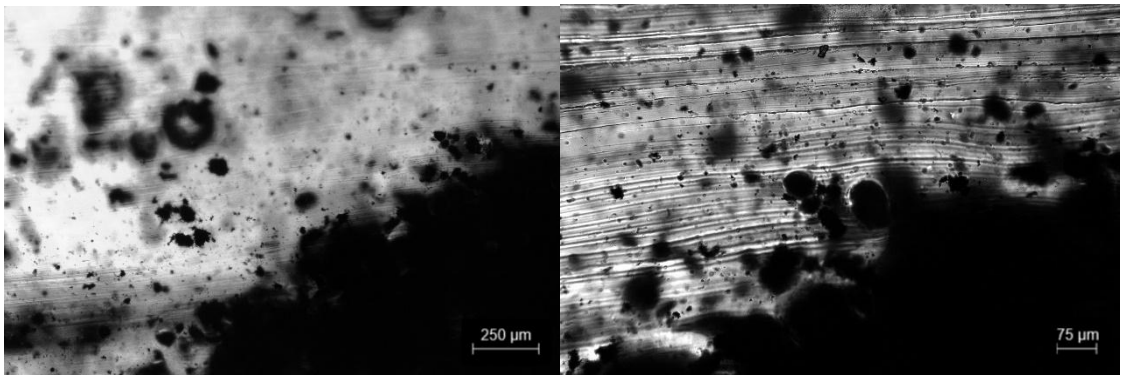

a)

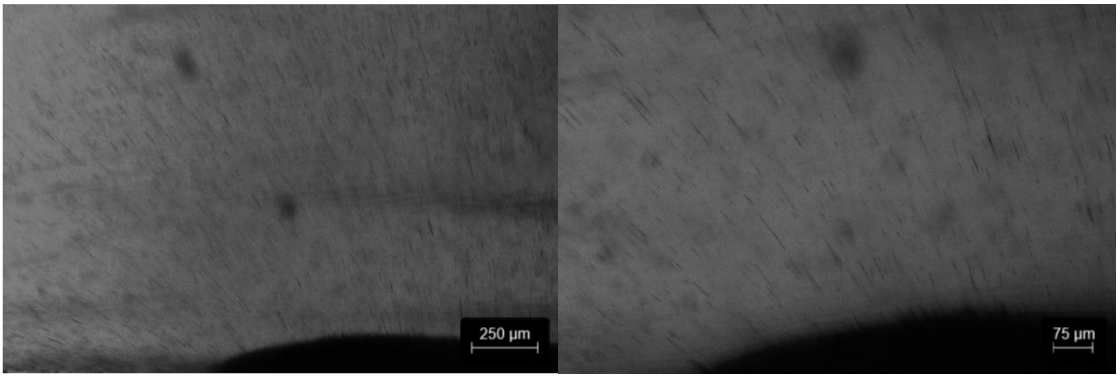

b)

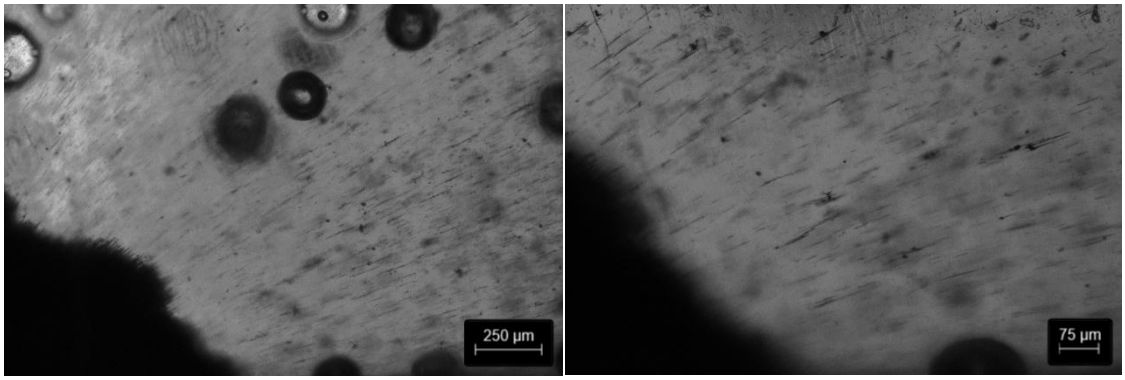

c)

Figure 4.8- Cross section images of the electrodes obtained by OM in transmission: a) 1 wt.% MWCNT/PU, b) 1 wt.% magnetite/PU and c) (1 wt.% MWCNT + 1 wt.% magnetite)/PU.

The distribution of the magnetite particles, MWCNT agglomerates and the combination of both inside the composites was analysed by micro CT, with a particular focus on the region close to the permanent magnets (formation of the electrodes in the composite). The micro CT images (Figure 4.9) highlight the location of high-density particles inside the polymer composite. Since the MWCNT density is slightly higher than the polymer, its location inside the matrix is difficult to identify (Figure 4.9 a). In contrast, the density of magnetite particles are much higher than the polymer and MWCNT, making it easier to localise in the composite (Figure 4.9 b). The results from OM and micro CT could be compared, showing that the composite with 1 wt.% of magnetite presents a similar magnetic pattern in Figure 4.7 b) (in the vicinity of one of the square permanent magnets) and Figure 4.9 b). Figure 4.9 c) depicts the composite formed by 1 wt.% MWCNT + 1 wt.% magnetite, showing the presence of the magnetite particles across the entire area close to the permanent magnet. The images show the distribution of magnetite particles and MWCNT agglomerates, indicating that their homogeneous mixture in the composite allowed a continuous distribution of both particles (MWCNT and magnetite particles) in the magnetic field generated by the permanent magnets. This continuous path of electrically conductive particles is expected to positively influence the quality of the electrodes formed in the composite.

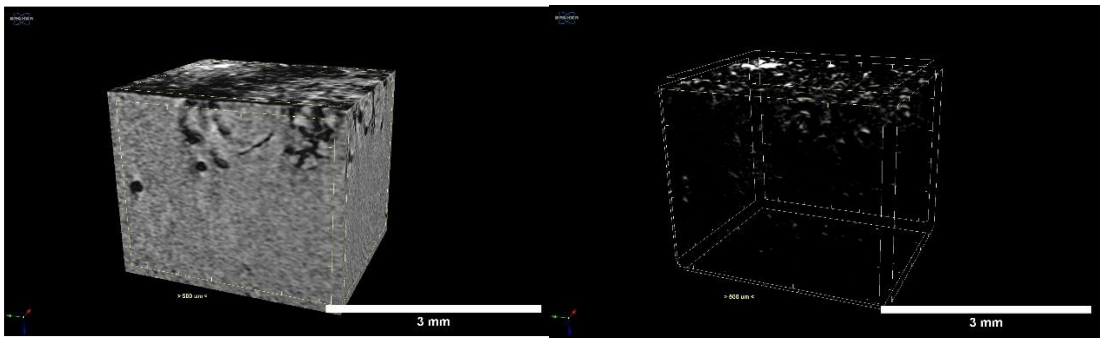

a)

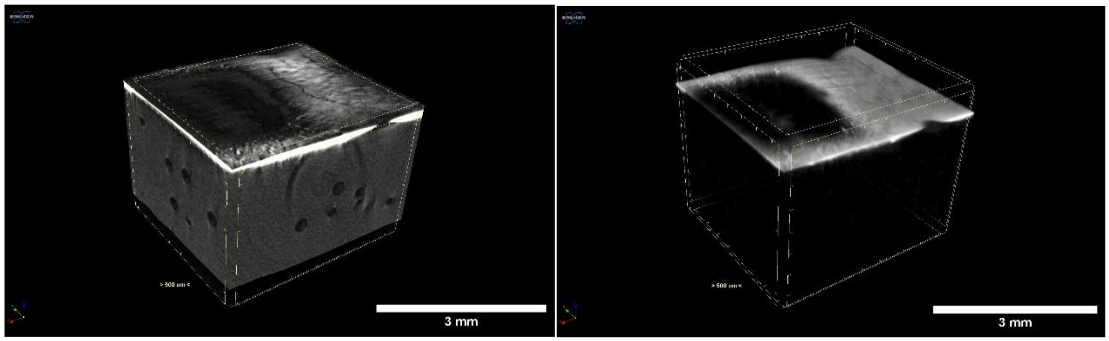

b)

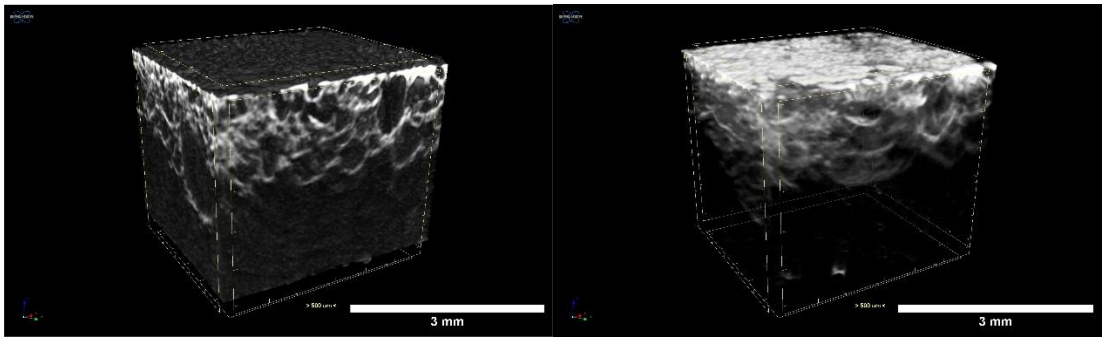

c)

Figure 4.9- Micro CT analysis of the particle distribution inside the PU matrix for a) 1 wt.% MWCNT/PU, b) 1 wt.% magnetite/PU and c) (1 wt.% MWCNT + 1 wt.% magnetite)/PU. The images on the left present the polymeric matrix and the particles, and the images on the right present just the particles.

The electrical resistance of each electrode formed in the composites was measured, and the results are presented in Figure 4.10. In this study it was confirmed that the electrical resistance measured for the composites with MWCNT and magnetite is attributed mainly to the MWCNT. When measuring composites with magnetite only, the electrodes were non-conductive, with an electrical resistance of $(13.8\pm3.4)\times10^{9}$ Ω. On the contrary, when measuring composites with MWCNT only, the electrical resistance of each electrode was

(8.8±3.0)x10^4 Ω. However, the interaction of the magnetite particles with the MWCNT agglomerates in the presence of a static magnetic field seems to increase the magnetic force exerted on the MWCNT, generating a "magnetic net" that drags the particles in the direction of the permanent magnet. As shown in the OM analysis (Figure 4.7 c)) and micro CT images (Figure 4.9 c)), the mixture (MWCNT plus magnetite particles) increases the concentration of conductive particles in the region of the static magnetic field, decreasing the electrical resistance of the electrode.

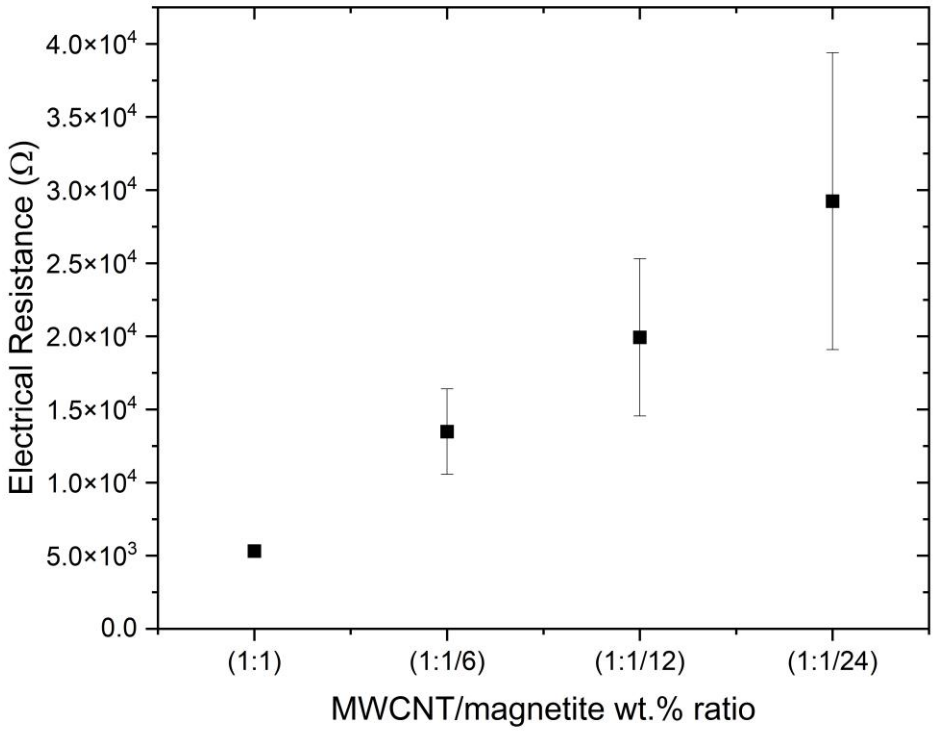

Figure 4.10- Electrical resistance of each electrode for composites with different ratios of magnetite added to 1 wt.% of MWCNT/PU.

A comparison of the electrical resistance of the composites with different ratios of magnetite added to 1 wt.% of MWCNT is plotted in Figure 4.10. A decrease in the weight percentage of magnetite is observed to increase the electrical resistance of the composites, although keeping them electrically conductive. The average electrical resistance measured for the electrodes of (1:1) composite (1 wt.% MWCNT + 1 wt.% magnetite) was (5.31±0.29)x10^3 Ω, while for the composite with 1 wt.% MWCNT + 0.04 wt.% magnetite (1:1/24) it increased to (29.2±10.1)x10^3 Ω. Therefore, a gradual decrease in the magnetite

content causes a gradual increase in both the electrical resistance and its standard deviation. Even though the composite with 1 wt.% magnetite is nonconductive, the addition of even a small amount of magnetite to MWCNT significantly decreases the electrical resistance and reproducibility of the fabrication process. The increase in the standard deviation of electrical resistance as the concentration of magnetite decreases is probably related to a decrease in the effectiveness of the “magnetic net” formed between MWCNT and magnetite in the composite. Decreasing the concentration of magnetite will hamper the continuous and homogeneous drag of the MWCNT agglomerates towards the permanent magnets, decreasing the concentration of the electrically conductive particles in their vicinity.

After the fabrication of the conductive composites with different magnetite concentrations added to 1 wt.% MWCNT, the composites were tested as triboelectric sensors. Figure 4.11 presents the result of the tests performed on triboelectric sensors composed of different MWCNT and magnetite ratios (1:1, 1:1/6, 1:1/12 and 1:1/24) with two different friction layers on top (PU and SR). Figures 4.11 a) and b) display a positive impact of the decrease in electrical resistance of the electrodes on the output voltage for the two friction layers tested. An increase of the triboelectric effect was also observed when the composition of the friction layer is different from the matrix polymer. For the combination of PU as the friction layer and as the polymeric matrix, the output voltage should be close to 0 V since it should not exist a flow of electrons between both materials during contact electrification. However, the fact that the PU samples still show some triboelectric effect could be associated with the interaction between the PU and the metallic parts of the tensile test machine tool under cyclic force [30].

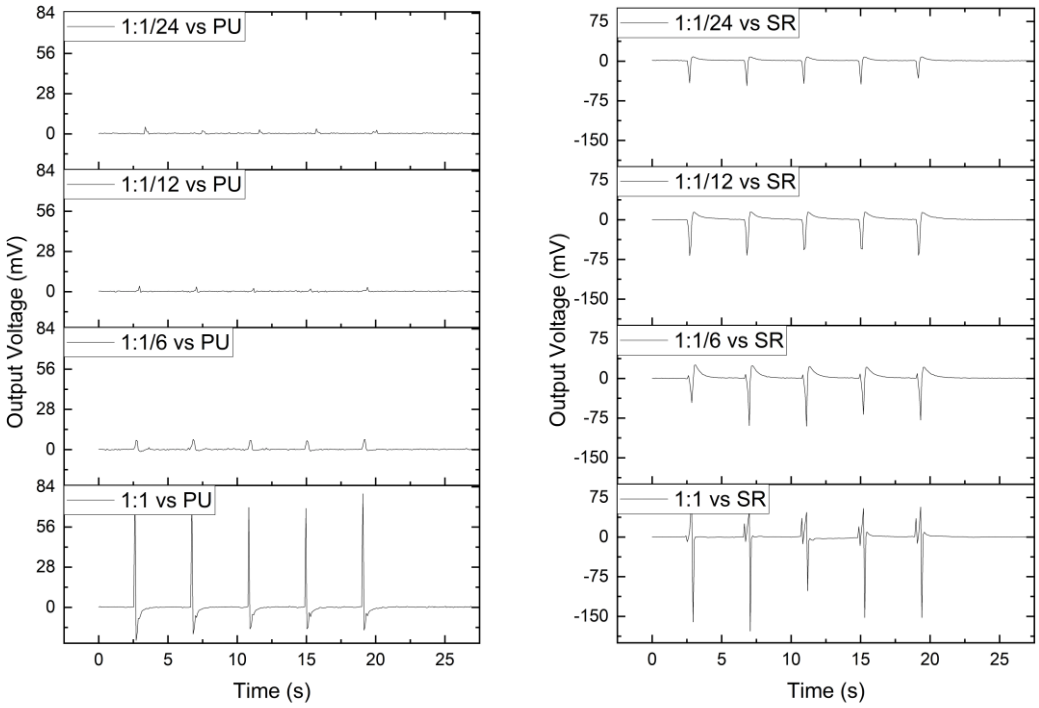

a) b)

Figure 4.11- Triboelectric sensor characterisation with a) a PU layer on top, compared with b) an SR layer on top.

The increase in the output voltage observed for the combination of PU with the SR may be interpreted as resulting from the tendency of the SR to attract electrons and the tendency of the PU to “give” electrons. When the surfaces of these materials contact each other, there is a flow of electrons that can be measured, and the opposite happens after the materials’ separation [31].

SR is a commonly used material in soft robotics applications, and, since it increases the output voltage of the triboelectric sensors, it was selected as the friction layer for the prototype.

4.3.3. Prototype development and testing

After characterising the triboelectric sensor, the next step was the design of an actuator that could be produced based on a PU rubber matrix and controlled by an Arduino Uno. Among the different types of soft robotics actuators, the tendon-driven actuator was selected, which bends the polymeric structure when a string is pulled (Figure 4.2). For the fabrication of the prototype presented in

Figure 4.12, two actuators and two micro servo motors were required. Then, the Arduino Uno was used to measure the triboelectric signal and control the micro servo motors. The developed system works by measuring voltage changes on the triboelectric sensor. Since the Arduino does not measure negative output voltage, the triboelectric sensor was connected to a 3.3 V power supply. The system working principle can be interpreted as a sum of signals, a direct current (DC) signal with an alternating current (AC) signal whenever the sensor works. This way, when an object touches the sensor, there is a peak that almost achieves 0 V (Figure 4.12 a). When the object is held by the actuator, there is no exchange of electrons between the materials, and the signal stays constant (Figure 4.12 b)). Finally, when the object is released from the actuator (Figure 4.12 c)), there is a positive peak achieving 5 V. By defining thresholds above and under 3.3 V, activating and deactivating the blue LED and the actuators was possible. The blue LED can be used to test the system without the actuators. The green LED is connected to the actuators, showing that the actuation system is on.

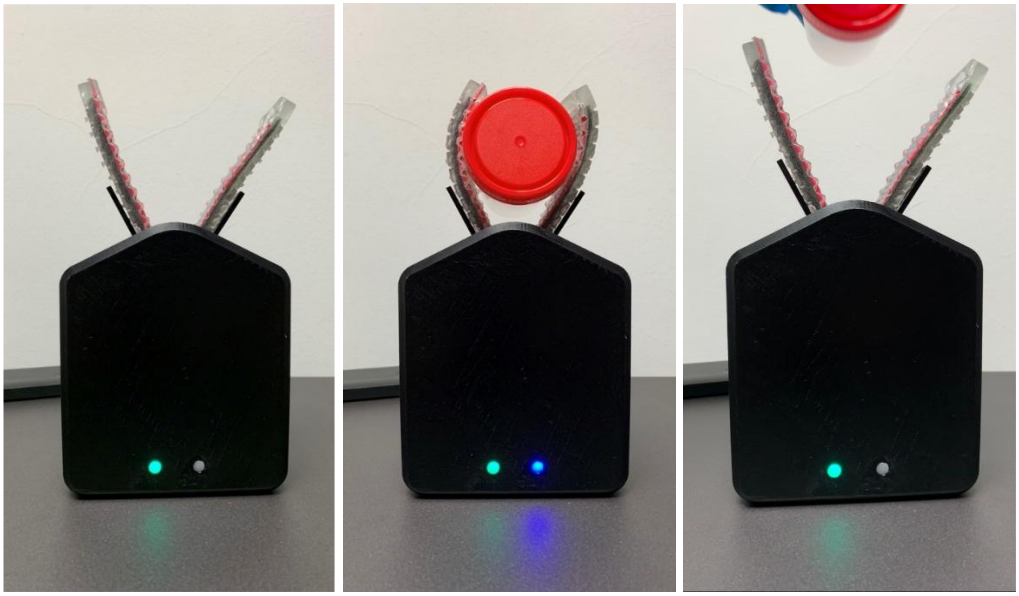

a) b) c)

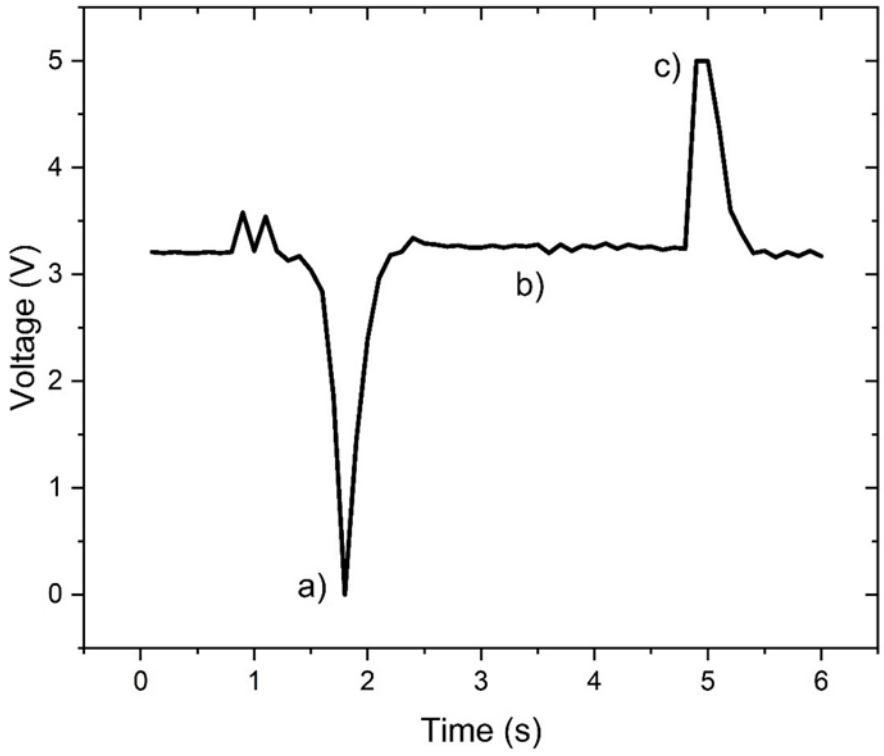

d)

Figure 4.12- Soft robotics prototype using a triboelectric sensor, a) catching, b) holding and c) releasing an object when pulled away. d) Output voltage signal at the three different stages.

The developed system successfully detects the presence of an object, closing its grip and grabbing it until it is pulled away from the gripper. When the system detects an opposite signal, the system automatically opens the grips. A

system that closes and opens automatically increases user interaction, which is useful for demonstration purposes. However, the sensor can be used as a preventive measure to detect problems on the soft robotic gripper, sending alerts to the user in case of slippage or malfunction.

4.4. Conclusions

This work reports the fabrication of low-cost triboelectric sensors using magnetic patterning. MWCNT and magnetite particles in a PU matrix formed the composites prepared for the magnetic patterning. During the curing of the PU, the MWCNT and magnetite particles were driven by a magnetic field to produce a pattern consisting of two parallel lines that formed the electrodes. These electrodes were used as triboelectric sensors, combined with SR friction layer. The developed sensors were integrated into a soft robotic actuator to demonstrate the applicability of the fabrication process.

The combination of magnetite with MWCNT increased the magnetic interaction of the filler particles with the magnetic field generated by the permanent magnets, leading to the good quality of the magnetic patterning in a viscous thermoset matrix, producing electrodes with low electrical resistance. A decrease in the electrical resistance of the electrodes produced based on MWCNT was observed with the addition of magnetite, as compared to electrodes with MWCNT alone. The effect of magnetite was that of a “magnetic net” that effectively dragged the MWCNT in the direction of the permanent magnets. This effect was illustrated by OM, observing the particles morphology along the PU cross-linking process, and by micro CT, which allowed the observation of the morphology of composites with 1 wt.% of MWCNT, 1 wt.% of magnetite, and a mixture of 1 wt.% of each (1:1). The addition of 1 wt.% of magnetite to 1 wt.% of MWCNT in the PU composite decreased the electrical resistance of the electrodes formed from $(88.5\pm30.9)\times10^3$ Ω to $(5.31\pm2.89)\times10^2$ Ω. The effect of reducing the wt.% of magnetite added to MWCNT was evaluated, showing that it increased the electrodes' electrical resistance and decreased the fabrication process reproducibility. Finally, it was observed that the composites with lower electrical resistance presented higher triboelectric properties. The combination of

PU and silicone rubber increased the output voltage under press and release motion, and this combination was used to develop a demonstration prototype.

The prototype consisted of a soft robotic grip with a sensor and actuator that could detect the presence of an object and close the grip automatically. The system automatically opens when the object is pulled away from the grip. The developed tendon-driven actuators were activated by two micro servo motors controlled by the developed triboelectric sensor.

The magnetic patterning process developed proved to be an effective method to decrease the electrical resistance of conductive patterns. This simple, versatile, low-cost method can be used to develop soft robotics solutions to monitor the interaction between the soft robot and external objects. Even though the presented prototype was developed for proof of concept only, it is possible to programme it for other applications, such as slippage detection, for the already available soft robotics in the food industry. It could also be used to develop smart prosthetics, making the movements and interaction with the objects more natural.

4.5. References

[1] Rus, D., & Tolley, M. T. (2015). Design, fabrication and control of soft robots. Nature, 521(7553), 467–475.

[2] Park, H. L., Lee, Y., Kim, N., Seo, D. G., Go, G. T., & Lee, T. W. (2020). Flexible neuromorphic electronics for computing, soft robotics, and neuroprosthetics. Advanced Materials, 32(15), 1903558.

[3] Kar, D., George, B., & Sridharan, K. (2022). A review on flexible sensors for soft robotics. Systems Printing Flexible Sensors, 1–15.

[4] White, E. L., Case, J. C., & Kramer, R. K. (2017). Multi-mode strain and curvature sensors for soft robotic applications. Sensors and Actuators A: Physical, 253, 188-197.

[5] Ren, L., Li, B., Wei, G., Wang, K., Song, Z., Wei, Y., ... & Liu, Q. (2021). Biology and bioinspiration of soft robotics: Actuation, sensing, and system integration. Iscience, 24(9).

[6] Zhang, Y., Li, P., Quan, J., Li, L., Zhang, G., & Zhou, D. (2022). Progress, challenges, and prospects of soft robotics for space applications. Advanced Intelligent Systems, 2200071.

[7] Verified Market Research. (2023). Soft robotics market. Retrieved May 7, 2023, from https://www.verifiedmarketresearch.com/product/soft-robotics-market/

[8] Terrile, S., Argüelles, M., & Barrientos, A. (2021). Comparison of different technologies for soft robotics grippers. Sensors, 21(9), 3253.

[9] Xie, M., Zhu, M., Yang, Z., Okada, S., & Kawamura, S. (2021). Flexible self-powered multifunctional sensor for stiffness-tunable soft robotic gripper by multimaterial 3D printing. Nano Energy, 79, 105438.

[10] Shintake, J., Cacucciolo, V., Floreano, D., & Shea, H. (2018). Soft robotic grippers. Advanced Materials, 30(29), 201707035.

[11] Wang, H., Totaro, M., & Beccai, L. (2018). Toward perceptive soft robots: Progress and challenges. Advanced Science, 5(9), 201800541.

[12] Chen, J., Han, K., Luo, J., Xu, L., Tang, W., & Wang, Z. L. (2020). Soft robots with self-powered configurational sensing. Nano Energy, 77, 105171.

[13] Jin, T., Sun, Z., Li, L., Zhang, Q., Zhu, M., Zhang, Z., ... & Lee, C. (2020). Triboelectric nanogenerator sensors for soft robotics aiming at digital twin applications. Nature communications, 11(1), 5381.

[14] Zhang, S., Zhang, B., Zhao, D., Gao, Q., Wang, Z. L., & Cheng, T. (2022). Nondestructive dimension sorting by soft robotic grippers integrated with triboelectric sensor. ACS Nano, 16(2), 3008–3016.

[15] Chen, S., Pang, Y., Yuan, H., Tan, X., & Cao, C. (2020). Smart soft actuators and grippers enabled by self-powered tribo-skins. Advanced Materials Technologies, 5(4), 201901075.

[16] Lee, Y., Song, W. J., & Sun, J. Y. (2020). Hydrogel soft robotics. Materials Today Physics, 15, 100258.

[17] Pagoli, A., Chapelle, F., Corrales-Ramon, J.-A., Mezouar, Y., & Lapusta, Y. (2022). Large-area and low-cost force/tactile capacitive sensor for soft robotic applications. Sensors, 22(11), 4083.

[18] Jang, H. G., Yang, B., Khil, M. S., Kim, S. Y., & Kim, J. (2019). Comprehensive study of effects of filler length on mechanical, electrical, and thermal properties of multi-walled carbon nanotube/polyamide 6 composites. Composites Part A: Applied Science and Manufacturing, 125, 105542.

[19] Esteves, D., Durães, N., Pedroso, R., Melo, A., & Pinto, M. (2023). Fabrication of low electrical percolation threshold multi-walled carbon nanotube sensors using magnetic patterning. Applied Sciences, 13(3), 1437.

[20] Gong, T., Peng, S. P., Bao, R. Y., Yang, W., Xie, B. H., & Yang, M. B. (2016). Low percolation threshold and balanced electrical and mechanical performances in polypropylene/carbon black composites with a continuous segregated structure. Composites Part B: Engineering, 99, 348-357.

[21] Wittmann, L., Turrina, C., & Steinmetz, S. (2021). The effect of pH and viscosity on magnetophoretic separation of iron oxide nanoparticles. Magnetochemistry, 7(6), 80.

[22] Huang, Y., Jiao, W., Niu, Y., Ding, G., & Wang, R. (2018). Improving the mechanical properties of Fe3O4/carbon nanotube reinforced nanocomposites by a low-magnetic-field induced alignment. Journal of Polymer Engineering, 38(8), 731–738.

[23] Wang, H., Jiang, H., Wang, S., Shi, W., He, J., Liu, H., & Huang, Y. (2014). Fe_3O_4–MWCNT magnetic nanocomposites as efficient peroxidase mimic catalysts in a Fenton-like reaction for water purification without pH limitation.

[24] Zheng, J., Zhang, M., Ling, Y., Xu, J., Hu, S., Hayat, T., ... & Yang, F. (2018). Fabrication of one dimensional CNTs/Fe3O4@ PPy/Pd magnetic composites for the accumulation and electrochemical detection of triclosan. Journal of Electroanalytical Chemistry, 818, 97-105.

[25] Zeng, X., Zhu, L., Yang, B., & Yu, R. (2020). Necklace-like Fe3O4 nanoparticle beads on carbon nanotube threads for microwave absorption and supercapacitors. Materials & Design, 189, 108517.

[26] Ghoderao, P., Sahare, S., Alegaonkar, P., Kulkarni, A. A., & Bhave, T. (2019). Multiwalled carbon nanotubes decorated with Fe3O4 nanoparticles for efficacious doxycycline delivery. ACS Applied Nano Materials, 2(1), 607–616.

[27] Arvand, M., & Hassannezhad, M. (2014). Magnetic core–shell Fe3O4@ SiO2/MWCNT nanocomposite modified carbon paste electrode for amplified electrochemical sensing of uric acid. Materials Science and Engineering: C, 36, 160-167.

[28] Dong, M., Tong, Z., Qi, P., & Qin, L. (2021). Enhanced electrical/dielectrical properties of MWCNT@Fe3O4/polyimide flexible composite

film aligned by magnetic field. Journal of Materials Science: Materials in Electronics, 32(1), 524–542.

[29] McCloskey, K. E., Chalmers, J. J., & Zborowski, M. (2003). Magnetic cell separation: Characterization of magnetophoretic mobility. Analytical Chemistry, 75(24), 6868–6874.

[30] Musa, U. G., Cezan, S. D., Baytekin, B., & Baytekin, H. T. (2018). The charging events in contact-separation electrification. Scientific reports, 8(1), 1-8.

[31] Li, Z., Zheng, Q., Wang, Z. L., & Li, Z. (2020). Nanogenerator-based self-powered sensors for wearable and implantable electronics. Research.

Chapter 5: Development of thermoplastic bi-component electrodes for triboelectric impact detection in smart textile applications

This chapter addresses the thesis's third objective: optimise thermoplastic material combinations to enhance composite properties. Achieving a balance between mechanical flexibility, electrical conductivity, and recyclability presents a significant challenge in flexible electronics. To address this, bi-component flexible conductive electrodes were developed, which were then used for triboelectric sensors. This approach demonstrated the potential of combining PP and TPE to overcome mechanical challenges, achieving the desired balance between electrical resistance and mechanical performance.

This article is part of the Special Issue Conductive and Magnetic Properties of Polymer Nanocomposites of Polymers, with reference: Esteves, D. S., Melo, A., Peliteiro, B., Durães, N., Paiva, M. C., & Sequeiros, E. W. (2025). Development of Thermoplastic Bi-Component Electrodes for Triboelectric Impact Detection in Smart Textile Applications. Polymers, 17(2), 210. https://doi.org/10.3390/polym17020210

Chapter 5: Development of thermoplastic bi-component electrodes for triboelectric impact detection in smart textile applications

Abstract:

Smart textiles provide a significant technological advancement, but their development must balance traditional textile properties with electronic features. To address this challenge, this study introduces a flexible, electrically conductive composite material that can be fabricated using a continuous bi-component extrusion process, making it ideal for sensor electrodes. The primary aim was to create a composite for the filament's core, combining MWCNTs, PP, and TPE, optimised for conductivity and flexibility. This blend, suitable for bi-component extrusion processes, exemplifies the role of advanced materials in combining electrical conductivity, mechanical flexibility, and processability, which are essential for wearable technology. The composite optimisation balanced MWCNT (2.5, 5, 7.5, and 10 wt.%) and TPE (0, 25, and 50 wt.%) in a PP matrix. There was a significant decrease in electrical resistivity between 2.5 and 5 wt.% MWCNT, with electrical resistivity ranging from $(7.6\pm4.0)10^{4}$ to $(1.1\pm0.1)10^{-1}$ Ω.m. Combining the composite with 25 wt.% TPE improved the flexibility, while with 50 wt.% TPE decreased tensile strength and hindered the masterbatch pelletising process. The final stage involved laminating the composite filament electrodes, with a 5 wt.% MWCNT/PP/ (25 wt.% TPE) core and a TPE sheath, into a textile triboelectric impact detection sensor. This sensor, responding to contact and separation, produced an output voltage of approximately 5 V peak-to-peak per filament and 15 V peak-to-peak with five filaments under a 100 N force over 78.54 cm^2. This preliminary study demonstrates an innovative approach to enhance the flexibility of conductive materials for smart textile applications, enabling the development of triboelectric sensor electrodes with potential applications in impact detection, fall monitoring, and motion tracking.

5.1. Introduction

Smart textiles offer responsive capabilities to external stimuli such as thermal, mechanical, chemical, electrical, magnetic, or optical changes. These materials interact intelligently with their surroundings, adapting to environmental changes with re-markable versatility [1–3]. The evolution of smart textiles has led to three distinct generations: passive smart textiles (first generation) that monitor environmental changes through sensors; active smart textiles (second

generation) that both sense and respond to stimuli; and highly intelligent textiles (third generation) that can react to and adapt to environmental conditions autonomously [4]. Smart textiles can be integrated into products using different methods, including weaving, knitting, embroidery, lamination, and braiding [4–7]. These integrated smart textiles have demonstrated trans-formative potential across diverse sectors such as healthcare, sports, automotive, aerospace, and military [8,9]. For example, in healthcare, wearable monitoring systems measure vital signs and perform gait analysis through capacitive or triboelectric sensing [10–13], while in the automotive and aerospace sectors, embedded sensor systems enhance safety [14,15].

Central to smart textile development is the selection of appropriate conductive materials [7,16,17]. MWCNTs have emerged as a particularly promising option, excelling in applications ranging from thermal regulation to electromagnetic shielding [18–21]. Their exceptional electrical conductivity and versatility have made MWCNT-based composites fundamental to sensor technologies, including piezoelectric, triboelectric, and thermoelectric devices [22–25]. These sensors have proven especially valuable in wearable technology and remote monitoring systems [26–29].

Within the field of passive smart textiles, triboelectric impact detection sensors have become increasingly necessary for real-time monitoring across various sectors. Healthcare applications include fall detection systems for elderly care [30,31], whilst aerospace implementations focus on damage detection from debris or collisions [32]. The effectiveness of these sensors depends on carefully calibrated operational parameters, including activation force thresholds and environmental condition tolerances [33].

This study advances the field of smart textiles, by introducing a novel approach for developing MWCNT-based triboelectric sensor electrodes, designed for continuous production and direct lamination within textile structures. By using optimised electrically conductive and flexible polymer composites, processed via bi-component extrusion melt spinning, it is possible to overcome some of the development limitations of conventional triboelectric devices, such as poor mechanical robustness, limited flexibility, insufficient environmental stability, and complex manufacturing processes [34,35]. Besides, this innovative approach provides a balanced solution, integrating a conductive core with a TPE

sheath that is compatible with low-temperature textile lamination processes, to ensure reliable adhesion for electrode integration.

5.2 Materials and Methods

The experimental process outlined in Figure S1 (supplementary materials), begins with the analysis of the electrical, mechanical, rheological, and thermal properties of polymer tapes containing varying weight percentages of MWCNT. To further enhance the mechanical properties of these composites, TPE was blended with PP. Once the optimal composite samples were identified, they were processed through a bi-component extrusion technique to produce sheath/core structured filaments. These filaments were subsequently laminated onto textile substrates, serving as electrodes for the fabrication of triboelectric sensors.

5.2.1 Materials

MWCNT were used as a PP masterbatch, containing approximately 20 wt.% of MWCNT, supplied by Nanocyl (PLASTICYL PP2001, Sambreville, Belgium). PP was bought from Repsol (ISPLEN PP 086, Madrid, Spain), while the thermoplastic elastomer (TPE) used was Vistamaxx 6202, supplied by ExxonMobil (Texas, USA). The polymer compatibilizer Exxelor, was sourced from The Compound Company (Enschede, Netherlands).

5.2.2 Tape Fabrication Process

Composites of PP/MWCNT were produced in a range of MWCNT concentrations aiming at electrical conductivity, from the early stages of electrical percolation to higher conductivity composites, based on previous experience and in the literature [3,36]. Thus, the weight % of 2.5, 5, 7.5 and 10 were selected for the PP composites preparation.

Seven distinct composites were synthesised using a twin-screw extruder to form and characterise the tapes. MWCNT masterbatch (PLASTICYL PP2001) with a nominal content of 20 wt.% MWCNT in PP was utilised by dilution to produce the different composites. The master batch was initially diluted with PP (ISPLEN PP 086) to achieve MWCNT concentrations of 2.5, 5, 7.5, and 10 wt.%

within the PP matrix. Subsequently, to enhance polymer flexibility, samples containing 5, 7.5, and 10 wt.% MWCNT in PP were blended with 25 wt.% TPE (Vistamaxx 6202). A final composition with 10 wt.% MWCNT and 50 wt.% TPE were also prepared by diluting the 20 wt.% MWCNT/PP masterbatch. Additionally, 2.5 wt.% of Exxelor PO 1020 was added to all samples to improve polymer compatibility.

The tapes were extruded using a co-rotating twin-screw extruder with L/D 25 (Rondol Technology Ltd, Staffordshire, UK) under specific conditions: temperature along the extruder was set at 200, 210, 215, 215, and 220 °C for screw zones 1 through 4 and the die, respectively. The drive torque was maintained at 40%, and the screw speed was 100 rpm. Extrusion was conducted using a flat die of 19 mm width and 0.7 mm thickness, and the tapes were collected using pulling rolls at constant speed.

5.2.3 Cross-section morphology analysis

Morphological analysis for the visualisation of the MWCNT distribution on the cross-section of the polymeric tapes was conducted using a Field Emission Gun Scanning Electron Microscope (FEG-SEM, NOVA 200 Nano SEM, FEI Company) in secondary electrons (SE) mode. Before analysis, specimens were cryo-fractured using liquid nitrogen and coated with a 1.5 nm film of Au-Pd (80-20 weight %) using a high-resolution sputter coater (208HR, Cressington Company), coupled with an MTM-20 High Resolution Thickness Controller (Cressington).

5.2.4 Mechanical properties

Tensile tests of the tapes were carried out to evaluate the impact of MWCNT and TPE on the mechanical properties of the composites. The tests were conducted on a Shimadzu AGX-V (Shimadzu Corporation, Kyoto, Japan) equipped with a 5 kN load cell and rubber-coated grips. The geometry of the test specimens was rectangular with 100 mm length, 10 mm wide and approximately 0.5 mm thickness, with a gauge length (L_0) of 30 mm. The tests were performed at a speed of 1000 mm/min and repeated three times for each composite.

5.2.5 Electrical properties

Electrical resistivity measurements for the composites were carried out using a two-point electrical resistance method, with a Keithley 6487 instrument (Keithley Instruments, Cleveland, OH, USA). To evaluate the electrical resistance of the electrodes, silver ink (CI 1036, EMS, Hatfield, PA, USA) was coated on the cross-section of the opposite sides of the composite. The length of each specimen was 25 mm, the width was 10 mm and the thickness was 0.5 mm. Therefore, the cross-section area of the silver electrodes was approximately 5 mm^2. Subsequently, the silver-coated composites were cured at 110 ºC for 20 minutes. Five replicates of each specimen composition were tested for statistical significance.

5.2.6 Rheological and thermal characterisation

Melt Flow Index (MFI) analysis was conducted to evaluate the influence of MWCNT and TPE on the flow of the composites. This analysis was carried out using a Ceast MF20 (Instron, Norwood, MA, USA), set at a temperature of 230 ºC, with a load of 2.16 kg and a pre-heating time of 120 seconds. To further investigate the impact of MWCNT on the composites' viscosity, loss, and storage modulus, oscillatory shear rheological analysis was performed. The tests were carried out on a Discovery HR 10 rheometer (TA Instruments, New Castle, DE, USA) at 230 ºC. The rheological properties were assessed using a parallel stainless-steel plate geometry, with the linear viscoelastic region determined through a stress sweep at a frequency of 1 Hz. Differential Scanning Calorimetry (DSC) analysis was performed to assess the effect of MWCNT and TPE on the composites melting temperature. The DSC was carried out on a DSC 214 instrument (Netzsch, Selb, Germany) over a temperature range from -40 to 300 ºC at a heating rate of 10 K/min.

5.2.7 Sheath/Core Extrusion Process

Bi-component filament extrusion was conducted using two extruders, namely, "A" for TPE and "B" for the composite, with temperatures at 196 ºC and 185 ºC, respectively. Each extruder is equipped with a melt pump that precisely

controls the volumetric throughput. Melt pump “A” has a flow rate of 0.6 cc per revolution, and was set at a velocity of 6 rpm, whilst melt pump “B” has a flow rate of 1.2 cc per revolution and was set at a velocity of 3 rpm. The transfer line temperature was maintained at 165 ºC, and the spinneret at 156 ºC. Spinneret pressures were 80 bar for extruder A and 119 bar for extruder B. The resulting filament consisted of a TPE sheath (extruder A) and a core comprising a 5 wt.% MWCNT/PP/TPE masterbatch, corresponding to a polymer blend of 25 wt.% TPE, 2.5 wt.% compatibiliser, and 67.5 wt.% PP. The lamination of the filaments onto commercially available knitted structures was achieved using a hot press at 130 ºC, 3 bar, for 2 minutes.

After extrusion and textile lamination, the filament characterisation was performed. Five filaments were tested and the dimensions of each filament were 25 mm in length and an internal diameter of approximately 250 µm. The electrical resistivity was measured using the same procedure and equipment described in 2.5, where silver ink was cured on each extremity of the composite to create a silver electrode in the cross-section of opposite sides of the composites. Finally, the cross-section of the bi-component structure was observed by optical microscopy (OM) on a Leica DM300 microscope (Leica Microsystems, Wetzlar, Germany) in transmission mode.

5.2.8 Triboelectric Sensor Development

For the triboelectric sensor, a metallic mould of squares with 1 cm side was positioned over the textile structure containing five laminated filaments. Silicone rubber (Ecoflex 00-30) was poured into the mould, forming 1 mm thick square shapes on top of the textile structure. Sensor testing consisted of applying a compression force of 100 N using a Shimadzu AGX-V equipped with two compression plates, 100 mm in diameter each, at 1500 mm/min speed. The output voltage signal generated by the sensor was recorded in single electrode mode using a B&K Precision model 2194 oscilloscope (B&K Precision Corporation, Yorba Linda, CA, USA) connected with a 10 MΩ probe.

5.3. Results and discussion

5.3.1 Cross section morphology analysis

The cryofractured surfaces of the composites prepared by twin screw extrusion were observed by SEM. Figure 5.1 shows the dispersed MWCNT for the composites with increasing MWCNT concentration for composites containing 2.5, 5 and 10 wt.% MWCNT. Figure 5.1 c), concerning PP/TPE blend, depicts good dispersion of the CNT and, at this magnification, does not show signs of PP/TPE phase separation, which can also be confirmed in Figure 5.2.

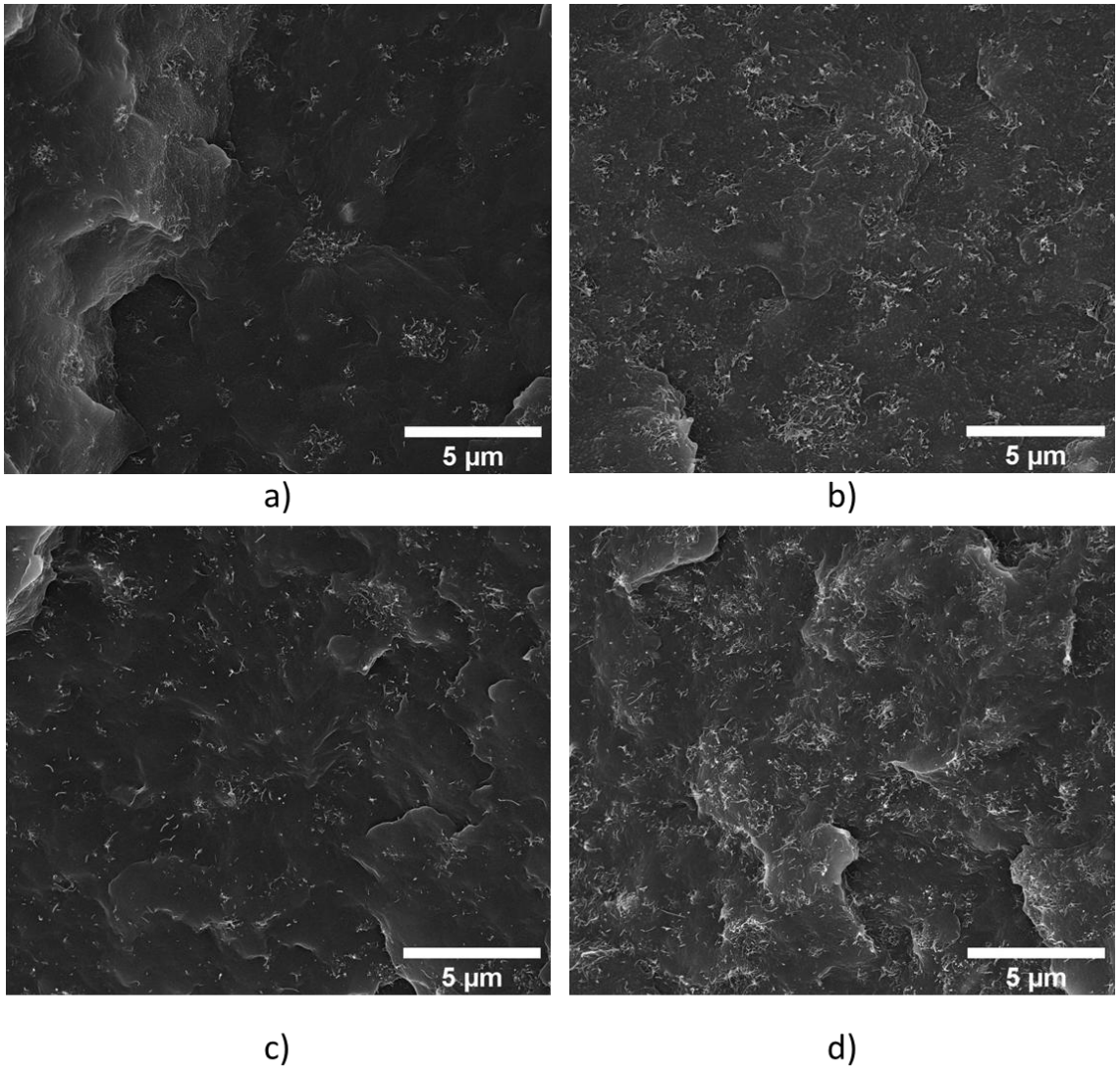

Figure 5.1- Cross section SEM images of the produced tapes: MWCNT distribution on composites with a) 2.5 wt.% MWCNT/PP; b) 5 wt.% MWCNT/PP; c) 5 wt.% MWCNT/PP/ (25% TPE) and d) 10 wt.% MWCNT/PP.

Figure 5.2 illustrates the cross-section of 5 wt.% MWCNT/PP and 5 wt.% MWCNT/PP/ (25% TPE) composites at different magnifications. At lower magnification, the individual MWCNT cannot be observed. However, the greyish spots detected with approximate diameters of 50 μm and below correspond to MWCNT agglomerates. At higher magnification, these agglomerates show a higher MWCNT concentration and entanglement.

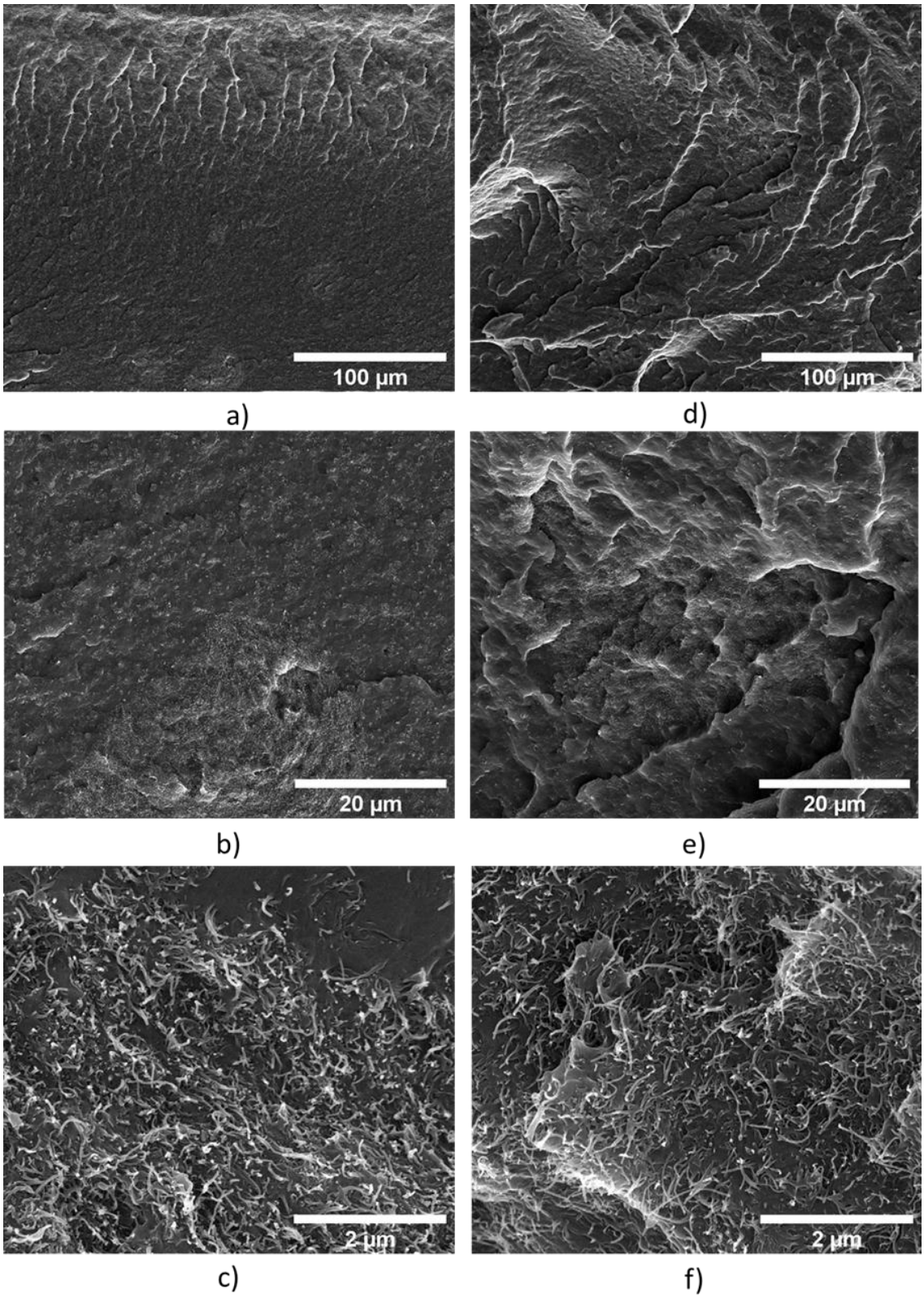

Figure 5.2- Cross section SEM images showing MWCNT agglomerates in composites tapes with 5 wt.% MWCNT, displayed at increasing magnifications from (a) to (c). Images (d) to (f) present composites of 5 wt.% MWCNT/PP with 25 wt.% TPE at the corresponding magnifications.

It is known that the presence of MWCNT agglomerates in the composites above a given concentration is detrimental to their mechanical properties, however it can be an advantage for the composite electrical conductivity. Thus, the tensile and electrical properties of the composites were measured to assess the extent of these effects.

5.3.2 Tensile properties

The tensile properties of all the composites prepared were assessed, and representative stress-strain curves are presented in Figure 5.3 a). Table 5.1 presents the tensile strength, elongation at break and Young's modulus calculated for the composites. Figure 5.3 a) illustrates the transition from brittle to ductile behaviour achieved with the addition of TPE and the increase in concentration in the blend [39].

Table 5.1-Summary of the mechanical and electrical properties of the composites. The tensile tests were performed at 1000 mm/min.

Sample	Tensile strength Rm (MPa)	Elongation at maximum load (%)	Young's modulus (MPa)	Electrical Resistivity (Ω.m)
2.5 wt.% MWCNT/PP	22.6±0.8	9.9±0.2	240.4±37.0	(7.6±4.0) $x10^{4}$
5 wt.% MWCNT/PP	21.1±2.5	9.7±0.2	226.5±29.0	(1.1±0.1) $x10^{-1}$
7.5 wt.% MWCNT/PP	21.1±2.3	9.1±0.9	230.8±37.5	(2.2±0.1) $x10^{-2}$
10 wt.% MWCNT/PP	24.8±2.1	9.2±1.1	220.5±42.3	(9.8±0.4) $x10^{-3}$
5 wt.% MWCNT/PP/ (25% TPE)	21.1±1.6	21.0±0.8	153.2±3.5	(1.0±0.5) $x10^{-1}$
7.5 wt.% MWCNT/PP/(25% TPE)	21.8±0.9	29.9±1.4	110.6±16.3	(2.7±0.1) $x10^{-2}$
10 wt.% MWCNT/PP/ (25% TPE)	24.4±0.2	26.8±0.9	117.5±25.5	(1.5±0.3) $x10^{-2}$
10 wt.% MWCNT/PP/(50% TPE)	15.7±0.2	51.8±5.8	68.7±17.2	(7.2±0.3) $x10^{-3}$

The MWCNT/PP composites display brittle behaviour, even at a low MWCNT concentration, resulting from the presence of MWCNT agglomerates and the high stiffness of the nanotubes. The composites of MWCNT/PP present tensile strength ranging from 21.1±2.5 to 24.8±2.1 MPa and elongation at maximum load (Rm) ranging from 9.0±0.8 to 9.8±0.2%. Interestingly, under the test conditions, it is observed that the tensile properties of the composites are not sensitive to composition. This is expected since nanocomposites present agglomerates with weaker bonding to the polymer which act as regions of stress concentration. At high deformation rates there is no time for plastic deformation in the polymer to reduce stress concentrations, failure occurring due to the localised stress concentration effects. These effects are associated to the presence of nanoparticle agglomerates, which are common to all the composite concentrations.

Conversely, incorporating TPE into the MWCNT/PP composite enhances the ductility of the composites. The elongation at break significantly increases to

double or triple with the addition of 25 wt.% TPE. The 10 wt.% MWCNT/PP/TPE blend with 50 wt.% of TPE has the highest ductility with average tensile strength and elongation at maximum load of 15.7±0.2 MPa and 51.8±5.8 %, respectively. However, the rubber-like behaviour of the composites with high TPE content presents additional challenges, such as cutting the extruded tape during the composite preparation for subsequent extrusion processes. Reducing the TPE content to 25 wt.% solved these processing limitations for the three different MWCNT concentrations (5, 7.5, and 10 wt.%) prepared. The results indicate an increase in ductility for all compositions compared to the MWCNT/PP composites. The tensile strength of the blends containing 25 wt.% TPE tapes was comparable to that of MWCNT/PP composites. The elongation at break for these blends increased significantly, in the case of 7.5 wt.% MWCNT, the elongation at break more than tripled, increasing from 9.1% to 29.9%, corresponding to an approximate 330% improvement. These mechanical characteristics are particularly beneficial for laminating the tapes onto the textile substrates, warranting a flexible and seamless integration.

In summary, in the present work the aim was to test PP/MWCNT composites at deformation rates that lead to a brittle stress-strain response, and test the composite blends with TPE under these extreme conditions. This allowed to identify that using TPE leads to an increased ductile response of the composite blends, relative to the PP/MWCNT composite alone. The results demonstrate the benefits of incorporating 25 wt.% TPE to enhance the ductility of PP/MWCNT composites, which is particularly relevant for application in textiles.

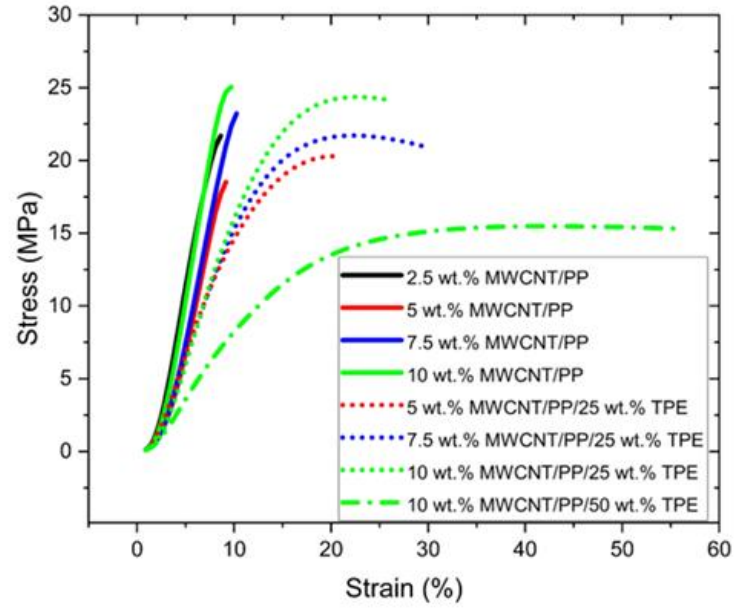

a)

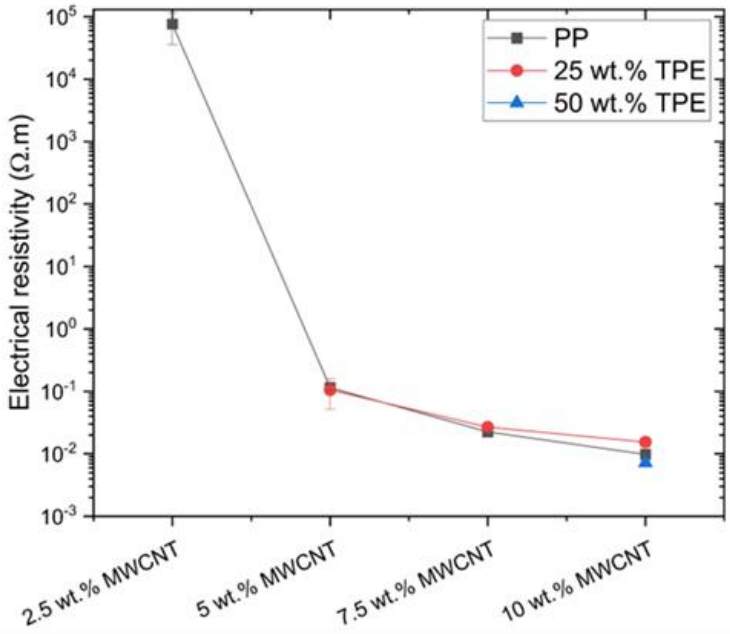

b)

Figure 5.3- a) Representative stress-strain curves of all the PP/MWCNT and MWCNT/PP/TPE composites tested at a speed of 1000 mm/min. b) Electrical resistivity of the MWCNT/PP composites and their TPE blends.

5.3.3 Electrical properties

Table 5.1 and Figure 5.3 (b) summarise the electrical properties of the composites. The electrical percolation threshold for the MWCNT/PP composites is observed near 2.5 wt.% MWCNT, as the resistivity of pure PP is reported to be approximately 10^{16} Ω.m, indicating its insulating nature. At 2.5 wt.% MWCNT, the resistivity is considerably reduced but remains relatively high due to the low MWCNT content, which is insufficient to form a large number of continuous conductive pathways for electrons to flow.

Above the percolation threshold, the electrical resistivity decreases significantly, ranging from $(7.6\pm4.0)\times10^{4}$ Ω.m to $(9.8\pm0.4)\times10^{-3}$ Ω.m for compositions with MWCNT content from 2.5 wt.% to 10 wt.%. This sharp reduction in resistivity reflects the formation of a robust conductive network built on MWCNT bridging. However, as the MWCNT content increases beyond the percolation threshold, the rate of resistivity reduction decreases, suggesting that additional MWCNTs contribute less to further enhancing conductivity once a sufficient conductive network is established [40].

Notably, the electrical properties of the PP/TPE blends are similar to those of pure PP composites. Thus, the miscibility of the polymers does not affect the electrical conductivity, meaning that the conductive network of MWCNTs is not affected by TPE blending. The morphological analysis presented in Figure 5.2 shows that the blend with TPE forms a homogeneous material, without phase separation, and that the MWCNT continue to be well dispersed. The increase in MWCNT content improves conductivity consistently for both PP and its TPE blends.

Given that TPE does not influence electrical resistivity but significantly enhances mechanical flexibility, particularly at 25 wt.% TPE, the composite with 5 wt.% MWCNT/PP/25 wt.% TPE emerges as a good choice since it provides low resistivity while maintaining enhanced flexibility. Further increase in MWCNT content (e.g., to 7.5 wt.% or 10 wt.%) does not significantly decrease the electrical resistivity.

5.3.4 Rheological characterisation

One of the objectives of this work was to prepare a flexible bicomponent filament with an electrically conductive core and an insulating sheath. This outer layer encapsulates the inner conductive composite core preventing short circuits and allowing the filament's lamination into textile structures while protecting the integrity of the conductive core. To facilitate the lamination process, the sheath polymer was selected with a low melting temperature. Additionally, manufacturing bicomponent filaments with a core/sheath morphology requires polymers with different melt viscosity for the core and sheath. Typically, the core material should have a higher melt viscosity than the sheath material under the filament processing conditions [41]. Thus, within an acceptable range, the composite core should have a lower MFI than the sheath polymer.

The MFI was measured for the polymers and composites, showing a large reduction of the MFI of the composites relative to the pure polymers. While the PP and TPE presented an MFI of 25 and 20 g/10 min, respectively, the MFI of the PP composites with 2.5 and 5 wt.% of MWCNT decreased to 15 and 5 g/10 min, respectively. Composites with higher MWCNT content did not flow under a 2.16 kg load and, thus, were not selected for the bi-component extrusion process. The MFI drop for the composites is a consequence of the formed MWCNT network, hindering the polymer flow, and it is comparable with the results reported by Stanciu *et al.* [37]. The composites with 5 wt.% MWCNT/PP and 5 wt.% MWCNT/PP/TPE exhibit similar MFI of 5 g/10 min, thus suggesting comparable flow characteristics. These results were confirmed by oscillatory rheology, illustrated in Figure 5.4, showing a viscosity increase with increasing MWCNT content, particularly at low frequencies. The network formed by increasing MWCNT content creates physical barriers that restrict the polymer chains through Van der Waals interactions and entanglements. The shear-thinning behaviour of the composites, evidenced by the decrease in complex viscosity with frequency, can be attributed to the breakdown of the MWCNT network and the subsequent alignment of both the MWCNTs and polymeric chains, which reduces viscosity [36,37]. The viscosity of PP exhibits a similar trend, although less pronounced, which reinforces that the shear-thinning behaviour can also be attributed to the alignment of the polymeric chains.

Storage and loss modulus analysis reveals that TPE inclusion slightly increases the storage modulus, indicative of enhanced elasticity while maintaining a similar loss modulus. The viscoelastic behaviour of MWCNT/PP composites, especially at higher MWCNT concentrations, suggests enhanced stiffness due to the denser MWCNT network, which constrains PP chain mobility. Conversely, the 2.5 wt.% MWCNT composite, closer to the PP viscoelastic response, presents G'' slightly higher than G', possibly indicating insufficient MWCNT dispersion, allowing for dominant viscous flow. The presence of MWCNT agglomerates is illustrated in the SEM images in Figure 5.1 and Figure 5.2.

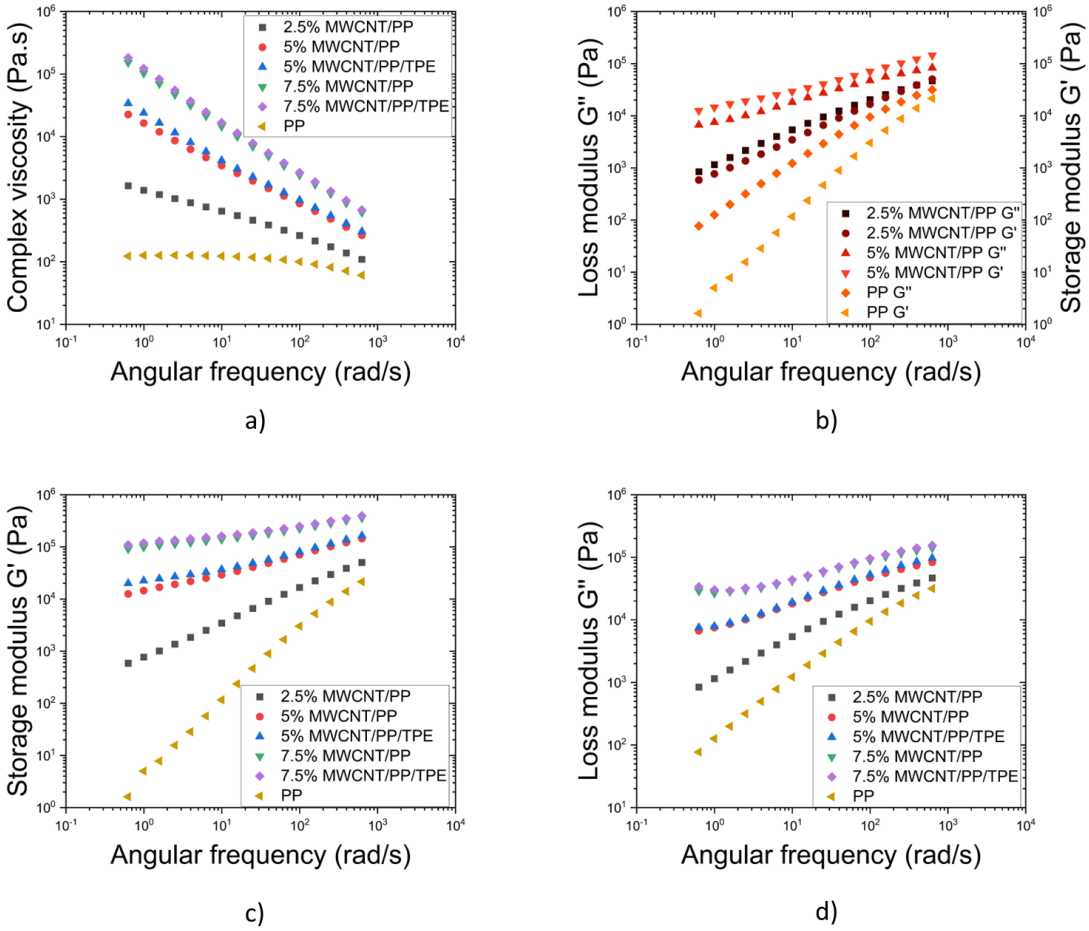

Figure 5.4- Rheology results for PP, 2.5, 5 and 7.5 wt.% MWCNT composites a) complex viscosity; b) storage modulus and loss modulus for MWCNT/PP composites; c) storage modulus and d) loss modulus for MWCNT/PP and MWCNT/PP/TPE composites;

In summary, the rheological behaviour of the composites highlights the influence of MWCNT content on viscosity and viscoelastic properties. The increase in viscosity at higher MWCNT loadings is attributed to the formation of

a dense MWCNT network, which limits the mobility of polymer chains [37]. At lower MWCNT concentrations, insufficient dispersion leads to dominant viscous flow, as evidenced by the slightly higher loss modulus (G″) compared to the storage modulus (G′) and supported by SEM images showing MWCNT agglomerates. Therefore, by combining the mechanical, electrical, and rheological analyses, it was determined that the most suitable composite is 5 wt.% MWCNT/PP/25 wt.% TPE. This composition offers enhanced mechanical and electrical performance while exhibiting rheological behaviour compatible with bi-component extrusion processes. Additionally, the inclusion of 25 wt.% TPE did not negatively impact the properties compared to MWCNT/PP samples.

5.3.5 Thermal characterisation

DSC analysis was conducted to investigate the impact of MWCNT on the thermal properties of the PP matrix and to evaluate the thermal properties of the composite blend with TPE. Specifically, it is important to assess the melting temperature of the pure polymers, their MWCNT composites and polymer/composite blend.

Two PP/MWCNT composite concentrations, 5 wt.% and 10 wt.%, were selected for this study. The influence of blending 25 wt.% of TPE with the PP/MWCNT composites was studied for the 5 wt.% MWCNT/PP/TPE blend. The thermograms are presented in Figure 5.5, consistent with the amorphous nature of TPE and allowing the measurement of the melting enthalpy of the PP, showing a melting temperature near 163.5 °C.

The melting temperature of the PP composites with 5 wt.% and 10 wt.% MWCNT were 166.6 °C and 166.7 °C, respectively, showing a slight increase relative to the pure polymer, however invariant with MWCNT concentration (within the concentration range studied). These results for the MWCNT/PP composites, are consistent with those reported by Stanciu *et al*. [37]. Blending 25 wt.% TPE with 5 wt.% MWCNT/PP composite slightly reduced the melting temperature to 165.7 °C, only 1 °C lower than the 5 wt.% MWCNT/PP alone, indicating the limited impact of MWCNTs and TPE on the crystalline structure of PP within the studied concentration range (Table 5.2). TPE is an amorphous polymer thus, above the glass transition temperature (Tg) its free volume continuously

increases, and the polymer decreases the viscosity until it becomes a polymer melt. TPE transforms into a melt at a lower temperature than PP, its composites and the 5 wt.% MWCNT/PP/TPE composite blend. This is important for the lamination process of the bicomponent filaments, performed at 130 °C, thus allowing the melting of the outer TPE layer of the filament while preserving the integrity of the composite core.

The crystallinity calculation was based on the enthalpy of fusion for the different samples and the fraction of the enthalpy of fusion of pure PP in each sample. For the calculations, an enthalpy of fusion of 209 J/g for pure PP was assumed [37].

The degree of crystallisation was calculated using the following equation:

$$\chi(\%) = \frac{\Delta \mathrm{Hm}}{\Delta \mathrm{H0} \cdot (1 - \varphi)} \cdot 100\%$$

Where ΔHm is the melting enthalpy of the sample, $\Delta H0$ is the melting enthalpy of 100% crystalline PP (209 J/g for PP) and φ is the weight fraction of MWCNTs and TPE.

According to the results presented in Table 5.2, pure PP exhibited a crystallinity of 54.8%, and the incorporation of 5 and 10 wt.% MWCNTs did not significantly affect its crystallinity. The addition of 25 wt.% TPE to a composite with 5 wt.% MWCNT resulted in a slight increase in crystallinity, reaching 59.0%, consistent with the tendencies found by Lu *et al*. [27]. This increase in crystallinity can be attributed to Vistamaxx's (TPE) ability to improve the compatibility between the composite materials. This improved compatibility facilitates better alignment and ordering of PP molecules, improving crystallization.

Table 5.2- Summary of the DSC results.

Sample	Onset temperature (ºC)	Peak temperature (ºC)	Enthalpy of fusion (J/g)	Crystallinity (%)
PP	157.9	163.5	114.5	54.8
5 wt.% MWCNT/PP	148.6	166.6	108.8	54.8
5 wt.% MWCNT/PP/25wt.% TPE	152.6	165.7	86.32	59.0
10 wt.% MWCNT/PP	148.9	166.7	103.6	55.1

Therefore, among the tested samples, the 5 wt.% MWCNT/PP/TPE blend was identified as an adequate core material, offering a balance of thermal stability, crystallinity, and processing compatibility. With a melting temperature above 150 °C, it provides the thermal performance required for lamination processes without compromising structural integrity, making it ideal for flexible and stable textile applications. Pure TPE was selected for the outer layer of the bi-component filament due to its low melting point, ensuring compatibility with textile lamination at 130 °C while preserving the core's structure.

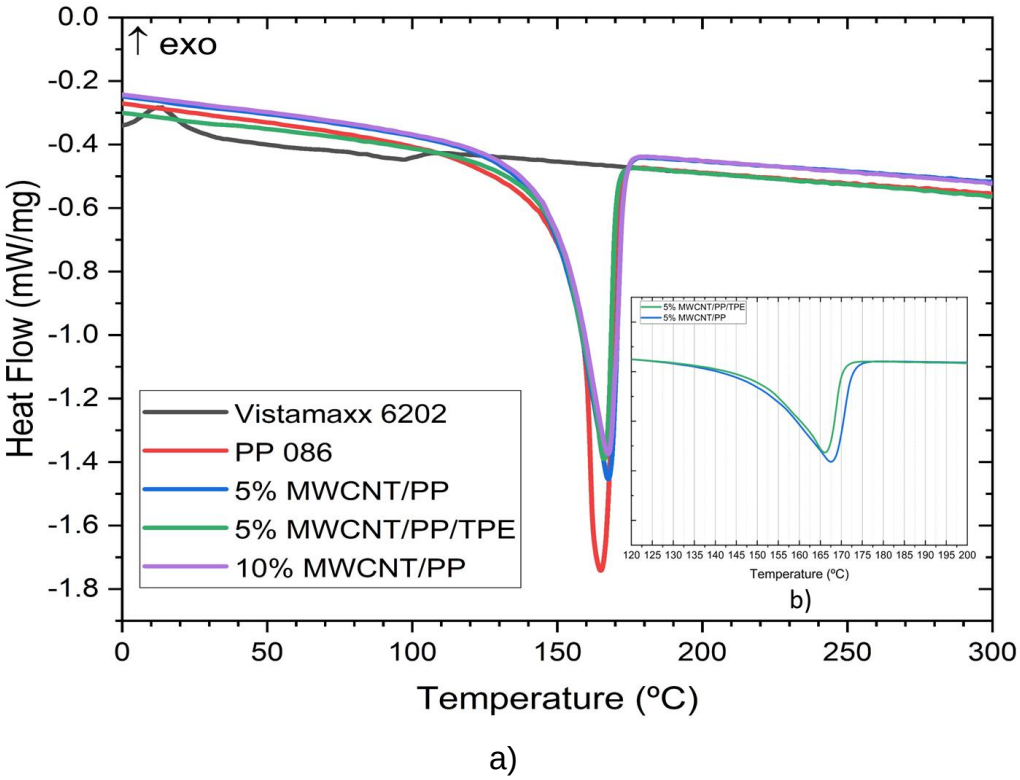

Figure 5.5- a) DSC results for TPE, PP, 5 wt.% MWCNT/PP, 5 wt.% MWCNT/PP/TPE and 10 wt.% MWCNT/PP; b) representation of the melting temperature for each 5 wt.% MWCNT composite.

5.3.6 Bi-component electrode integration and triboelectric sensor testing

The analysis of the composite blends provided a comprehensive evaluation of their mechanical, electrical, rheological, and thermal properties, enabling the selection of the optimal core and sheath materials for the bi-component filament extrusion process. Among the tested materials, the 5 wt.% MWCNT/PP/TPE composite blend with 25 wt.% TPE emerged as the best choice for the core. This selection was justified by the balance it offered across all critical performance metrics. Electrical resistivity results showed that increasing MWCNT content from 2.5 wt.% to 5 wt.% significantly reduced resistivity due to the formation of an electrically conductive network, while higher concentrations (e.g., 7.5 and 10 wt.%) increased viscosity, which limited the processability required for filament extrusion. In addition, the mechanical testing revealed that the inclusion of 25 wt.% TPE improved flexibility and reduced brittleness, which is critical for wearable applications under dynamic conditions. Thermal analysis further

confirmed that the addition of TPE did not adversely affect the melting temperature or structural integrity of the composite core, making it compatible with the lamination process at 130 °C. The core of the filaments was therefore formed with the 5 wt.% MWCNT/PP/TPE (with 25 wt.% TPE) composite blend, while the sheath was based on pure TPE.

Subsequent electrical testing of the bi-component filaments showed similar resistivity to the composite blends. The bi-component filament and the extruded tape with the same composition presented electrical resistivities of $(3.1\pm1.0)x10^{-1}$ Ω.m and $(1.0\pm0.5)x10^{-1}$ Ω.m, respectively. Thus, the filament processing and the decrease in cross-section did not hinder the electrical resistivity.

Then, a hydraulic hot press was used to melt the TPE sheath of the filaments against the textile structure for the smart textile integration. Since TPE softens at temperatures above 50 °C and the core melts above 160 °C, the fibre core keeps its integrity by performing the lamination process at 130 °C. In contrast, the sheath of the fibre melts and attaches to the textile surface. This can be observed in the optical images presented in Figure 5.6 (a), where the core is cylindrical and the TPE presents a rectangular shape due to the applied pressure during lamination.

Finally, to perform a preliminary demonstration of an application of these structures, a triboelectric sensor was used to detect impacts through contact and separation, as demonstrated in Video S2 in the supplementary materials. The bi-component sensor electrodes were integrated into the textile structure by lamination, and the textured silicone rubber was cured on top of the textile structure and electrodes, as shown in Figure 5.6 c). Silicone rubber is commonly used in triboelectric devices for energy harvesting and sensing because of its ability to gain and donate electrons. Its high dielectric constant improves the charge storage properties and the material's flexibility and softness optimise contact interfaces, improving electron exchange efficiency and allowing easy customisation into various shapes, suitable for several applications [21,43–46].

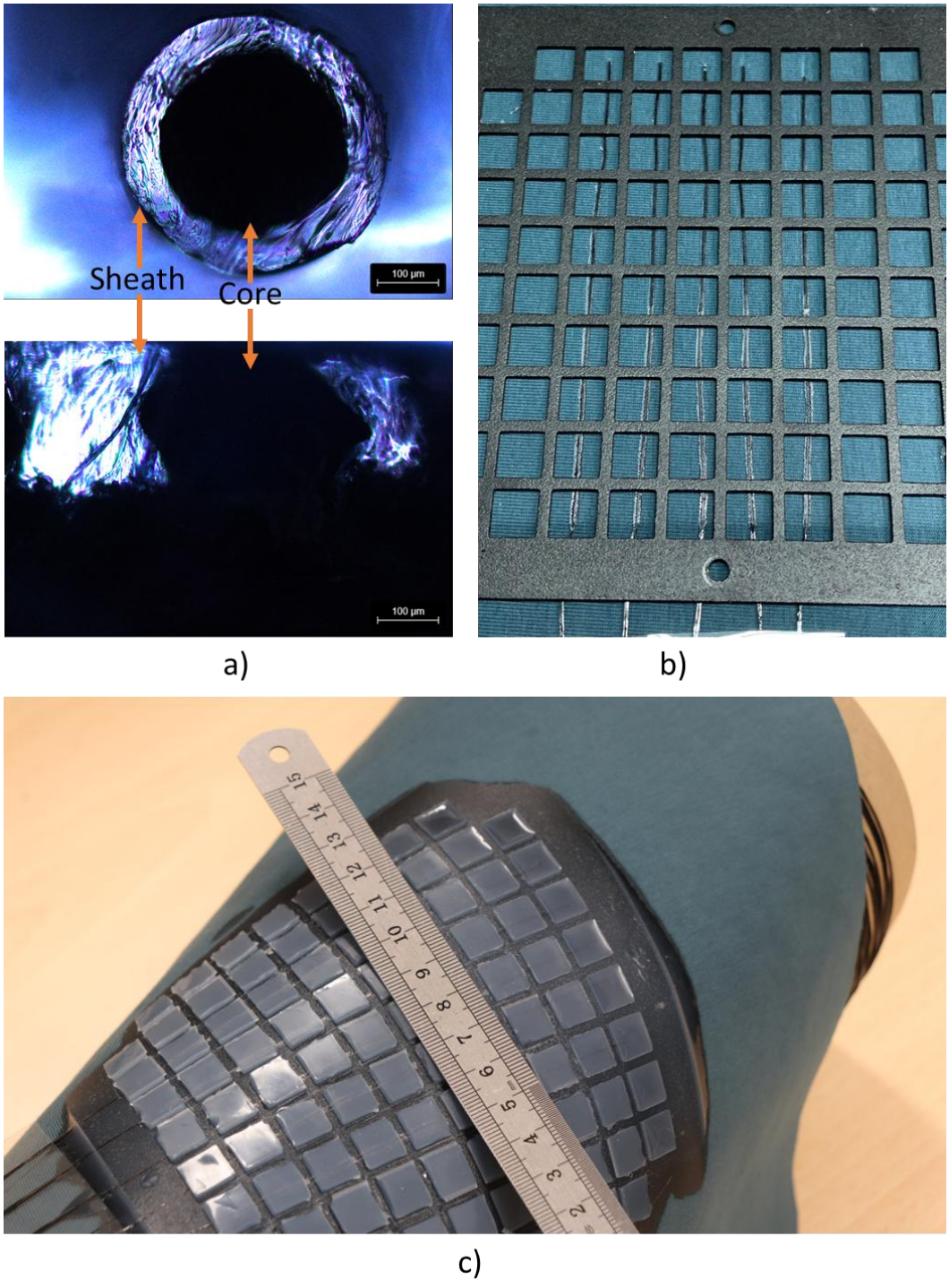

Figure 5.6- a) Bi-component filament cross section before and after hot pressing. b) lamination of the filaments on a textile structure and metallic mould for the silicone rubber. c) Triboelectric sensors prepared with 5 laminated filaments.

Figure 5.7 illustrates the impact of the sensor surface area on the output voltage of the composite. The characterisation of the triboelectric sensors revealed similar output voltage for individual filaments. When these filaments

were combined, the cumulative output voltage increased, which may be attributed to the increase in sensor surface area. The 100 N of applied force from a 10 cm diameter disc ensured optimal contact with the silicone rubber surface, which is critical for consistent charge generation. The filaments were spaced 1.2 cm apart, and incorporating additional filaments expanded the effective surface area, amplifying the output voltage. The electric field resulting from the triboelectric effect facilitated the sensors' capacity to detect impacts. Figure 5.7 shows that the voltage increment is residual when the number of filaments increases from 4 to 5, indicating that triboelectric coverage may be already maximised. With the silicone rubber dimensions remaining constant, 3 to 4 filaments appear sufficient to harvest the majority of the triboelectric potential between the testing disc and the silicone layer. This phenomenon was also demonstrated in the work of Xie *et al*. [47], who showed that increasing the mesh density beyond a certain threshold, results in diminishing returns due to the saturation of effective charge collection. At this point, the system already optimally covers the triboelectric surface area and establishes a uniform electric field. A similar principle is observed in the design of electrostatic discharge (ESD) garments, where strategically spaced electrically conductive filaments efficiently dissipate static electricity without requiring full coverage [48]. This suggests that the surface area of silicone rubber interacting with the pressing element generates charges that can be effectively captured with only a few spaced filaments. Furthermore, the system’s overall capacitive properties are influenced by the addition of more filaments, each acting as a small capacitor. This can alter the charge distribution and storage, leading to a non-linear increase in voltage output.

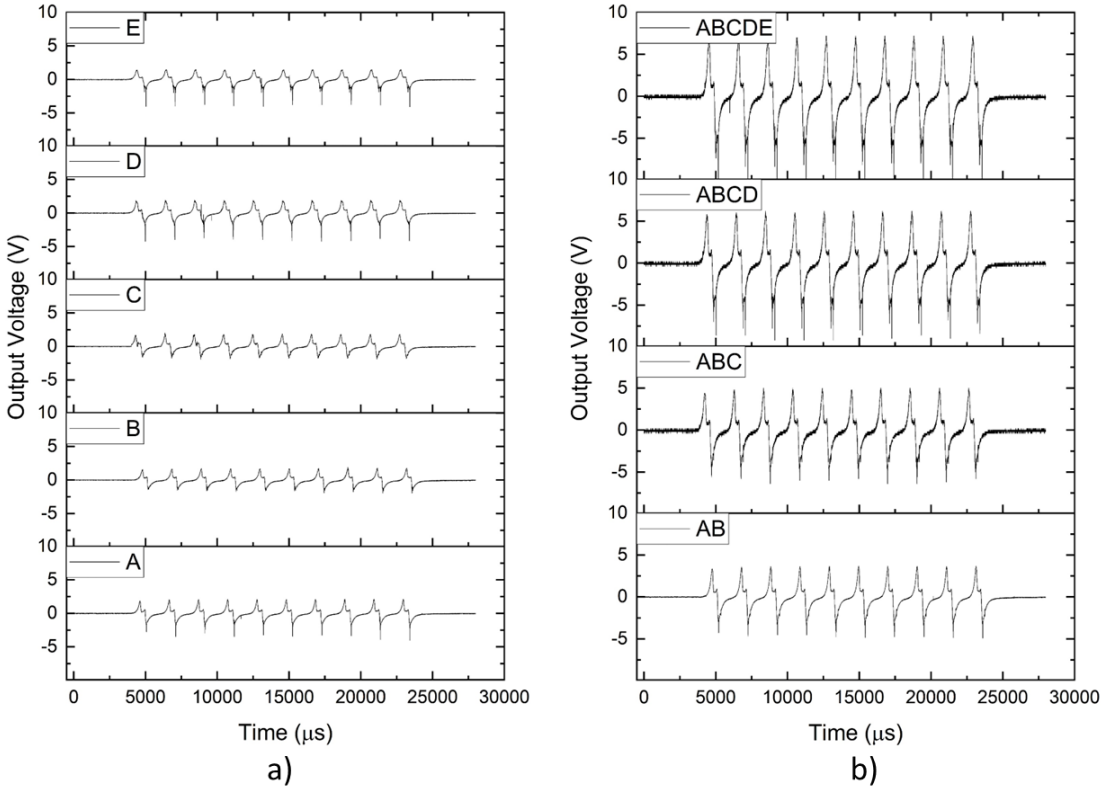

Figure 5.7- Triboelectric performance of the fabricated composite. a) individual output voltage for each filament and b) a combination of multiple filaments under the same applied force.

In conclusion, the relationship between the number of filaments and triboelectric performance was primarily guided by the objective of maximising sensor coverage. The selected spacing configuration efficiently utilised the triboelectric potential of the silicone rubber surface in combination with the applied force, ensuring consistent performance and broad coverage. This approach was particularly suited to large-scale sensing applications where maximising charge generation and distribution across the sensor area is a priority. While this study focused on sensor coverage, we recognise the importance of investigating other objectives, such as improving sensor precision through the individualisation of filaments. Therefore, future work should explore how varying filament spacing affects the sensitivity and accuracy of each filament as an independent sensing element. Such an approach could provide valuable insights into the relationship between filament spacing and the spatial resolution of the sensor.

5.4. Conclusions

This study successfully demonstrates the development of thermoplastic bi-component electrodes, optimised for continuous bi-component extrusion processes, emphasising their potential for textile triboelectric impact detection sensors. The findings illustrate the ability to finetune the properties of thermoplastic composites to produce bi-component filaments, featuring a conductive core and an outer layer compatible with lamination processes. These filaments, fabricated through continuous extrusion, could be well-suited for large-scale manufacturing. Then, once laminated on textile substrates, they would serve as effective electrodes for triboelectric impact sensors.

The optimised composition of 5 wt.% MWCNT within a PP matrix blended with 25 wt.% TPE achieved a good balance of electrical conductivity, mechanical ductility, rheological properties and thermal stability. The inclusion of TPE significantly enhanced the flexibility of the composites, reducing brittleness and ensuring durability under dynamic conditions such as repeated mechanical impacts.

The observed decrease in electrical resistivity with increasing MWCNT content confirmed the formation of a robust conductive network. Rheological and DSC analyses further validate the compatibility of PP/TPE for the core with the low melting point of the TPE sheath, enabling efficient lamination processes without compromising the structural integrity of the composite core. These properties make the material highly suitable for integration into textile substrates for wearable electronics, energy-harvesting systems, and safety applications.

The fabricated triboelectric sensors demonstrated reliable performance in detecting impacts, with output voltage increasing as the number of filaments increased, up to a saturation point. This highlights the need to optimise filament arrangements to balance coverage and precision effectively.

Finally, this study provides interesting results for the development of sustainable and cost-effective electrode solutions, that can be used for smart textiles. Future research should focus on dynamic testing under diverse operational conditions and on conducting a detailed life-cycle assessment of these composites, to quantify their environmental impact, including energy consumption during production and recycling. Additionally, exploring methods to

further enhance the recyclability of these materials and their integration into large-scale industrial processes could improve their economic and environmental viability, expanding their potential impact across diverse applications. From an economic perspective, the use of widely available and cost-effective materials such as PP and TPE, enhances the scalability and affordability of the composites, making them highly attractive for commercial applications. By combining environmental advantages with economic feasibility, these composites pro-vide a compelling solution for industries seeking to balance performance, sustainability, and cost-effectiveness.

5.5. References

[1] Van Langenhove, L. (2007). Smart textiles for medicine and healthcare: Materials, systems and applications. Elsevier.

[2] Maity, S., Singha, K., & Pandit, P. (2021). Advanced applications of green materials in wearable e-textiles. In Applications of Advanced Green Materials (pp. 239–263). Elsevier.

[3] Mahesh, G., & Sornapudi, S. (2017). Techniques and application of smart textiles. International Journal of Computer Science, 5(10).

[4] Sajovic, I., Kert, M., & Boh Podgornik, B. (2023). Smart textiles: A review and bibliometric mapping. Applied Sciences, 13(18), 10489.

[5] Foroughi, J., et al. (2016). Knitted carbon-nanotube-sheath/spandex-core elastomeric yarns for artificial muscles and strain sensing. ACS Nano, 10(10), 9129–9135.

[6] Lai, M.-F., Huang, C.-H., Lou, C.-W., Chuang, Y.-C., Wei, C.-Y., & Lin, J.-H. (2022). Multi-walled carbon nanotubes/polypropylene-based coating layer on the composite metal filaments: Characteristic evaluations and radiation-shielded fabric. Fibers and Polymers, 23(3), 768–774.

[7] Tseghai, G. B., Malengier, B., Fante, K. A., Nigusse, A. B., & Van Langenhove, L. (2020). Integration of conductive materials with textile structures, an overview. Sensors, 20(23), 6910.

[8] Dubal, D. P. (2018). Advances in flexible supercapacitors for portable and wearable smart gadgets. In Emerging Materials for Energy Conversion and Storage (pp. 209–246). Elsevier.

[9] Wang, L., Lou, Z., Jiang, K., & Shen, G. (2019). Bio-multifunctional smart wearable sensors for medical devices. Advanced Intelligent Systems, 1(5), 1900040.

[10] Khan, A., Rashid, M., Grabher, G., & Hossain, G. (2024). Autonomous triboelectric smart textile sensor for vital sign monitoring. ACS Applied Materials & Interfaces.

[11] Zhang, Z., et al. (2020). Deep learning-enabled triboelectric smart socks for IoT-based gait analysis and VR applications. npj Flexible Electronics, 4(1), 29.

[12] Hu, X., Ma, Z., Zhao, F., & Guo, S. (2024). Recent advances in self-powered wearable flexible sensors for human gait analysis. Nanomaterials, 14(14), 1173.

[13] Wang, C., Kim, Y., Shin, H., & Min, S. D. (2019). Preliminary clinical application of textile insole sensor for hemiparetic gait pattern analysis. Sensors, 19(18), 3950.

[14] Chaudhary, B., Winnard, T., Oladipo, B., Das, S., & Matos, H. (2024). Review of fiber-reinforced composite structures with multi-functional capabilities through smart textiles. Textiles, 4(3), 391–416.

[15] Decaens, J., Vermeersch, O., Lachapelle, D., & Forcier, P. (2020). Use case of smart textiles bio-sensors development and integration for the automotive industry. In IOP Conference Series: Materials Science and Engineering, 827(1), 012018.

[16] Grancarić, A. M., et al. (2018). Conductive polymers for smart textile applications. Journal of Industrial Textiles, 48(3), 612–642.

[17] Rayhan, M. G. S., et al. (2023). Conductive textiles for signal sensing and technical applications. Signals, 4(1), 1–39.

[18] Stoppa, M., & Chiolerio, A. (2014). Wearable electronics and smart textiles: A critical review. Sensors, 14(7), 11957–11992.

[19] Shahidi, S., & Moazzenchi, B. (2018). Carbon nanotube and its applications in textile industry—A review. Journal of the Textile Institute, 109(12), 1653–1666.

[20] Hughes-Riley, T., Dias, T., & Cork, C. (2018). A historical review of the development of electronic textiles. Fibers, 6(2), 34.

[21] Esteves, D. S., Pereira, M. F. C., Ribeiro, A., Durães, N., Paiva, M. C., & Sequeiros, E. W. (2023). Development of MWCNT/Magnetite flexible triboelectric sensors by magnetic patterning. Polymers, 15(13), 2870.

[22] Bhatia, R., Kumari, K., Rani, R., Suri, A., Pahuja, U., & Singh, D. (2018). A critical review of experimental results on low-temperature charge transport in carbon nanotubes based composites. Reviews in Physics, 3, 15–25.

[23] Esteves, D., Durães, N., Pedroso, R., Melo, A., & Paiva, M. (2023). Fabrication of low electrical percolation threshold multi-walled carbon nanotube sensors using magnetic patterning. Applied Sciences, 13(3), 1437.

[24] Lin, Z.-I., et al. (2017). Conductive fabrics made of polypropylene/multi-walled carbon nanotube coated polyester yarns: Mechanical properties and electromagnetic interference shielding effectiveness. Composites Science and Technology, 141, 74–82.

[25] Lund, A., van der Velden, N. M., Persson, N.-K., Hamedi, M. M., & Müller, C. (2018). Electrically conducting fibres for e-textiles: An open playground for conjugated polymers and carbon nanomaterials. Materials Science and Engineering R Reports, 126, 1–29.

[26] Su, M., Brugger, J., & Kim, B. (2020). Simply structured wearable triboelectric nanogenerator based on a hybrid composition of carbon nanotubes and polymer layer. International Journal of Precision Engineering and Manufacturing Technology, 7(3), 683–698.

[27] Ning, C., et al. (2021). Flexible and stretchable fiber-shaped triboelectric nanogenerators for biomechanical monitoring and human-interactive sensing. Advanced Functional Materials, 31(4), 2006679.

[28] He, X., et al. (2017). A highly stretchable fiber-based triboelectric nanogenerator for self-powered wearable electronics. Advanced Functional Materials, 27(4), 1604378.

[29] Bobinger, M., et al. (2018). Light and pressure sensors based on PVDF with sprayed and transparent electrodes for self-powered wireless sensor nodes. IEEE Sensors Journal, 19(3), 1114–1126.

[30] Wang, S., et al. (2023). Human motion recognition by a shoes-floor triboelectric nanogenerator and its application in fall detection. Nano Energy, 108, 108230.

[31] Li, R., et al. (2021). Smart wearable sensors based on triboelectric nanogenerator for personal healthcare monitoring. Micromachines, 12(4), 352.

[32] Sun, Y., et al. (2023). Conformable multifunctional space fabric by metal 3D printing for collision hazard protection and self-powered monitoring. ACS Applied Materials & Interfaces, 15(49), 57726–57737.

[33] Baburaj, A., et al. (2023). Factors affecting the performance of flexible triboelectric nanogenerators (F-TENGs) and their sensing capabilities: A comprehensive review. Nano Energy, 108983.

[34] Huang, X., et al. (2022). Overview of advanced micro-nano manufacturing technologies for triboelectric nanogenerators. Nanoenergy Advances, 2(4), 316–343.

[35] Davoudi, M., An, C.-Y., & Kim, D.-E. (2024). A review on triboelectric nanogenerators, recent applications, and challenges. International Journal of Precision Engineering and Manufacturing Technology, 11(4), 1317–1340.

[36] Li, C., Jiao, Z., Xiong, L., & Yang, W. (2017). Electrical conductivity of carbon nanotube/polypropylene composites prepared through microlayer extrusion technology. Journal of Polymer Engineering, 37(8), 795–804.

[37] Stanciu, N.-V., Stan, F., Sandu, I.-L., Fetecau, C., & Turcanu, A.-M. (2021). Thermal, rheological, mechanical, and electrical properties of polypropylene/multi-walled carbon nanotube nanocomposites. Polymers, 13(2), 187.

[38] Tamayo-Vegas, S., et al. (2022). The effect of agglomeration on the electrical and mechanical properties of polymer matrix nanocomposites reinforced with carbon nanotubes. Polymers, 14(9), 1842.

[39] Nagler, J. (2019). Failure mechanics of multi-material laminated systems review analysis-based project. School of Mechanical Engineering, University of Tel Aviv.

[40] Rahaman, M., et al. (2017). A new insight in determining the percolation threshold of electrical conductivity for extrinsically conducting polymer composites through different sigmoidal models. Polymers, 9(10), 527.

[41] Chung, C. I. (2019). Extrusion of polymers: Theory & practice. Carl Hanser Verlag GmbH Co KG.

[42] Lu, Y., Sun, Y., Li, L., & Men, Y. (2017). Influence of propylene-based elastomer on stress-whitening for impact copolymer. Journal of Applied Polymer Science, 134(20).

[43] Xiao, T. X., et al. (2018). Silicone-based triboelectric nanogenerator for water wave energy harvesting. ACS Applied Materials & Interfaces, 10(4), 3616–3623.

[44] Natarajan, T. S., et al. (2020). Robust triboelectric generators by all-in-one commercial rubbers. ACS Applied Electronic Materials, 2(12), 4054–4064.

[45] Burgo, T. A. L., Batista, B. C., & Galembeck, F. (2017). Electricity on rubber surfaces: A new energy conversion effect. ACS Omega, 2(12), 8940–8947.

[46] Du, T., et al. (2022). A robust silicone rubber strip-based triboelectric nanogenerator for vibration energy harvesting and multi-functional self-powered sensing. Nanomaterials, 12(8), 1248.

[47] Xie, Y., et al. (2023). An internal electrode strategy for enhancing the stability and durability of triboelectric nanogenerator. Composites Science and Technology, 237, 110014.

[48] Fast, L., & Paasi, J. (2006). ESD protective requirements for cleanroom clothing. In 37th R3-Nordic Contamination Control Symposium (pp. 343–356).

5.6. Supplementary materials

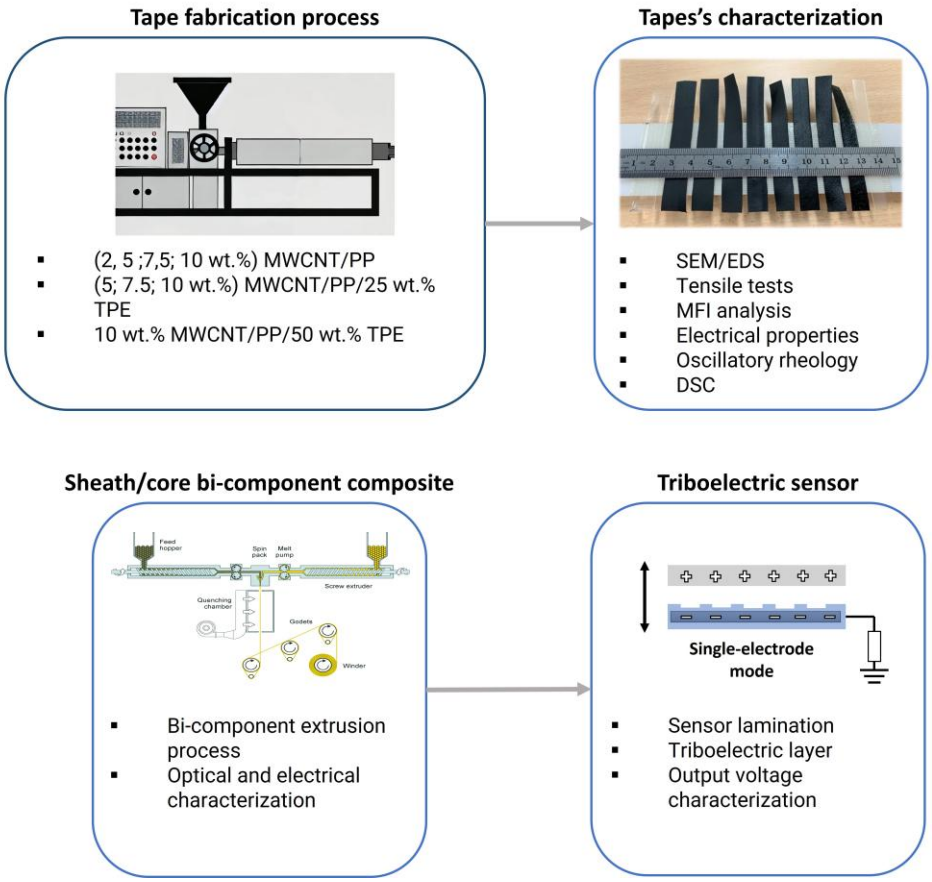

Figure 5.8- S1:Workflow outline for the development of thermoplastic bi-component electrodes for triboelectric impact detection sensors

Chapter 6: Magnetic field-assisted orientation and positioning of magnetite for flexible and electrically conductive sensors

This chapter addresses the thesis's fourth objective: Investigate magnetic field-assisted particle alignment in thermoplastics. Restricted particle mobility due to high viscosity presents a key challenge for achieving effective magnetic alignment in thermoplastic matrices. This study explores how fabrication processes and material selection influence alignment efficiency, identifying viscosity as a critical factor affecting particle orientation. The findings demonstrate that combining magnetic positioning with laser cutting offers a promising approach to overcoming these processing limitations and advancing the scalability of flexible sensor manufacturing.

This article is part of the Special Issue Materials and Processing, of Micromachines, with reference: Esteves, D. S., Melo, A., Alves, S., Durães, N., Paiva, M. C., & Sequeiros, E. W. (2025). Magnetic Field-Assisted Orientation and Positioning of Magnetite for Flexible and Electrically Conductive Sensors. Micromachines, 16(1), 68. https://doi.org/10.3390/mi16010068

Abstract

Magnetic field-assisted control of magnetite location is a promising strategy for developing flexible, electrically conductive sensors with enhanced performance and adjustable properties. This study investigates the effect of static magnetic fields applied on TPE composites with magnetite and MWCNT. The composites were prepared by compression moulding and the magnetic field was applied on the mould cavity during processing. Composites were prepared with a range of concentrations of magnetite (1, 3, and 6 wt.%) and MWCNT (1 and 3 wt.%). The effect of particle concentration on composite viscosity was investigated. Rheological analysis showed that MWCNTs significantly increased the composite viscosity while magnetite had minimal impact, ensuring stable processing and facilitating particle orientation under a static magnetic field. Particle orientation and electrical conductivity were evaluated for the composites prepared with different particle concentrations under different processing temperatures. Magnetic field application at 190 °C enhanced magnetite/MWCNT interactions, substantially reducing electrical resistivity while preserving thermal stability. The composites showed no degradation at 220 °C and above, demonstrating suitability for high-temperature applications requiring thermal resilience. Furthermore, magnetite's magnetic response facilitated precise sensor positioning and strong adhesion to polyimide substrates at 220 °C. These findings demonstrate a scalable and adaptable approach for enhancing sensor performance and positioning, with broad potential in flexible electronics.

6.1. Introduction

The field of composite materials has advanced significantly in recent decades, driven by research and innovations in manufacturing and advanced materials design [1]. Among these innovations, incorporating magnetic and conductive fillers into a polymer matrix is a promising approach for enhancing and diversifying the functional capabilities of flexible composite materials. The ability to control the orientation of these fillers within the matrix can substantially improve mechanical strength [2–3], thermal stability [4], and electrical conductivity [5–6]. The use of thermoplastic matrices in the development of flexible and conductive composites has demonstrated key advantages relative to

other matrix materials, offering superior processability, recyclability, and adaptability [7]. TPE combine flexibility with ease of moulding and reshaping, making them particularly well-suited for applications demanding both adaptability and sustainability. This contrasts with thermoset polymers, which, despite their stiffness, lack reusability after curing, limiting their versatility and reducing their alignment with modern sustainability goals [8].

Therefore, this study introduces a novel methodology for controlling filler orientation within TPE polymer matrices by employing magnetically induced particle alignment. Specifically, magnetite particles were chosen for their inherent magnetic responsiveness, which facilitates their precise orientation within the polymer matrix when subjected to an external magnetic field [9–10]. This targeted orientation optimises the distribution of fillers, which could improve the overall performance of the composite. While magnetite alone provides moderate electrical conductivity in combination with magnetic properties, the level of conductivity required for advanced flexible electronics often necessitates a hybrid material approach [9–10]. To address this, magnetite may be combined with MWCNTs, which possess exceptionally low resistivity [11–12]. Integrating MWCNTs can significantly reduce the composite electrical resistance, even at minimal concentrations, while maintaining magnetic responsiveness [9–12].

Several techniques are available to enhance composite electrical conductivity through particle orientation, each with specific mechanisms that influence particle alignment and significantly impact the material’s properties [3, 13–22]. Among these, magnetic field orientation presents unique advantages, especially for magnetic or magnetically responsive particles. By leveraging the particles' magnetic susceptibility, a magnetic field can be applied during composite fabrication to align particles along the field lines, forming an organised internal structure. Unlike mechanical or electric field methods, magnetic orientation is non-intrusive and can be applied uniformly across the material, enabling fine control over particle alignment and distribution [23–27]. In addition to potential enhancements associated with controlled particle orientation, the multifunctional characteristics of magnetite have drawn substantial interest in a wide range of electronic applications [28]. In a sense, magnetite nanoparticles enhance systems for detecting magnetic fields and other critical targets, making them highly valuable in medical diagnostics [28]. In the energy sector, magnetite's

high theoretical capacity makes it a promising candidate for use as an anode material in lithium-ion batteries. Additionally, it exhibits intriguing properties for wireless charging technologies [29–31]. Moreover, magnetite's magnetic loss properties render it highly effective for EMI shielding, mainly when employed in combination with carbon-based materials [32–33].

In the present work, TPE hybrid composites incorporating magnetite and MWCNT were produced by melt processing, a method that is highly scalable and environmentally friendly. Using low filler contents, the composites were moulded under the effect of magnetic fields to induce particle/nanoparticle orientation and enhance the composite response under different stimuli. Therefore, the work presented contributes to the development of multifunctional composites with potential applications in several fields, including sensors, actuators, electromagnetic shielding, soft robotics and flexible electronics [34–38].

6.2. Materials and methods

This study examined TPE composites reinforced with magnetite and MWCNT and studied the influence of these fillers on the composite's morphology, rheology, and electrical properties. The workflow diagram in Figure 6.1 illustrates the sequential stages of composite preparation, characterisation, and testing employed in this study. The first stage was the composite materials preparation where magnetite, MWCNTs, and TPE are combined by melt mixing using twin-screw extrusion. From these composites, samples were moulded with and without the application of magnetic fields to investigate its effect on particle distribution. The next stage consisted of the composites' characterisation using different analytical techniques to assess the morphology, structure and properties of the composites. Morphological analysis was conducted by SEM and Micro-CT to visualise particle distribution and orientation within the composite. Rheological analysis of the composite melt assessed the viscosity, loss and storage moduli, providing insight into the effect of the addition of magnetite and MWCNTs on the viscoelastic behaviour of the TPE composite. Thermogravimetric analysis (TGA) characterised the thermal stability of the composites, defining their maximum processing temperature. In the final stage, electrical and functional testing was conducted on the final composites to compare the electrical resistivity with and

without magnetic field application and assess the impact of magnetic alignment on conductivity. Finally, a laser cutting technique was used to create sensor patterns in the composite films. These patterned films were then bonded to flexible substrates with magnetic assistance. The stability and performance of the sensors were evaluated through bending cycles, simulating repeated mechanical stress to assess adhesion durability.

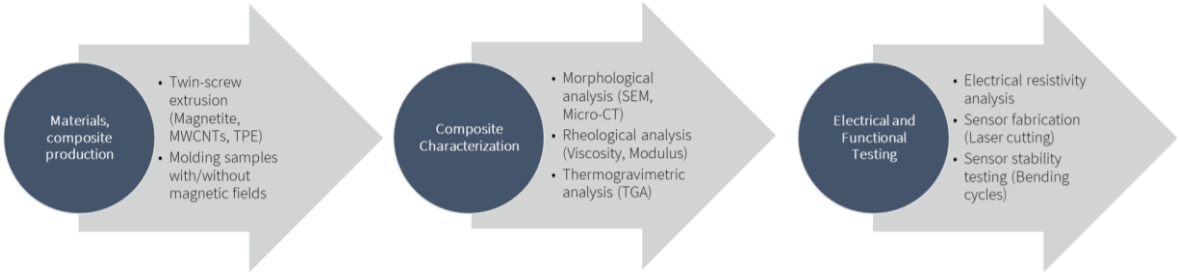

Figure 6.1- Experimental Workflow.

6.2.1. Materials

MWCNTs used in this study were obtained from Nanocyl, the NC 7000 grade (Sambreville, Belgium). The TPE employed was Engage 8401, a high-performance elastomer supplied by Dow Chemical Company (Midland, Michigan, USA). Rectangular Samarium Cobalt (SmCo) permanent magnets with dimensions of 25x9.5x12 mm were acquired from Superimanes S.L. (Madrid, Spain). Synthetic magnetite was purchased from Inoxia Ltd. (Alton, Hampshire, UK), providing magnetic particles for composite production.

6.2.2. Composite production

Composite production by extrusion: For the sample production, five distinct composites were produced using a twin-screw extruder, incorporating 1%, 3%, and 6% by weight (wt.%) of magnetite and 1% and 3% by weight (wt.%) of MWCNT. Subsequently, hybrid composites were prepared as follows: 6 % of magnetite was added to 500 g of the 1% or 3% MWCNT composites, to fabricate composites containing 1% or 3% wt.% MWCNT with 6 wt.% magnetite each. The magnetite powder was added to the TPE/MWCNT composite using a gravimetric dosing system Movacolor B.V. (Friesland, Netherlands), calibrated beforehand for accuracy. The filaments were produced using a co-rotating twin-screw

extruder with a length-to-diameter (L/D) ratio of 25 Rondol Technology Ltd (Staffordshire, United Kingdom). The extrusion process was conducted under specific conditions: the temperature along the extruder was set at 140 °C for the first and last zones and 145 °C for zones 2 through 4. The drive torque was maintained at 30%, and the screw speed was set to 150 rpm.

Composite sample preparation by compression moulding: To ensure accurate process control, the mould cavity temperature was initially monitored due to its importance in the thermal dynamics and resulting properties of the manufactured material. Temperature variations between the set values on processing equipment and real mould cavity temperatures can impact material properties. A Type J thermocouple connected to a UNI-T UT320 A thermometer was used to monitor cavity temperature, with data recorded every 30 seconds for a 20 minute duration at each set temperature. Results showed significant discrepancies between the set and real cavity temperatures, with measured temperatures consistently lower within the cavity. For example, a set temperature of 160 °C resulted in a cavity temperature of approximately 130 °C, while set temperatures of 190 °C and 220 °C yielded cavity temperatures of approximately 160 °C and 190 °C, respectively, after 20 minutes. The samples were prepared from the extruded composites using a stainless steel mould with a thickness of 3 mm. Each mould contained two 40 × 20 × 3 mm cavities, one designated for samples with permanent magnets and another as a control. Samples were processed using compression moulding (Galaxy XL5880, Acosgraf) at specified temperatures and durations, as detailed in Table 6.1 and Figure 6.13-S1 in supplementary materials, applying a constant pressure of 2 bar to protect the integrity of the permanent magnets.

Table 6.1- Summary of process conditions for the composites

Sample	Magnetite Concentration (wt. %)	Set temperature (°C)	Real temperature (°C)	Duration (minutes)
a)	1%	220	190	10
b)	3%	220	190	10
c)	6%	220	190	10
d)	6%	220	180	5
e)	6%	220	190	10
f)	6%	220	190	20
g)	6%	160	130	10
h)	6%	190	160	10
i)	6%	220	190	10

Magnetic field application on the mould cavity: The first two SmCo permanent magnets (25 × 9.5 × 12 mm each), were aligned in a North-South (NS) configuration and securely attached. Two additional magnets, arranged in a South-North (SN) configuration, were positioned parallel to the first pair, spaced 3 mm apart, as shown in Figure 6.2. All four magnets were firmly fixed to a 5 mm thick iron base to ensure stability during the composite fabrication process. Precise alignment of the magnets in the NSNS configuration was essential for achieving a continuous and uniform particle alignment within the composite material [6].

The magnetic properties of the SmCo magnets were characterised using a 3D magnetic field mapper (M3D-2A-Port, Senis, Canton Zug, Switzerland) over a mapped area of 75 × 35 mm. Measurements were taken at two key distances: 0.2 mm and 3 mm from the magnet surface. At 0.2 mm, the magnetic flux density peaked at 400 mT, while at 3 mm, it decreased to approximately 200 mT, demonstrating the expected attenuation with distance. These measurements confirmed the consistency and reliability of the magnetic field, which is essential for effective particle alignment during composite processing.

To optimise magnetic interaction with the composite material while ensuring insulation and protecting the mould setup, a 150 µm thick Teflon film was used as a barrier. This thin yet durable layer minimised the distance between the magnets and the composite, allowing sufficient magnetic exposure to orient the

magnetite particles effectively. At the same time, the Teflon film preserved the mechanical and thermal integrity of the setup during the heating and compression stages.

As illustrated in Figure 6.2, the consistent magnetic flux density of 350 mT, combined with the precise positioning of the magnets in an NSNS configuration, created a stable magnetic field gradient between 0.2 mm and 3 mm from the magnet surface. Both the flux density and field direction were carefully controlled to ensure reproducibility of the process and its results. Additionally, exposure duration and process temperature were varied to investigate their effects on particle alignment within the composite.

6.2.3 Composite characterisation

6.2.3.1 Morphological analysis

Micro CT analysis: The micro CT assessed composites' three-dimensional (3D) microstructural and compositional heterogeneities. Digital radiographs were acquired on a micro CT SkyScan 1275 scanner (Bruker, Billerica, MA, USA) using an X-ray cone incident on a rotating specimen. The following operating conditions were used: source voltage of 48 kV, current of 80 µA, a distance of 9-10 µm and an average of four radiographs per position. The acquisition was performed by rotating the specimen over 360° with a 0.25° rotational step. The reconstructions were obtained with the NRecon, and volumetric visualisation was achieved with CTvox programs, which integrate the instrument software packages.

SEM analysis: The MWCNT and the magnetite on the cross-section of the polymeric tapes was visualised using a Field Emission Gun Scanning Electron Microscope (FEG-SEM, NOVA 200 Nano SEM, FEI Company). Before analysis, specimens were cryo-fractured using liquid nitrogen and coated with a 1.5 nm film of Au-Pd (80-20 weight %) using a high-resolution sputter coater (208HR, Cressington Company), coupled with an MTM-20 High Resolution Thickness Controller (Cressington). The topographic images were obtained with a secondary electron (SE) detector at an acceleration voltage of 10 kV. The atomic contrast images were obtained with a Backscattering Electron Detector (BSED) at an acceleration voltage of 15 kV. The chemical analyses of samples were

performed with the EDS technique, using an EDAX Si(Li) detector at an acceleration voltage of 20 kV.

6.2.3.2 Rheological analysis

Oscillatory shear rheological analysis was conducted to evaluate the impact of MWCNT and magnetite on the composites' viscosity, loss, and storage modulus. The experiments were performed using a Discovery HR 10 rheometer from TA Instruments (Delaware, USA), which provides precise control and measurement capabilities. The tests were conducted at various temperatures (160, 190, and 220 °C) to assess the thermal influence on rheological properties. The analysis employed a parallel stainless-steel plate geometry ideal for uniform shear distribution. The linear viscoelastic region was identified through a stress sweep at a frequency of 1 Hz to ensure accurate characterisation of the materials' viscoelastic behaviour. Initially, a frequency sweep analysis was conducted on all samples ranging from 0.1 to 1000 rad/s. This test provided insights into how the composites respond to dynamic shear stresses over a wide frequency range. Subsequently, a time sweep analysis, at a frequency of 1 Hz, was performed during 20 minutes within the linear viscoelastic region. This analysis focused on samples containing 1 wt.% MWCNT, 6 wt.% magnetite, and the combined 1 wt.% MWCNT with 6 wt.% magnetite. This allowed for the assessment of time-dependent changes in rheological properties, offering a detailed understanding of the stability and performance of the composites under sustained shear conditions at temperatures of 160, 190 and 220 °C.

6.2.3.3 Thermogravimetric analysis (TGA)

TGA was conducted using the equipment TGA 209 F1 Libra instrument from Netzsch (Bavaria, Germany) to evaluate the thermal stability and thermal decomposition of the composites produced. The TGA was performed under a nitrogen atmosphere. Each sample was heated from 30 to 700 °C at a consistent rate of 20 °C/min. Alumina crucibles were used throughout the testing process. The samples tested consisted of composites with 1 wt.% MWCNT, 3 wt.% MWCNT, 1 wt.%, 3 wt.% and 6 wt.% magnetite, and a combination of 1 wt.% MWCNT with 6 wt.% magnetite and 3 wt.% MWCNT with 6 wt.% magnetite.

These concentrations were selected to investigate the influence of MWCNT and magnetite loadings on the thermal properties of the composites. To ensure that the observed changes in rheological behaviour over time were not due to thermal degradation, TGA was conducted over a temperature range from ambient to 220 °C, and maintained at 220 °C for 20 minutes.

6.2.3.4 Electrical and functional testing

Electrical resistivity analysis: Electrical resistivity measurements for the composites were performed using the two-point electrical resistance method, employing a Keithley 6487 picoammeter/voltage source. To ensure electrical contact, the cross-sections of the opposite sides of each composite sample were coated with silver ink (CI 1036, Engineered Materials Systems Inc, Ohio, USA). The dimensions of each specimen were 40 mm in length, 20 mm in width, and 3 mm in thickness, yielding an electrode cross-sectional area of approximately 60 mm^2. After applying silver ink, the composites were thermally treated at 110 °C for 10 minutes to ensure the cure of the ink, its adhesion and conductivity. Electrical resistance measurements were conducted on five replicates per composite formulation.

Sensor fabrication: To explore a complementary application of MWCNT/magnetite/TPE composites in flexible electronics, laser-cut patterns with 1 mm wide zig-zag lines were fabricated using a Laser Spirit LS machine (GCC, New Taipei City, Taiwan). These patterns were then bonded to a PI substrate pre-printed with silver ink electrical pads.

Sensor pattern positioning was achieved using SmCo permanent magnets (characterised in Figure 6.2) with a surface magnetic flux density of 350 mT. Arranged in a North-South configuration (Figure 6.2), these magnets generated a strong, uniform magnetic field, even at elevated temperatures. This field facilitated precise alignment and secure positioning of the sensor patterns, allowing adjustment of the zig-zag line spacing for specific applications. The magnetic force ensured uniform pressure across the sensor patterns, enhancing adhesion to the PI substrate during the subsequent 220 °C, 10 minute bonding process in an oven. This temperature was carefully selected to avoid melting the substrate while enabling the TPE to melt and form a strong bond between the

composite and the substrate. The pressure required for bonding was provided by the magnetic interaction between the SmCo magnets and the magnetite particles within the composite. After the heating process, the magnets and sensor were carefully removed from the oven and allowed to cool to ambient temperature to stabilise the bonded structure.

The electrical resistance of the bonded sensor patterns was measured using a Keysight U1282A multimeter connected to a computer, enabling precise data acquisition to verify sensor functionality and adhesion quality to the PI substrate. This magnetic field-assisted fabrication process simplifies sensor positioning and ensures robust adhesion and alignment, offering a practical and scalable solution for flexible electronics.

Sensor stability testing: The preliminary analysis of the sensor's stability was assessed by performing 100 bending cycles under 10 mm deformation in a Shimadzu AGX-V (Shimadzu Corporation, Kyoto, Japan) at the rate of 150 mm/min. The stability of the sensor was also tested with 10 mm deformation and 10 s holding under deformation cycles. Then, an extra bending step with 5 mm deformation was tested, followed by a 10 mm deformation step.

6.3. Results and discussion

6.3.1. Morphological analysis

To investigate the impact of the magnetic field on particle orientation, a 6 wt.% magnetite/TPE composite was analysed using micro-CT imaging. The micro-CT images, shown in Figure 6.2 c) and f), reveal variations in particle density within the TPE matrix. Brighter areas in these images indicate higher concentrations of magnetite, as magnetite absorbs more X-rays due to its higher density. The micro-CT analysis provides insight into particle orientation patterns induced by the magnetic field. In addition to the observed particle orientation with the magnetic field lines, the images reveal a hole in the composite, which aligns with regions of low magnetic field intensity from the magnetic mapping data. This phenomenon suggests that magnetite particles are drawn toward areas of higher magnetic flux density, as illustrated in the magnetic mapping images in Figure 6.2 b) and e). The movement of magnetite particles toward stronger magnetic fields creates defects in regions with weaker magnetic fields. The formation of such

defects could be reduced in composites with a low-viscosity polymer matrix, as shown in studies performed on thermoset polymers like PDMS and PU [11,31]. On the one hand, in low-viscosity thermoset matrices, magnetic particles can move more freely toward areas of higher magnetic flux density, allowing particles to accumulate in regions of strong magnetic fields without dragging the surrounding matrix. On the other hand, high-viscosity thermoplastic matrices like TPE behave differently. Here, the viscosity is high enough that magnetic particles cannot move independently. Instead, as the particles attempt to migrate toward stronger magnetic fields, they also drag the surrounding polymer matrix, creating defects in the composites. The magnetic field mapping highlighted the influence of the magnetic poles on particle orientation within the composite. The presence of north and south poles affects how magnetite particles orient and aggregate, impacting the material's density, as observed in the micro-CT images (Figure 6.2 c) and f)). The images reveal that the magnetite particles align parallel to the north-south poles direction. With the four magnets arranged in a north-south

configuration, the particles exhibit a circular orientation around the central region, with low magnetic flux density.

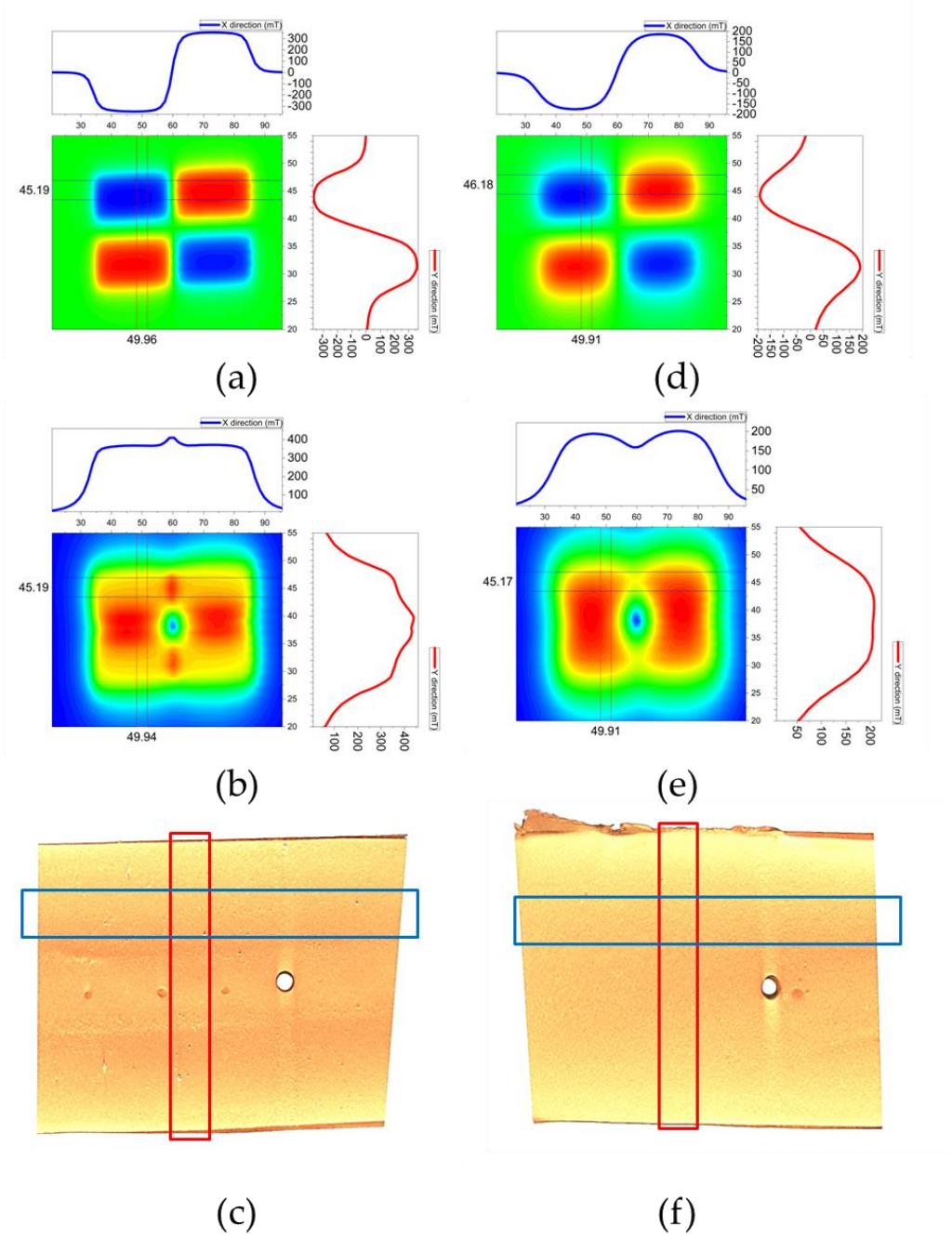

Figure 6.2- Magnetic field mapping and micro-CT analysis of a 6 wt.% magnetite composite. The magnetic flux density (mT) is represented using a color scale, with green to red indicating increasing intensity. The blue line at the top of each subplot represents the magnetic flux density in the x-direction (horizontal), while the red line on the right side of each subplot shows the magnetic flux density in the y-direction (vertical). (a) NS polarity at a distance of 0.2 mm (b) magnetic field interaction between north and south pole at 0.2 mm (c) and bottom view of the sample, near the location of the permanent magnets. (d) NS polarity at a distance of 3 mm (e) magnetic field interaction between north and south pole at 3 mm (f) and top view of the sample, 3 mm away from the location of the permanent magnets.

The particle orientation mechanism was studied through a detailed analysis of the effect of the composition and processing parameters on the orientation of

magnetite. In particular, the effects of magnetite concentration and compression moulding parameters were analysed using micro-CT imaging, to visualise changes in particle orientation, as shown in the cross-section images in Figure 6.3. The impact of the weight percentage of magnetite on the particle alignment is depicted in Figure 6.3 a), showing that 1 wt.% of magnetite is insufficient to induce a uniform magnetic alignment. However, increasing magnetite content to 3 and 6 wt.% leads to particle orientation in the magnetic field, as shown in Figure 6.3 b) and c). At lower magnetite concentrations the distance between particles is too large to facilitate their interaction in the magnetic field. This leads to weaker magnetic interactions within the material, hampering the attainment of uniform magnetic alignment. Additionally, the magnetic moments of individual particles are often insufficient to counteract the random thermal motion and orientation within the polymer matrix. In contrast, at higher concentrations (3 and 6 wt.%), the density of magnetic particles in the composite is large enough to induce an overall magnetic responsiveness [39]. The shorter distance between particles fosters stronger collective magnetic interactions, facilitating more effective alignment in response to a magnetic field. Furthermore, the increased particle density provides a continuous and interconnected pathway for magnetic forces to act upon, thereby improving alignment uniformity [40,41].

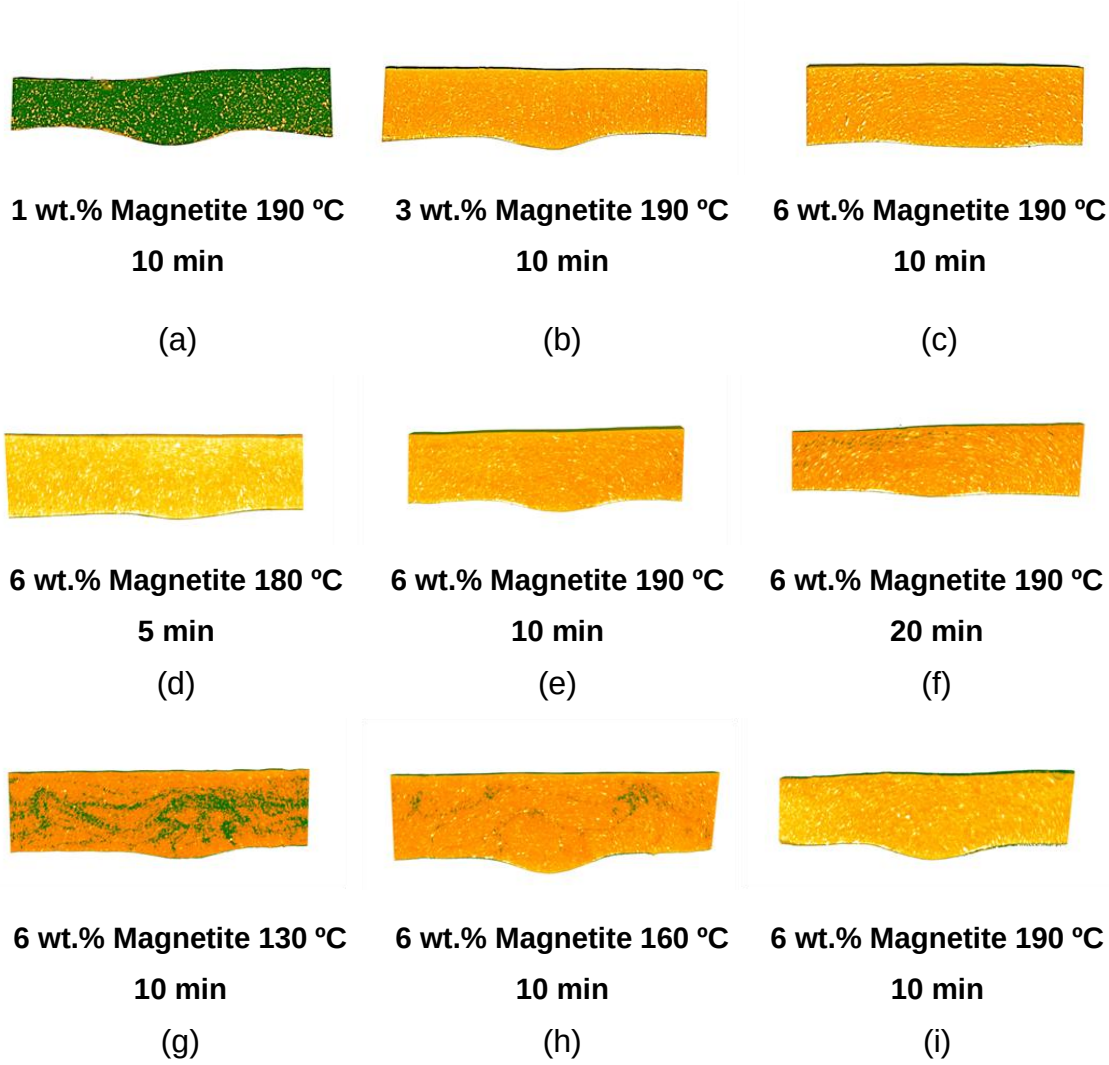

Figure 6.3- Micro-CT images of cross-section samples: (a) 1% magnetite with 220 ºC set temperature, during 10 minutes (b) 3% magnetite with 220 ºC set temperature, during 10 minutes (c) 6% magnetite with 220 ºC set temperature, during 10 minutes (d) 6% magnetite with 220 ºC set temperature, during 5 minutes (e) 6% magnetite with 220 ºC set temperature, during 10 minutes (f) 6% magnetite with 220 ºC set temperature, during 20 minutes (g) 6% magnetite with 160 ºC set temperature, during 10 minutes (h) 6% magnetite with 190 ºC set temperature, during 10 minutes (i) 6% magnetite with 220 ºC set temperature, during 10 minutes.

Additionally, the micro-CT analysis of process parameters, specifically temperature and moulding time, reveals that increasing the processing time enhances the orientation of magnetic particles within the composite, Figure 6.3 d), e) and f). Significant particle alignment is evident within the initial 10 minutes, indicating that an efficient orientation process can be achieved relatively fast, thus conserving time and resources. Decreasing the compression moulding time to 5 minutes hampers particle orientation, as it is not enough time for the polymer to reach 190 °C. Concerning temperature effects, there is a positive correlation between elevated temperatures and improved particle alignment, Figure 6.3 g), h), and i). Setting a temperature of 220 °C effectively reaches a mould cavity

temperature of approximately 190 °C after 10 minutes and improves particle alignment. This temperature setting is consistent with the recommendations provided in the polymer datasheet, ensuring that processing conditions are ideal without compromising the integrity of the material. To further confirm the magnetite orientation in the magnetic field observed by micro-CT analysis, the particle alignment was confirmed by SEM imaging and represented in Figure 6.4 a). The brighter particles observed in the Micro-CT images were analysed using SEM/EDS, as shown in Figure 6.4. Back scattered electrons (BSE) mode imaging was used to identify elements with higher atomic numbers, allowing straightforward detection of magnetite.

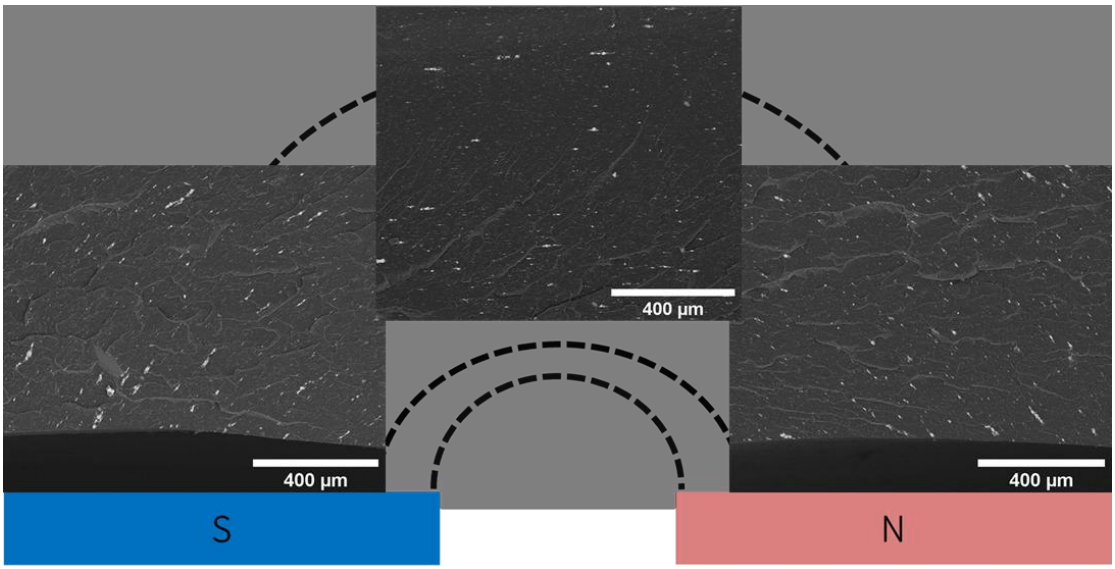

(a)

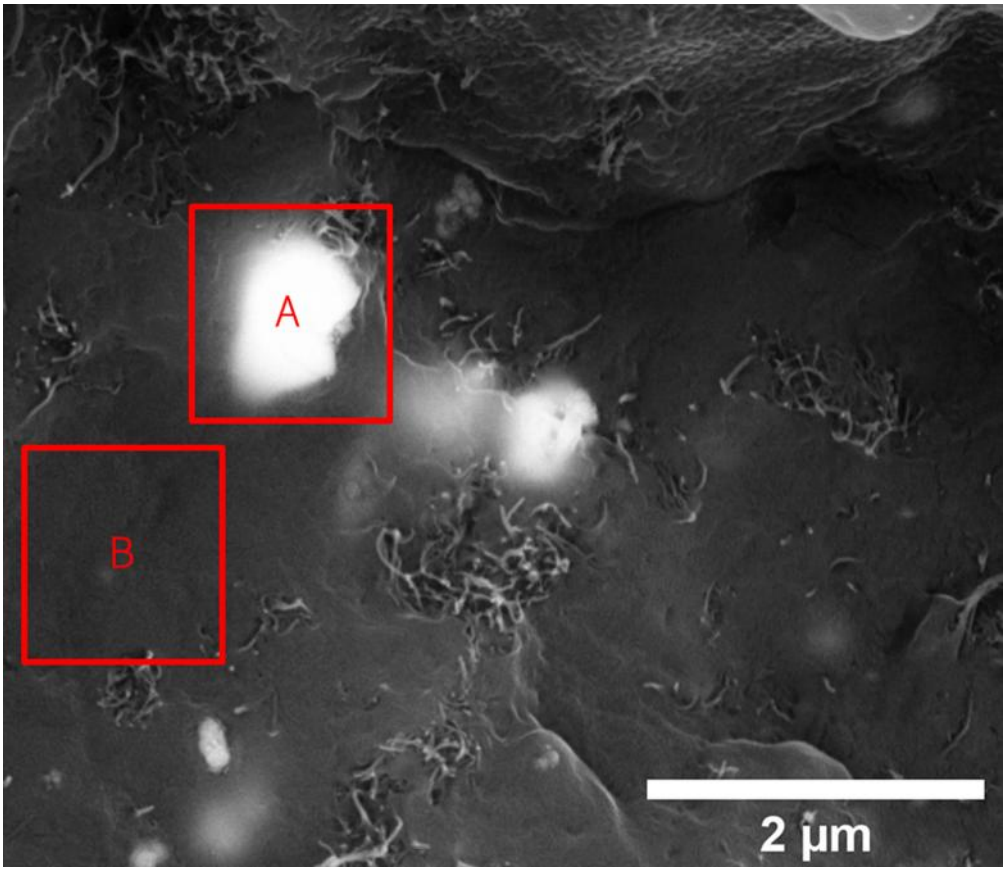

(b)

Figure 6.4- SEM images: (a) Reconstruction of the magnetite alignment inside the TPE composite after being fabricated under a static magnetic field. (b) BSED analysis to demonstrate the correspondence of the white spots to the location of magnetite.

EDS analysis then confirmed the elemental composition of the analysed areas, showing strong iron peaks in magnetite-rich regions and lower iron signals in areas with less magnetite (Figure 6.4 (b) and Table 6.2).

Table 6.2- Normalized chemical composition of Zone A and Zone B.

	Chemical Composition (At.%)		
Zone	**C**	**O**	**Fe**
A	82.5	5.9	10.9
B	96.3	2.9	0.6

In addition to the BSE analysis of composites with magnetite, the interaction be-tween magnetite and MWCNT in the same polymer matrix was examined, as shown in Figure 6.5. The results showed that specimens containing 1 wt.% MWCNT and 6 wt.% magnetite, subjected to a magnetic field in the melt state, demonstrated clear alignment along the magnetic field lines near the location of the permanent magnet, where the magnetic flux density is highest (Figure 6.5 b). This structured orientation is notably less pronounced when compared to the pure 6 wt.% magnetite sample (Figure 6.4 a), suggesting that the presence of MWCNT affects the particle orientation process, possibly by increasing the composite viscosity, which was confirmed by the rheological results. The composite with 3 wt.% MWCNT and 6 wt.% magnetite depict even lower orientation of the magnetite particles (Figure 6.5 c), resulting from the higher viscosity of this composite with higher MWCNT concentration. The resulting pattern of magnetic particles resembles that of the composite with 1 wt.% MWCNT and 6 wt.% magnetite fabricated in the absence of a magnetic field (Figure 6.5 a).

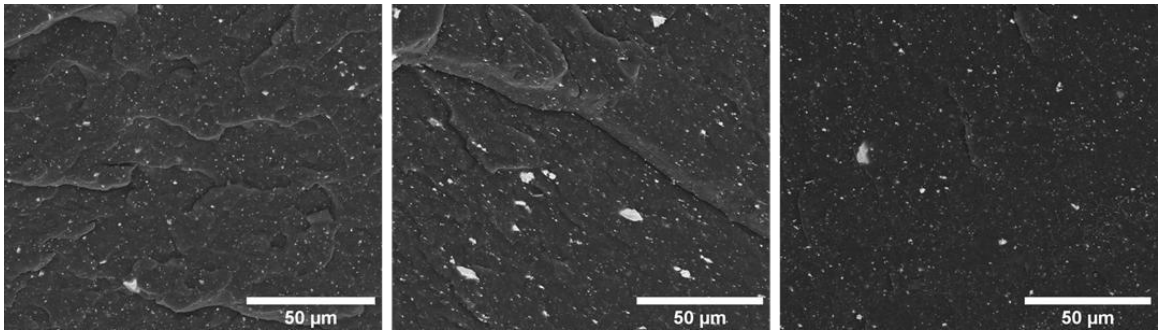

(a) (b) (c)

Figure 6.5- SEM images of the specimens cross-section at the corresponding magnifications performed in the same region: (a) 1% MWCNT_6% Magnetite without an applied magnetic field, (b) 1% MWCNT_6% Magnetite with an applied magnetic field and (c) 3% MWCNT_6% Magnetite with an applied magnetic field.

Figure 6.6 shows the morphology of the 1 wt.% MWCNT and 6 wt.% magnetite composite prepared with the application of a magnetic field, at higher magnification, to investigate the interaction between magnetite and MWCNT further. In these images, the alignment of magnetite and MWCNT particles in response to the magnetic field is visible, with BSE imaging providing evident contrast (Figure 6.6 a) and c)). The images effectively highlight the alignment and distribution of magnetite particles along the magnetic field lines, with MWCNTs also showing some orientation induced by the localised movement of magnetite within the matrix. In the absence of a magnetic field, magnetite particles and MWCNTs are dispersed randomly throughout the TPE matrix (Figure 6.13-S2 of Supplementary material).

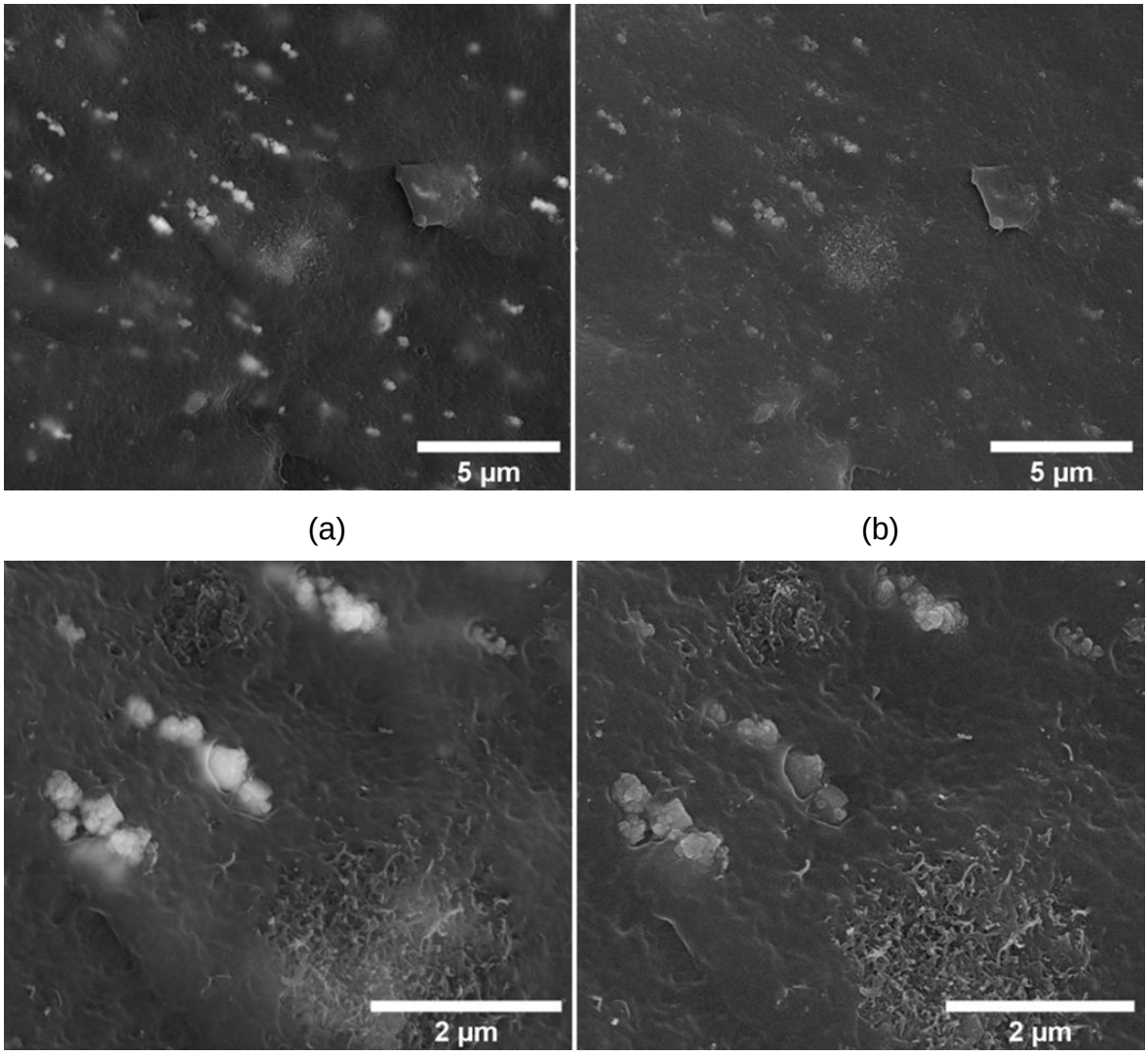

Figure 6.6- SEM images of a composite with 1% MWCNT and 6% magnetite under an applied magnetic field, shown in: (a) BSE and (b) SE modes, and (c) BSE and (d) SE modes at different magnification.

6.3.2. Rheological analysis

The rheological analysis of TPE composites containing varying concentrations of MWCNT and magnetite provides insight into the influence of these fillers on the properties of the composite melt. The results indicate that MWCNTs have a significant impact on the complex viscosity, loss modulus (G''), and storage modulus (G') of the composites. In contrast, adding magnetite at 1, 3, and 6 wt.%, shows minimal effect on complex viscosity, loss modulus, or storage modulus, compared to the pure TPE matrix (Figure 6.7 a), b), c) and d)). The similarity in the rheological response of TPE and magnetite-filled TPE composites, and the large shift observed for the nano-size MWCNT/TPE composites, confirms the influence of the particle size on the melt rheology. However, the combination of MWCNT with magnetite leads to a slight increase in complex viscosity, storage modulus, and loss modulus compared to the samples containing only MWCNT. This synergistic interaction between MWCNT and magnetite enhances the material's storage modulus and its ability to dissipate energy. Furthermore, the analysis shows that the complex viscosity of all materials decreases with increasing frequency, which suggests that the alignment of polymer chains under shear may contribute to a reduction in viscosity. This shear-thinning behaviour is characteristic of viscoelastic materials and highlights the importance of polymer chain dynamics in determining the flow properties of the composite [42].

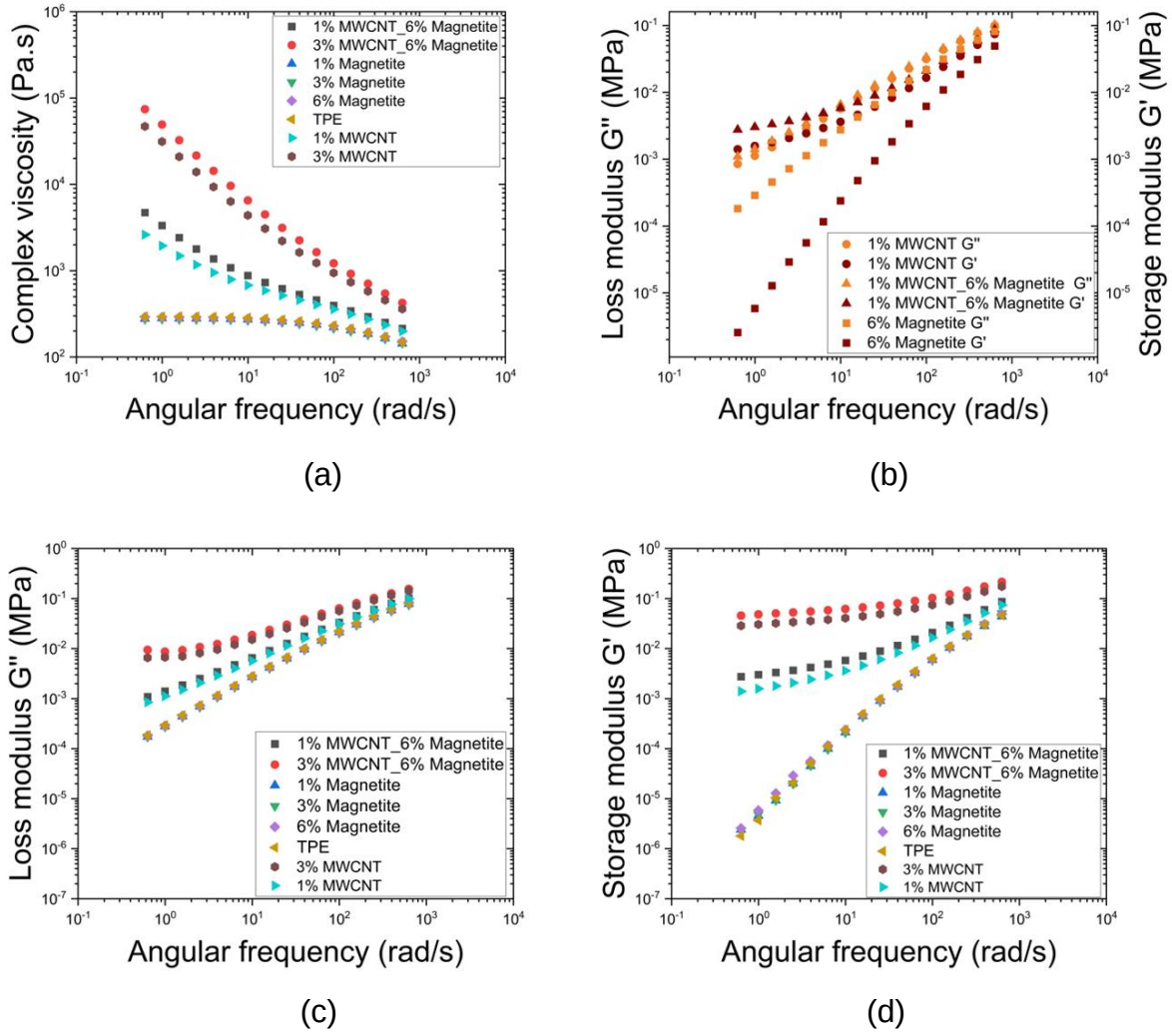

Figure 6.7- Rheology results obtained by frequency sweep for TPE, 1,3 and 6% magnetite, 1 and 3% MWCNT and the combination of 1% MWCNT with 6% magnetite and 3% MWCNT with 6% magnetite composites performed at 190 °C. (a) complex viscosity; (b) storage modulus and loss modulus for 1% MWCNT, 6% magnetite and 1% MWCNT with 6% magnetite composites; (c) storage modulus and (d) loss modulus for all the composites.

Interestingly, it is observed that the composite containing 6 wt.% magnetite presents the loss modulus consistently above the storage modulus, across the tested frequency range (Figure 6.7 b). This indicates the dominant viscous component of the complex modulus (G'' > G'), with energy dissipation dominating over elastic energy storage. In contrast, the samples containing 1% MWCNT and those containing 1% MWCNT combined with 6% magnetite exhibit a frequency-dependent transition: the viscous component dominates at low frequencies (G'' > G'), however, as the frequency increases, the storage modulus becomes dominant (G' > G''). This transition suggests that at higher deformation rates, the material's ability to store energy elastically becomes more significant, possibly

due to the enhanced network formation and interaction between the MWCNTs and the polymer matrix.

A time sweep analysis was performed at different temperatures to further investigate the rheological behaviour of the composites. Figure 6.8 illustrates individual materials storage and loss modulus at 160, 190, and 220 °C. This analysis depicts the evolution of the material's viscoelastic properties over 20 minutes at constant temperature. Additionally, a comparison of the complex viscosity for all samples was conducted at 160 and 190 °C, reflecting the highest real temperature achieved during the compression moulding process, which was 190 °C. The storage and loss modulus analysis extended to 220 °C to study the influence of higher temperature on the polymer's rheological behaviour.

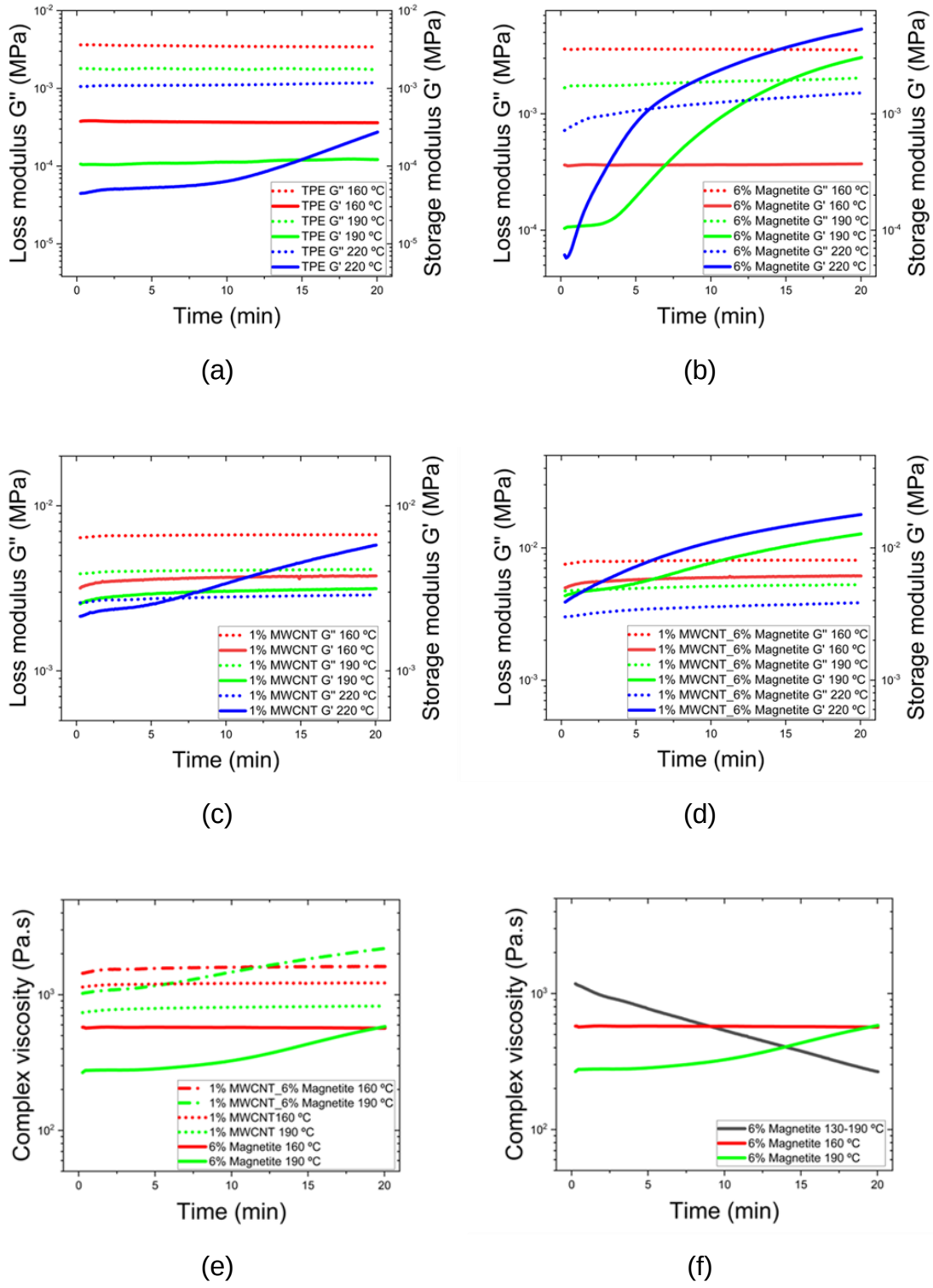

Figure 6.8- Time sweep rheology results, with storage and loss modulus for (a) TPE at 160, 190 and 220 °C; (b) 6% magnetite at 160, 190 and 220 °C; (c) 1% MWCNT at 160,190 and 220 °C; (d) 1% MWCNT with 6% magnetite at 160, 190 and 220 °C; and (e) complex viscosity for the samples of 1% MWCNT, 6% magnetite and 1% MWCNT with 6% magnetite at 160 and 190 °C. (f) Complex viscosity of TPE composites containing 6% magnetite at various temperature conditions: constant temperatures of 160 °C and 190 °C, and a gradually increasing temperature from 130 °C to 190 °C.

The rheological studies revealed the influence of fillers such as MWCNT and magnetite, as well as their combination, on the elastic and viscous responses

of the composite materials under constant thermal conditions. For the TPE composites, illustrated in Figure 6.8 a), storage and loss modulus remain relatively stable over time at temperatures of 160 and 190 °C, indicating stable elastic and viscous properties within this range. However, at 220 °C, the storage modulus shows a noticeable increase, suggesting that the material undergoes structural changes, possibly due to the onset of cross-linking or other thermal effects, which enhance its elastic response [43]. The loss modulus for TPE does not exhibit significant changes, implying that its ability to dissipate energy as heat remains constant across the temperature range.

The TPE composite containing 6 wt.% magnetite (Figure 6.8 b) depicts a pronounced increase in the storage modulus at both 190 °C and 220 °C, exhibiting a response similar to TPE but starting earlier and reaching a greater magnitude. This suggests that magnetite significantly enhances the material's stiffness as temperature increases, making the composite more resistant to deformation under elastic strain. At 160°C, the loss modulus remains higher than the storage modulus over the 20 minutes, indicating a predominantly viscous behaviour. However, as the temperature rises to 190 °C, the storage modulus approaches or exceeds the loss modulus, signalling a shift towards an elastic behaviour, with the material achieving gelation in less than 15 minutes. At 220 °C, gelation occurs faster, within 7 minutes, indicating that at this temperature the initial storage modulus is lower than at 190 °C but quickly surpasses the storage modulus observed at 160 °C. This demonstrates that the composite rapidly transitions to a more elastic state at elevated temperatures, highlighting the significant impact of temperature on its rheological properties.

The TPE composite containing 1 wt.% MWCNT (Figure 6.8 c)) shows the stable behaviour of the storage and loss modulus at 160 and 190 °C, with a pronounced increase at 220 °C, particularly in the storage modulus. This suggests that MWCNTs contribute to the material's energy dissipation capabilities, enabling gelation in approximately 7 minutes at 220 °C, although not to the extent observed in the sample with 6 wt.% magnetite. This observation is further supported by the analysis of the composite containing 1 wt.% MWCNT combined with 6 wt.% magnetite, which shows the most significant changes across the studied temperatures (Figure 6.8 d)). At 160 °C, the storage modulus displays a balanced increase, reflecting the synergistic effect of MWCNT and

magnetite in enhancing the composite's elastic properties over time. At 190 °C, the storage modulus increases substantially, indicating that the combination of these fillers strongly reinforces the material's elastic network at higher temperatures. At 220 °C, the test begins with G' already higher than G", indicating that the composite is stiffer at this temperature compared to other tested temperatures, highlighting the significant reinforcement provided by both MWCNT and magnetite.

Finally, the evolution of complex viscosity of the three composites at 160 °C and 190 °C over 20 minutes is compared in Figure 6.8 e). At 160 °C, complex viscosity remains relatively stable throughout the 20 minute test period. However, at 190 °C, after some time a noticeable increase in viscosity over time is observed, particularly for composites containing 6 wt.% magnetite, and 1 wt.% MWCNT with 6 wt.% magnetite. To provide insight into the contradictory enhanced particle alignment observed in Figure 6.3 f), Figure 6.8 f) shows the complex viscosity of the composites under a range of temperatures, simulating the mould cavity temperature evolution. With a set temperature of 220 °C, the cavity temperature gradually increases from 130 to 190 °C, allowing the sample to remain at lower temperatures initially. This gradual heating keeps the viscosity lower than at constant temperatures of 190 °C, delaying crosslinking that would otherwise increase viscosity. As a result, particle mobility and alignment are enhanced within the composite material. This gradual temperature increase reflects the real moulding process, where sustained lower viscosity over 20 minutes facilitates alignment.

6.3.3. Thermogravimetric analysis (TGA)

Figure 6.9 presents the results of the TGA. The TGA curves in Figure 6.9 (a) show that incorporating MWCNTs and magnetite at the specified concentrations significantly enhances the thermal stability of the composites compared to the neat TPE matrix. The thermal decomposition of the composites may be characterised by two parameters: the temperature at which mass losses of 5% (T5%) and 50% (T50%) are reached. As detailed in Table 6.3, composites containing 1 wt.% MWCNT and either 1 wt.% or 3 wt.% magnetite exhibit a T5% comparable to that of the neat TPE. However, composites with 3 wt.% MWCNT

show a notable 20 °C increase in T5%, while those with 6 wt.% magnetite exhibit a 12 °C increase. This behaviour aligns with previous studies [44–46], where the thermal stability increase was attributed to the heat dissipation properties of MWCNTs and magnetite and their ability to hinder the diffusion of volatile degradation products. Notably, the synergistic interaction between MWCNTs and magnetite amplifies this stabilising effect. The composite containing 1 wt.% MWCNT with 6 wt.% magnetite exhibits a 16 °C increase in T5%, while the composite containing 3 wt.% MWCNT with 6 wt.% magnetite shows a more pronounced increase of 36 °C. A similar trend is observed for T50%, the fillers delaying thermal decomposition for all composite samples. These results confirm the potential of MWCNT and magnetite to increase the thermal stability of TPE based composites.

Table 6.3- Thermal decomposition temperatures of the composites containing different percentages of MWCNT, magnetite and their combination

Samples	T5% (°C)	T50% (°C)
TPE	418	465
1% MWCNT/TPE	426	476
3% MWCNT/TPE	438	486
1% Magnetite/TPE	420	468
3% Magnetite/TPE	421	470
6% Magnetite/TPE	430	475
1 wt.% MWCNT/6 wt.% Magnetite/TPE	434	484
3 wt.% MWCNT/6 wt.% Magnetite/TPE	454	492

In a separate test (Figure 6.9 (b)), the thermal stability of a composite containing 6 wt.% magnetite was assessed by applying a controlled temperature ramp from ambient temperature to 220 °C over a period of 10 minutes, and then holding for 20 minutes at that temperature. During the isothermal stage, the weight loss percentage (TG%) remained nearly constant, with a small variation of approximately 1% observed, possibly due to residual humidity within the composite, showing the thermal stability at this temperature.

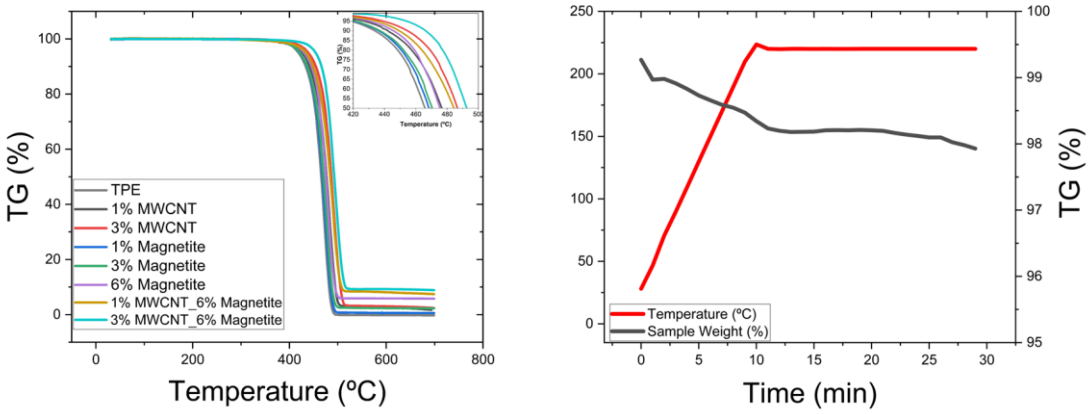

(a) (b)

Figure 6.9- (a) TGA for the 1, 3 and 6 wt.% magnetite, 1% MWCNT with 6 wt.% magnetite and 3 wt.% MWCNT with 6 wt.% magnetite samples. (b) isothermal thermogravimetric analysis for the sample with 6% magnetite at 220 °C for 20 minutes.

6.3.4. Electrical and functional testing

The electrical resistivity characterisation of the composites, formulated with different concentrations of MWCNT and magnetite within the TPE matrix, was done, revealing the influence of magnetite on the composite's resistivity (Table 6.4). Specifically, samples containing magnetite without a magnetic field applied during production exhibited slightly higher resistivity than those with an applied magnetic field. This suggests that simply adding magnetite without subsequent applied magnetic field may not enhance conductivity and might slightly disrupt the MWCNT conductive network. Conversely, applying a magnetic field during composite production appears to positively impact resistivity. This effect was particularly evident in the 1 wt.% MWCNT composites with 6 wt.% magnetite, where samples prepared under a magnetic field exhibited an electrical resistivity of $(8.8\pm7.5)\times10^{1}$ Ω.m compared to those processed without magnetic alignment, with $(4.5\pm6.9)\times10^{5}$ Ω.m, or the control sample with just 1 wt.% MWCNT and electrical resistivity of $(1.4\pm2.7)\times10^{5}$ Ω.m. Increasing the MWCNT content to 3 wt.% further decreased resistivity, especially when combined with an applied magnetic field on the mould cavity, achieving a value of $(9.5\pm6.1)\times10^{-1}$ Ω.m. These preliminary results indicate that including magnetite on conductive composites produced under a magnetic field seems to decrease their electrical resistivity. This increase could be attributed to the orientation of particles, which is reported in the literature as an effective method for enhancing

electrical conductivity [47], or potentially due to some degree of internal particle compaction.

The variability in electrical resistivity, particularly for samples with lower MWCNT concentrations, likely comes from challenges during composite preparation. Specifically, feeding low MWCNT concentrations proved difficult, leading to non-uniform particle distribution within the extruded filaments. This non-uniformity increased the variability in electrical resistance measurements, a common issue when working with low-density nanoparticles like MWCNTs, whose dispersion within the polymer matrix can be inconsistent during processing. Another contributing factor could be that 1 wt.% MWCNT appears to be near the electrical percolation threshold. Near this threshold, the critical concentration of conductive fillers at which a continuous conductive network forms, significantly decreasing resistivity, even small variations in MWCNT distribution or concentration can substantially impact the composite's electrical resistivity, resulting in higher measurement variability [48].

The variability in electrical resistivity, particularly for composites with low MWCNT concentration near the percolation threshold, is frequently observed. Small variations in nanoparticle dispersion and distribution across the composite can significantly impact conductivity [48]. To mitigate this variability, more precise feeding systems may be used to improve the control on MWCNT concentration during extrusion. However, this is a general limitation for compositions of small additive concentrations. Alternatively, a masterbatch dilution approach may be adopted, pre-dispersing a high concentration of MWCNT in the polymer matrix and then diluting it to the desired lower concentration. This method enhances the nanoparticle distribution and reduces challenges associated with feeding low-density materials.

Table 6.4- Summary of the electrical resistivity of the composites.

Samples	Resistivity with applied magnetic field (Ω.m)	Resistivity without applied magnetic field (Ω.m)
1% MWCNT/TPE	-	$(1.4\pm2.7)\times10^{5}$
1% CNT_6%magnetite TPE	$(8.8\pm7.5)\times10^{1}$	$(4.5\pm6.9)\times10^{5}$
3% MWCNT/TPE	-	(2.4±1.6)
3% CNT_6%magnetite/TPE	$(9.5\pm6.1)\times10^{-1}$	$(2.6\pm2.9)\times10^{1}$

Despite the observed variability in electrical resistance, the results highlight the potential of using magnetic fields and magnetite to align and distribute conductive fillers within the matrix. This approach is particularly advantageous for applications involving low-viscosity polymers and processing techniques like compression or injection moulding, as it effectively decreases electrical resistivity and enhances composite conductivity. Another potential application of magnetite in conductive composites involves sensor positioning and geometry control. This involves producing films from these composites, laser cutting sensor patterns, and then using permanent magnets to precisely immobilise the sensor pattern on flexible substrates, as demonstrated in Figure 6.10. This magnetic positioning technique applies pressure to the sensor pattern, allowing it to bond to the flexible substrate under temperature. The elevated curing temperature of 220 °C ensures adhesion between the sensor and the PI substrate, providing resistance to delamination even under cyclic deformation, as shown in Figure 6.11(e) and (f) [49].

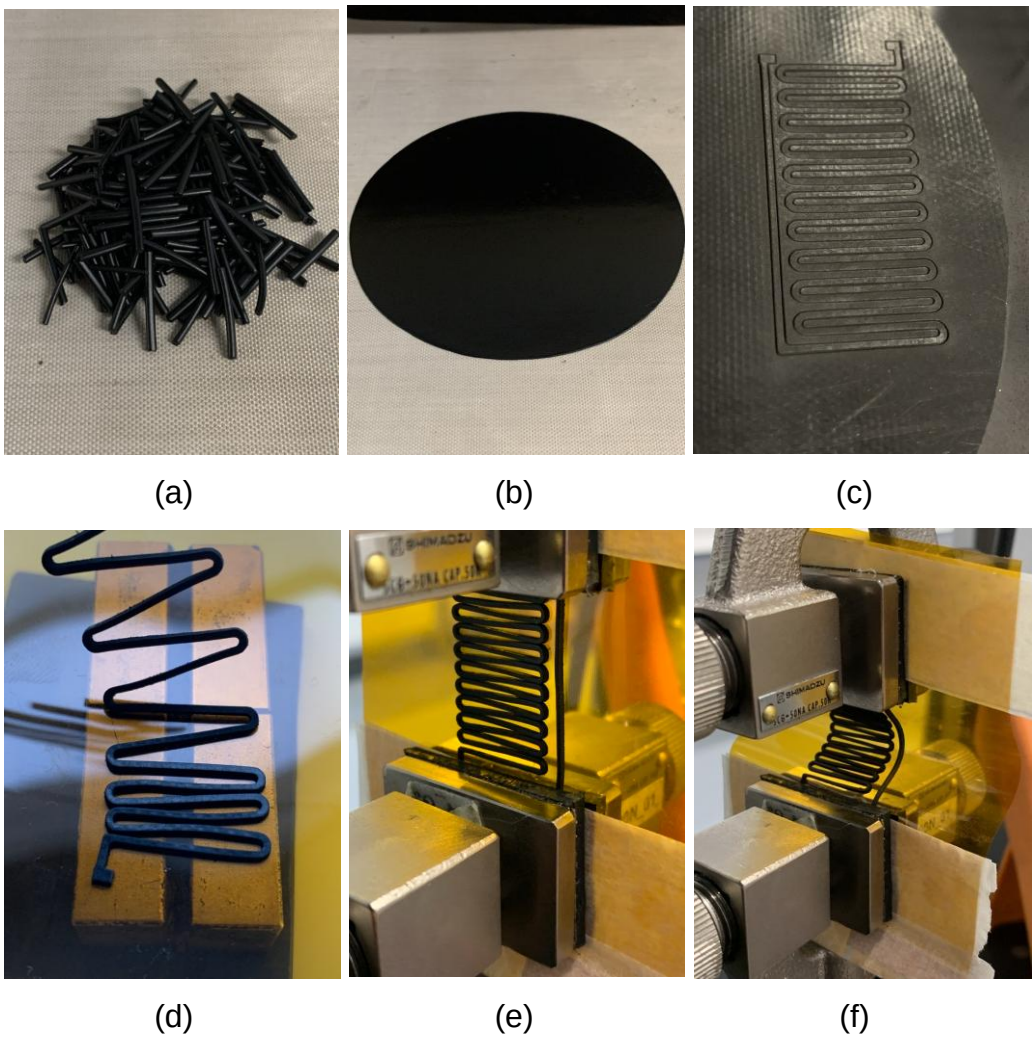

Figure 6.10- a) extruded material, b) compression moulding step to create a 0.3 mm film, c) laser cutting process, d) sensor positioning under magnetic field, e) sensor bonded to the polyimide substrate, f) sensor testing under cyclic bending.

To demonstrate the stability and functionality of the sensor, the composite with 3 wt.% MWCNT and 6 wt.% magnetite was assembled into a bending sensor and subjected to 100 bending cycles. As illustrated in Figure 6.11 (a), the sensor maintained its structural integrity with no signs of delamination, which would be evident in changes of the electrical resistance values. Subsequently, the sensor underwent 10 deformation cycles with a 10 second hold at the extreme positions, Figure 6.11 (b). Then, an additional 10 cycles were performed across three distinct bending positions, as demonstrated in Figure 6.11 (c). The sensor exhibited excellent stability in detecting different levels of deformation, highlighting its value as a tool for qualitative deformation analysis. These preliminary results present a promising approach for developing resilient sensors that endure repeated deformation cycles.

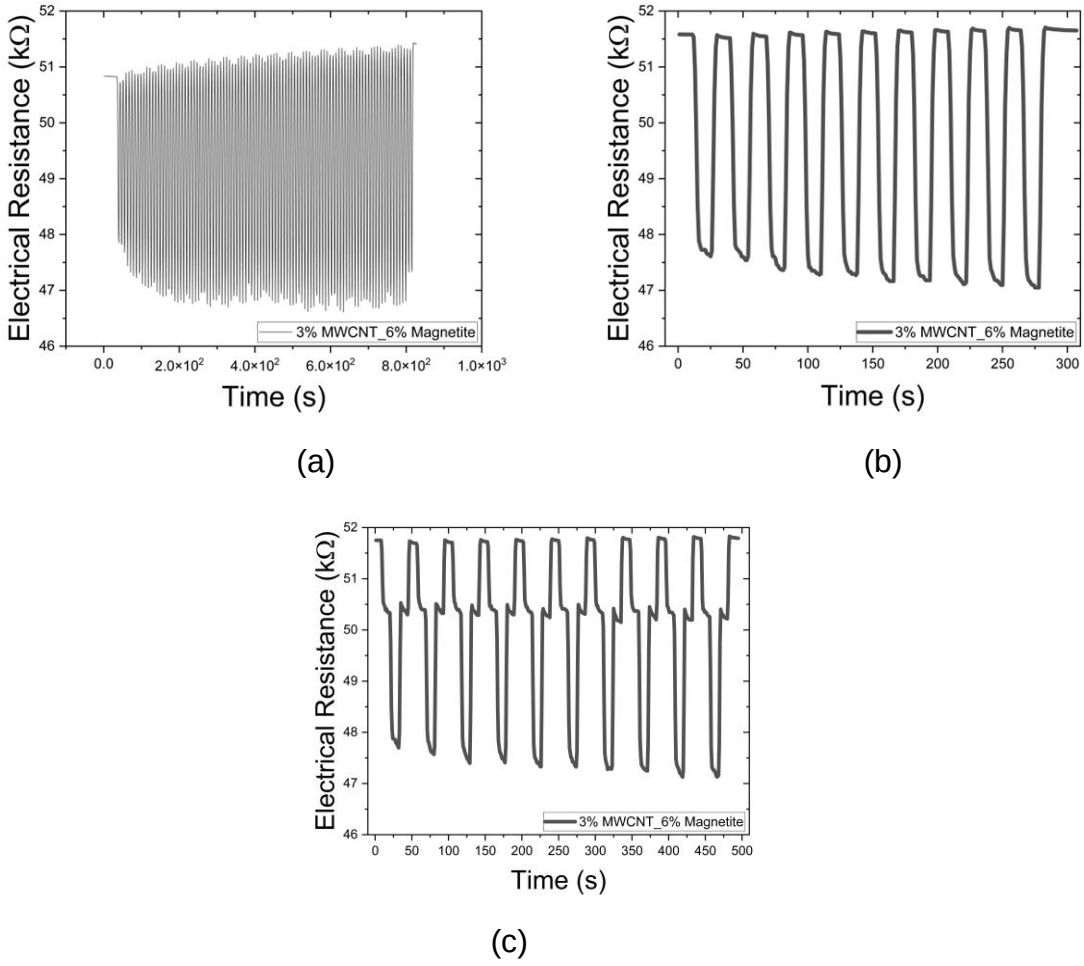

Figure 6.11- (a) Demonstration of the sensor stability under 100 bending cycles at 150 mm/min. (b) 10 bending cycles with 10 s holding time between bending cycles. (c) demonstrating the stability of the sensor at three different bending phases (no bending, medium bending, and full bending).

Table 6.5 compares bending sensors produced by different methods, their general characteristics and performance, for sensors reported in the literature [50,51], to compare with the sensor developed in the present work and a commercial sensor [52]. The sensor presented in the present work has a simple fabrication process and is versatile in terms of applications. While techniques such as scraping-coating or stencil printing require specific conditions and material properties [50, 51], the method proposed in this work is simple, robust and scalable. A key advantage is the use of a thermoplastic elastomer (TPE) instead of thermoset polymers as PDMS, commonly used in similar studies [50,51]. TPE advantages include recyclability, high processability, and compatibility with screen printing, simplifying the often challenging printing of electrodes and contacts in PDMS-based bending sensors. TPE is cost-effective,

its composites may be produced using large-scale production methods, making it highly suitable for industrial applications. These advantages position the sensor proposed in this work as a promising candidate for applications in wearable electronics, robotics, and soft robotics. Furthermore, integrating advanced techniques such as laser cutting and incorporating magnetite and MWCNT composites, aligns these sensors with contemporary advancements in bio-inspired designs and graphene-based devices, joining multifunctionality and durability under mechanical stress [53,54]. The robustness and operational stability demonstrated through repeated deformation cycles, combined with the adaptable design, broadens the scope of potential applications in flexible electronics and multifunctional actuator systems [55].

Table 6.5- Comparative fabrication techniques for bending sensors.

Reference	**Materials**	**Sensor fabrication method**	**Tested deformation range**	**Key Features**	**Applications**
This work	3 wt.% MWCNT/6 wt.% Magnetite /TPE	Laser cutting and magnetic field assisted lamination	0-90°	Simple, scalable; good stability over 100 cycles	Wearable electronics, robotics, soft robotics
Wang *et al*. [50]	2 wt.% Carbon Black/PDMS	Stencil printing	-0.6% to +0.6 % strain	High sensitivity; low hysteresis; scalable	Soft robotic skins, human motion detection
Zhao *et al*. [51]	8 wt.% MWCNT/ PDMS	Scrapping coating method	0-180°	Multi-functional; good cyclic stability	Human motion/ perception detection
Yu *et al*. [52]	Commercial bending sensor	Bending sensor sewn into the fabric	180 mm curvature range	High precision; robust gesture recognition	Gesture-controlled robotics

6.4 Conclusions

This work highlights the versatility of magnetite as an additive in flexible and electrically conductive composites, emphasising its promise in magnetic field-assisted orientation and positioning applications. Magnetite's magnetic responsiveness enables precise particle orientation within the TPE matrix, significantly enhancing the electrical conductivity of MWCNT/magnetite composites when exposed to a magnetic field. Magnetite does not impact TPE viscosity, facilitating particle mobility and alignment under magnetic influence. This characteristic enables the distribution of MWCNT particles when combined with 6 wt.% magnetite, enhancing the formation of conductive pathways and reducing electrical resistivity. This demonstrates magnetite’s suitability in applications requiring controlled particle orientation to boost conductivity without compromising the processability of the composite. Additionally, preliminary results were obtained for a bending sensor composed of 3 wt.% MWCNT and 6 wt.% magnetite, precisely adjusted and immobilised on a flexible substrate using permanent magnets, demonstrated stable performance across multiple bending positions and cycles, indicating a promising approach for flexible electronics.

Future work should refine these findings by exploring additional or alternative conductive additives to optimise composite performance. Improved MWCNT feeding methods to produce composites with low nanoparticle content are also relevant, to enhance particle homogeneity and reduce variability in conductivity measurements.

6.5. References

[1] Rajak, D. K., Wagh, P. H., & Linul, E. (2021). Manufacturing technologies of carbon/glass fiber-reinforced polymer composites and their properties: A review. Polymers, 13(21), 3721.

[2] Moaseri, E., Karimi, M., Baniadam, M., & Maghrebi, M. (2014). Improvements in mechanical properties of multi-walled carbon nanotube-reinforced epoxy composites through novel magnetic-assisted method for

alignment of carbon nanotubes. Composites Part A: Applied Science and Manufacturing, 64, 228–233.

[3] Mao, Z., Zhou, Z., Zhang, J., & Wang, T. (2022). Comparison between randomly distributed structure and 3D segregated structure in chlorinated polyethylene/MWCNT composites: Electrical conductivity, mechanical property, flame resistance, and rheological property. Composites Science and Technology, 221, 109338.

[4] Park, J. G., et al. (2012). Thermal conductivity of MWCNT/epoxy composites: The effects of length, alignment, and functionalization. Carbon, 50(6), 2083–2090.

[5] Kim, I. T., Tannenbaum, A., & Tannenbaum, R. (2011). Anisotropic conductivity of magnetic carbon nanotubes embedded in epoxy matrices. Carbon, 49(1), 54–61.

[6] Esteves, D. S., et al. (2023). Fabrication of low electrical percolation threshold multi-walled carbon nanotube sensors using magnetic patterning. Applied Sciences, 13(3), 1437.

[7] Dhanasekar, S., et al. (2022). Study of polymer matrix composites for electronics applications. Journal of Nanomaterials, 2022, 8605099.

[8] Cetin, M. S., & Karahan Toprakci, H. A. (2021). Flexible electronics from hybrid nanocomposites and their application as piezoresistive strain sensors. Composites Part B: Engineering, 224, 109199.

[9] Koch, I., et al. (2021). 3D arrangement of magnetic particles in thin polymer films assisted by magnetically patterned exchange bias layer systems. Particle & Particle Systems Characterization, 38(12), 2100072.

[10] Gaska, K., Kmita, G., Rybak, A., Sekula, R., Goc, K., & Kapusta, C. (2015). Magnetic-aligned, magnetite-filled epoxy composites with enhanced thermal conductivity. Journal of Materials Science, 50, 2510–2516.

[11] Esteves, D. S., et al. (2023). Development of MWCNT/Magnetite flexible triboelectric sensors by magnetic patterning. Polymers, 15(13), 2870.

[12] Krajewski, M., et al. (2019). Hybrid electrode composed of multiwall carbon nanotubes decorated with magnetite nanoparticles for aqueous supercapacitors. Journal of Energy Storage, 26, 101020.

[13] Wu, S., Peng, S., & Wang, C. H. (2018). Multifunctional polymer nanocomposites reinforced by aligned carbon nanomaterials. Polymers, 10(5), 542.

[14] Salehiyan, R., & Ray, S. S. (2019). Tuning the conductivity of nanocomposites through nanoparticle migration and interface crossing in immiscible polymer blends: A review on fundamental understanding. Macromolecular Materials and Engineering, 304(2), 1800431.

[15] Downes, R., Wang, S., Haldane, D., Moench, A., & Liang, R. (2015). Strain-induced alignment mechanisms of carbon nanotube networks. Advanced Engineering Materials, 17(3), 349–358.

[16] Eken, A. E., Tozzi, E. J., Klingenberg, D. J., & Bauhofer, W. (2011). A simulation study on the effects of shear flow on the microstructure and electrical properties of carbon nanotube/polymer composites. Polymer, 52(22), 5178–5185.

[17] Wang, M.-W., Hsu, T.-C., & Weng, C.-H. (2008). Alignment of MWCNTs in polymer composites by dielectrophoresis. European Physical Journal: Applied Physics, 42(3), 241–246.

[18] Gao, J.-F., Yan, D.-X., Yuan, B., Huang, H.-D., & Li, Z.-M. (2010). Large-scale fabrication and electrical properties of an anisotropic conductive polymer composite utilizing preferable location of carbon nanotubes in a polymer blend. Composites Science and Technology, 70(13), 1973–1979.

[19] Yang, J., Qi, X., Zhang, N., Huang, T., & Wang, Y. (2018). Carbon nanotubes toughened immiscible polymer blends. Composites Communications, 7, 51–64.

[20] Abbasi, S., Carreau, P. J., & Derdouri, A. (2010). Flow induced orientation of multiwalled carbon nanotubes in polycarbonate nanocomposites: Rheology, conductivity, and mechanical properties. Polymer, 51(4), 922–935.

[21] Dijkstra, D. J., Cirstea, M., & Nakamura, N. (2010). The orientational behavior of multiwall carbon nanotubes in polycarbonate in simple shear flow. Rheologica Acta, 49(7), 769–780.

[22] Zhu, Y.-F., Ma, C., Zhang, W., Zhang, R.-P., Koratkar, N., & Liang, J. (2009). Alignment of multiwalled carbon nanotubes in bulk epoxy composites via electric field. Journal of Applied Physics, 105(5), 054319.

[23] Dong, M., Tong, Z., Qi, P., & Qin, L. (2021). Enhanced electrical/dielectrical properties of MWCNT@Fe3O4/polyimide flexible composite film aligned by magnetic field. Journal of Materials Science: Materials in Electronics, 32(1), 524–542.

[24] Roskov, K. E., Atkinson, J. E., Bronstein, L. M., & Spontak, R. J. (2012). Magnetic field-induced alignment of nanoparticles in electrospun microfibers. RSC Advances, 2(11), 4603–4607.

[25] Kumar, S., Kaur, H., Kaur, H., Kaur, I., Dharamvir, K., & Bharadwaj, L. M. (2012). Magnetic field-guided orientation of carbon nanotubes through their conjugation with magnetic nanoparticles. Journal of Materials Science, 47, 1489–1496.

[26] Jia, X., Li, W., Xu, X., Li, W., Cai, Q., & Yang, X. (2015). Numerical characterization of magnetically aligned multiwalled carbon nanotube--Fe3O4 nanoparticle complex. ACS Applied Materials & Interfaces, 7(5), 3170–3179.

[27] Piao, G., et al. (2007). Alignment and micropatterning of carbon nanotubes in polymer composites using modulated magnetic field. Polymer Journal, 39(6), 589–592.

[28] Nguyen, M. D., Tran, H.-V., Xu, S., & Lee, T. R. (2021). Fe3O4 nanoparticles: Structures, synthesis, magnetic properties, surface functionalization, and emerging applications. Applied Sciences, 11(23), 11301.

[29] Wu, Y., et al. (2015). Magnetite/carbon nanotubes nanocomposite: Facile hydrothermal synthesis and enhanced cycling performance and high-rate capability as anode material for lithium-ion batteries. Ionics, 21, 635–643.

[30] Mahmud, M. H., Elmahmoud, W., Barzegaran, M. R., & Brake, N. (2017). Efficient wireless power charging of electric vehicles by modifying the magnetic characteristics of the transmitting medium. IEEE Transactions on Magnetics, 53(6), 1–5.

[31] Esteves, D. S., et al. (2022). Modified mortar for wireless powered lighting systems. Structural Concrete, 23(6), 3718–3726.

[32] Durmus, Z., Durmus, A., Bektay, M. Y., Kavas, H., Unver, I. S., & Aktas, B. (2016). Quantifying structural and electromagnetic interference (EMI) shielding properties of thermoplastic polyurethane--carbon nanofiber/magnetite nanocomposites. Journal of Materials Science, 51, 8005–8017.

[33] Kaidar, B., et al. (2024). Magnetite-incorporated 1D carbon nanostructure hybrids for electromagnetic interference shielding. Nanomaterials, 14(15), 1291.

[34] Kalita, H., & Karak, N. (2013). Hyperbranched polyurethane/Fe3O4 nanoparticles decorated multiwalled carbon nanotube thermosetting nanocomposites as microwave actuated shape memory materials. Journal of Materials Research, 28(16), 2132–2141.

[35] Ramazanov, M. A., Shirinova, H. A., Hajiyeva, F. V., & Bychanok, D. (2020). New polymeric three-phase nanocomposites based on polyvinylidene fluoride, magnetite nanoparticles, and multi-walled carbon nanotubes: Production, structure, and properties. Journal of Inorganic and Organometallic Polymers and Materials, 30, 4783–4791.

[36] Yang, J., et al. (2020). Fabrication of lightweight and flexible silicon rubber foams with ultra-efficient electromagnetic interference shielding and adjustable low reflectivity. Journal of Materials Chemistry C, 8(1), 147–157.

[37] Hekmatara, H., Seifi, M., & Forooraghi, K. (2013). Microwave absorption property of aligned MWCNT/Fe3O4. Journal of Magnetism and Magnetic Materials, 346, 186–191.

[38] Demidenko, N. A., et al. (2022). Flexible strain-sensitive silicone-CNT sensor for human motion detection. Bioengineering, 9(1), 36.

[39] Li, Z., et al. (2023). Low-field actuating magnetic elastomer membranes characterized using fibre-optic interferometry. Advanced Functional Materials, 33(50), 1–12.

[40] Andreu, J. S., Camacho, J., & Faraudo, J. (2011). Aggregation of superparamagnetic colloids in magnetic fields: The quest for the equilibrium state. Soft Matter, 7(6), 2336–2339.

[41] Faraudo, J., Andreu, J. S., & Camacho, J. (2013). Understanding diluted dispersions of superparamagnetic particles under strong magnetic fields: A review of concepts, theory, and simulations. Soft Matter, 9(29), 6654–6664.

[42] Ganguly, S., & Das, N. C. (2019). Rheological properties of polymer–carbon composites. Springer Singapore.

[43] Wallner, G. M., Adothu, B., Pugstaller, R., Costa, F. R., & Mallick, S. (2022). Comparison of crosslinking kinetics of UV-transparent ethylene-vinyl acetate copolymer and polyolefin elastomer encapsulants. Polymers, 14(7).

[44] Zhou, T. Y., Tsui, G. C. P., Liang, J. Z., Zou, S. Y., Tang, C. Y., & Mišković-Stanković, V. (2016). Thermal properties and thermal stability of PP/MWCNT composites. Composites Part B: Engineering, 90, 107–114.

[45] Kong, I., Ahmad, S. H., & Shanks, R. (2016). Properties enhancement in multiwalled carbon nanotube-magnetite hybrid-filled polypropylene natural rubber nanocomposites through functionalization and processing methods. Science and Engineering of Composite Materials, 23(3), 257–267.

[46] Carosio, F., Fina, A., & Coïsson, M. (2010). Polypropylene-based ferromagnetic composites. Polymer Bulletin, 65, 681–689.

[47] Tian, Z., Li, S., & Li, Y. (2021). Aligning conductive particles using magnetic field for enhanced piezoresistivity of cementitious composites. Construction and Building Materials, 313, 125582.

[48] Rahaman, M., et al. (2017). A new insight in determining the percolation threshold of electrical conductivity for extrinsically conducting polymer composites through different sigmoidal models. Polymers, 9(10), 527.

[49] Maynard, L. A., DeButts, B. L., & Barone, J. R. (2019). Mechanical and thermal properties of polyolefin thermoplastic elastomer blends. Plastics, Rubber and Composites, 48(8), 338–346.

[50] Wang, Y.-F., Yoshida, A., Takeda, Y., Sekine, T., Kumaki, D., & Tokito, S. (2023). Printed directional bending sensor with high sensitivity and low hysteresis for human motion detection and soft robotic perception. Sensors, 23(11), 5041.

[51] Zhao, X., et al. (2023). Strain and pressure sensors based on MWCNT/PDMS for human motion/perception detection. Polymers, 15(6), 1386.

[52] Yu, Z., Lu, C., Zhang, Y., & Jing, L. (2024). Gesture-controlled robotic arm for agricultural harvesting using a data glove with bending sensor and OptiTrack systems. Micromachines, 15(7), 918.

[53] Weng, M., et al. (2023). Multi-functional and integrated actuators made with bio-inspired cobweb carbon nanotube-polymer composites. Chemical Engineering Journal, 452, 139146.

[54] Li, M., et al. (2023). Graphene: Preparation, tailoring, and modification. Exploration, 3(1), 20210233.

[55] Ye, Y., Zhu, Y., Zhou, P., & Weng, M. (2023). Multi-functional and integrated actuator based on carbon nanotube-cellulose nanofiber composites. Cellulose, 30(11), 7221–7234.

Supplementary materials

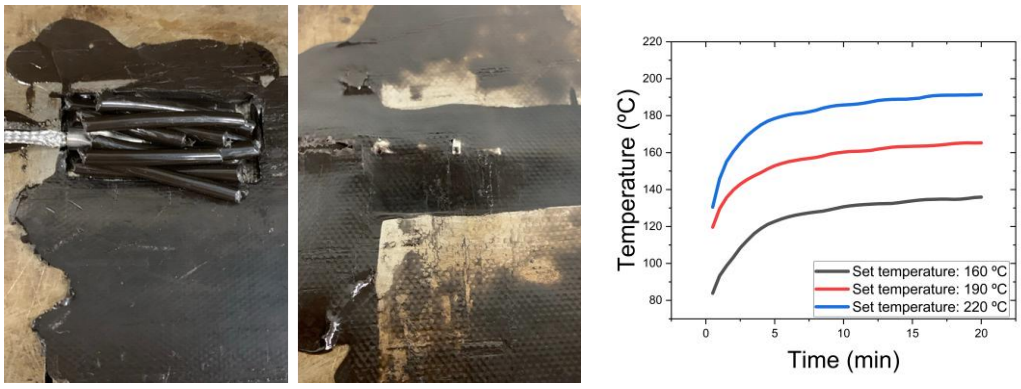

a) b) c)

Figure 6.12- S1: Temperature monitoring on the hot press cavity. a) sensor integration on the mould cavity. b) sensor inside the molten polymer. c) temperature profile for each set temperature for 20 minutes.

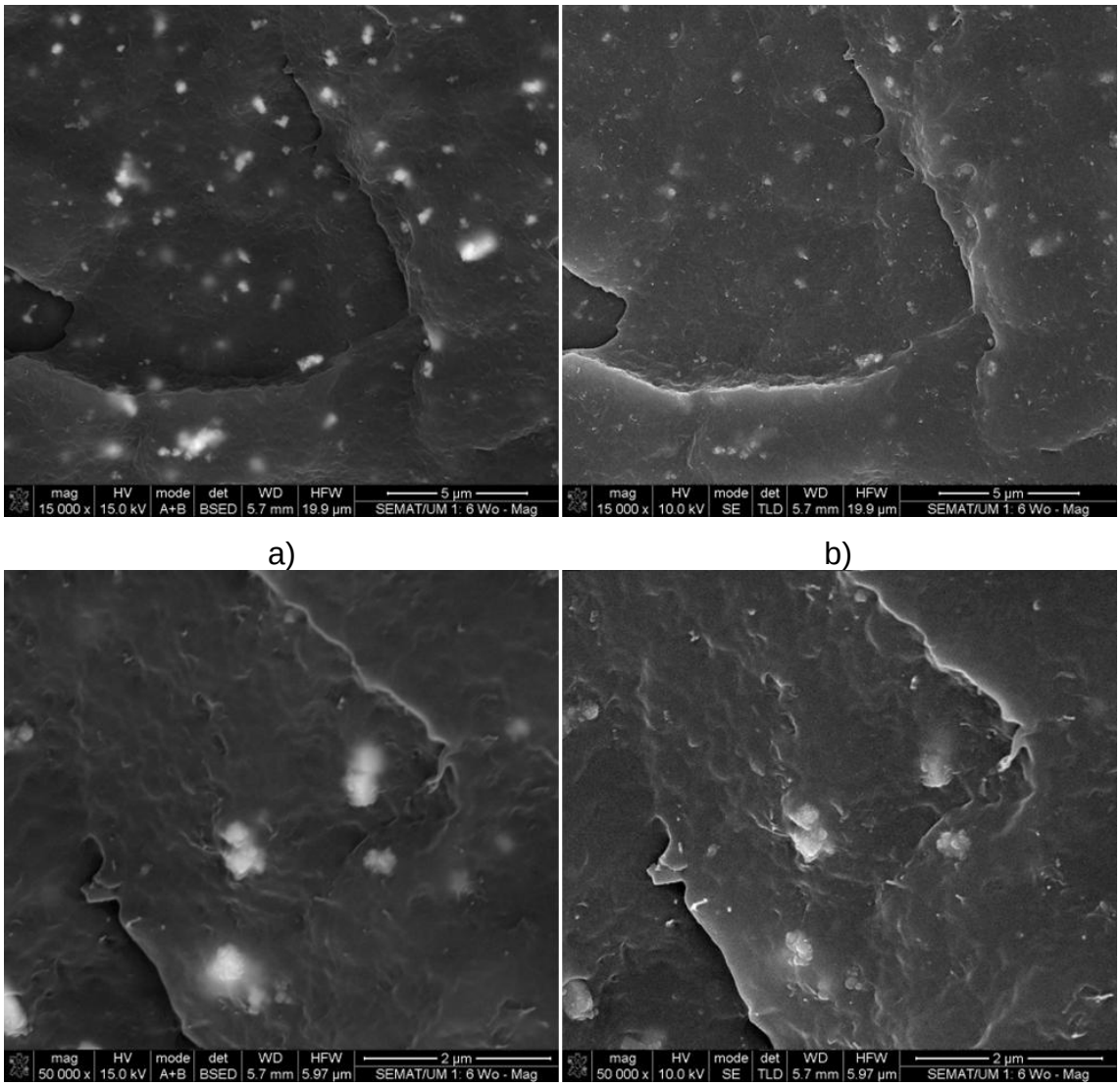

Figure 6.13- S2: 1% MWCNT 6% magnetite without magnetic field in a) BSE and b) SE at and c) BSE and d) SE.

Chapter 7: Conclusions and Future Work

The studies presented in chapters 3, 4, 5 and 6 of this PhD thesis contribute to the knowledge and development of MWCNT-based polymer composites for flexible sensors. These works emphasise the importance of magnetic patterning, polymeric matrix selection, and material preparation in optimising the electrical and mechanical properties of the composites produced. While challenges such as matrix viscosity and complex particle-polymer interactions were encountered, the research successfully demonstrated strategies to mitigate these hindrances, enhancing sensor performance, versatility, and integration into applications like soft robotics and smart textiles. The combination of the research topics contributed to the final objective: comparing thermosets and thermoplastics as polymeric matrices for conductive composite applications, providing insights into the trade-offs between these material classes for different sensor requirements.

7.1. Conclusions

This thesis investigated the development of flexible sensors, addressing five interconnected objectives: (1) investigating the influence of MWCNT arrangement on composite conductivity and electrical percolation threshold; (2) examining the impact of polymer matrix viscosity on particle arrangement and conductivity under magnetic fields in thermosets; (3) optimising thermoplastic material combinations to enhance composite properties; (4) evaluating magnetic field-assisted alignment in thermoplastics; and (5) comparing thermosets and thermoplastics as polymeric matrices for conductive composite applications.

Addressing the first objective, one of the key achievements of this work was the development of a novel, low-cost fabrication technique for low-percolation-threshold sensors. Leveraging the inherent magnetic properties of MWCNTs, magnetic field-assisted alignment within a PDMS matrix reduced the required nanomaterial concentration. It enabled patterned electrodes suitable for stable piezoresistive and triboelectric sensors under bending, demonstrating the potential for touch detection and soft robotics.

Regarding the second objective, thermoset matrix viscosity significantly influenced MWCNT mobility and alignment under magnetic fields. Lower thermoset viscosity facilitated particle movement and conductive pathway formation. While magnetite did not directly improve electrical conductivity, it conferred magnetic functionality, enabling sensor geometry control.

For the third objective, optimising thermoplastic blends identified a 5 wt.% MWCNT, 25 wt.% TPE, and PP composition as ideal for balancing flexibility, electrical properties, and mechanical strength. While increasing TPE composition enhanced flexibility, it reduced the composite's tensile strength and processing ease.

The fourth objective investigated the magnetic manipulation of magnetite/MWCNT/TPE composites in thermoplastics. While the higher thermoplastic viscosity, induced by MWCNT addition, limited magnetic patterning effectiveness, magnetite imparted magnetic properties without compromising electrical performance, enabling sensor positioning and geometry control. This

enabled the fabrication of a polymer-based resistive sensor that was thermally bonded to a PI substrate and successfully detected bending motion.

Addressing the fifth objective, the research provided an integrated understanding of MWCNT-based polymer composites for flexible sensors, emphasising the importance of magnetic patterning, matrix selection, and material blending. While challenges such as matrix viscosity and particle-polymer interactions were encountered, effective strategies to mitigate these issues were demonstrated, enhancing sensor performance, versatility, and integration into applications like soft robotics and smart textiles.

In conclusion, this work validated the hypothesis that static magnetic fields can enhance MWCNT-based polymer composites for sensor applications. Applying static magnetic fields in low-viscosity polymer matrices (PDMS and PU) effectively controlled MWCNT alignment and positioning, significantly reducing the electrical percolation threshold. The synergistic addition of magnetite further enhanced this control, demonstrating a straightforward, versatile magnetic patterning technique that improves conductive pathways while reducing MWCNT content. Magnetic field-driven particle migration was less effective in high-viscosity thermoplastics, a composite of 5 wt.% MWCNT and 25 wt.% TPE in a PP matrix was successfully developed using commercially available materials and industrially compatible processes. This composite achieved an optimal balance of low electrical resistivity and mechanical flexibility, making it suitable for wearable sensor applications. Its integration into textiles demonstrated the potential for multifunctional fabrics combining electrical and mechanical properties, offering promising opportunities for wearable electronics and adaptive clothing. Furthermore, incorporating MWCNTs into various polymer matrices yielded triboelectric sensors effectively responding to physical interactions, demonstrating the potential for robotics, wearable electronics, and other smart systems. By providing scalable, adaptable solutions for fabricating versatile composites, this work contributes to developing next-generation products in sectors such as healthcare, robotics, and smart textiles, facilitating the implementation of advanced, commercially viable sensor technologies at the intersection of material science and industrial innovation.

7.2. Future works

Using static magnetic fields to enhance the properties of MWCNT/magnetite-based polymer composites presents a promising strategy for developing advanced sensor technologies. However, there are still several areas that require further exploration. Therefore, the following future studies are proposed:

Firstly, to ensure these materials are viable for commercial applications, it will be necessary to examine the scalability of the fabrication processes used in the current studies. Future research should explore adapting static magnetic field alignment techniques for large-scale manufacturing while maintaining the quality and consistency of the composite's electrical properties. This could involve optimising the processing parameters for different fabrication methods, such as extrusion, injection moulding, or 3D printing, to ensure that the unique benefits of magnetic patterning can be preserved in mass production.

Then, exploring alternative matrices and fillers would significantly expand the versatility of MWCNT/magnetite-based composites. While the present work has primarily focused on flexible polymer matrices, investigating a wider range of materials could lead to novel composites with tailored properties for various applications. One example could be exploring biodegradable polymers to develop environmentally friendly sensors, thus meeting the growing demand for sustainable electronic solutions.

Another critical area for future research is evaluating the long-term stability of these composites. While initial tests show promise in electrical performance, a comprehensive knowledge of their durability under real-world conditions is essential. Long-term assessments should focus on stability, wear resistance, and electrical properties across various environmental factors, such as temperature fluctuations, humidity and continuous mechanical stress. This will provide insights into the composites' reliability and functionality over time, ensuring their suitability for various applications, particularly in fields where prolonged operational lifespans are necessary.

Additionally, investigating multifunctional sensor systems would be an interesting progression of this work. Future research could integrate the

developed MWCNT/magnetite-based sensors with other sensing modalities, such as temperature, humidity, and pressure detection, to create comprehensive, responsive, smart systems. Combining triboelectric sensors with different types of sensors could create all-in-one platforms capable of simultaneously monitoring a range of environmental and physiological parameters.